INSTITUTE
FOR
AEROSPACE STUDIES

UNIVERSITY OF TORONTO

AN INTERFEROMETRIC INVESTIGATION OF THE DIFFRACTION OF PLANAR SHOCK WAVES OVER A HALF-DIAMOND CYLINDER IN AIR

by

D. L. Zhang and I. I. Glass

March 1988

UTIAS Report No. 322
CN ISSN 0082-5255

AN INTERFEROMETRIC INVESTIGATION OF THE DIFFRACTION OF PLANAR SHOCK WAVES OVER A HALF-DIAMOND CYLINDER IN AIR

by

D. L. Zhang and I. I. Glass

Submitted October 1987

March 1988

UTIAS Report No. 322
CN ISSN 0082-5255

Acknowledgements

The first author is grateful to have had the opportunity of both studying and doing research at the Insitute for Aerospace Studies, University of Toronto, under the guidance of Prof. I. I. Glass. He is grateful to the Institute of Mechanics, Chinese Academy of Sciences, Beijing, China and to UTIAS for making it possible.

The authors thank Dr. George Ullrich and Dr. Allen Kuhl for suggesting this problem. We are also indebted to R. L. Deschambault, J. Kaca and T. C. J. Hu for providing assistance with the experimental work done at UTIAS.

The financial assistance received from Natural Science and Engineering Research Council of Canada under grant No. A1647, the U.S. Air Force under grant No. AF-AFOSR 87-0124 and from the U. S. Defence Nuclear Agency under DNA contract No. DNA 001-85-C-0368 is acknowleged with thanks.

Summary

In this study an experimental investigation was conducted on the diffraction of planar shock waves over a half-diamond (45° wedge angles) cylinder (28 mm x 28 mm x 56 mm cross-section) in air at initial pressures ranging from 6.67 Kpa to 80.3 Kpa (50 torr to 605 torr), at an initial temperature near 300 K in all cases and at initial Mach numbers ranging from $1.35 \leqslant M_s \leqslant 2.82$. Over 150 experiments were conducted including models with smooth, spongy (plastic), rough (sandpaper) and saw-tooth surfaces. Infinite fringe interferograms were used throughout. The UTIAS 10 cm x 18 cm hypervelocity shock tube and the 23 cm diam field-of-view Mach-Zehnder interferometer were utilized for this purpose. The induced flows behind the incident shock waves were subsonic, transonic and supersonic. The subsequent intersections with the initial wedge produced regular, single Mach, complex Mach and double Mach reflections. The isopycnics over the entire flowfields were evaluated and the pressure fields determined using the isentropic equation of state. A half-size model was also used to study the effects of longer flow durations. The present experimental data should prove very useful for comparison with numerical simulations and for evaluating the blast loading of structures.

Table of Contents

Notation

a	speed of sound
C	wedge corner
CMR	complex Mach reflection
DMR	double Mach reflection
e	specific total energy
h	height of cylinder, specific enthalpy
I	incident shock wave, specific internal energy
K	kink of reflected shock wave, degrees Kelvin, Gladstone-Dale constant
L	width of test section
M, M'	Mach stems
M_i	flow Mach number in state (i)
M'_1	induced flow Mach number behind the incident shock wave
MR	Mach reflection
M_s	incident shock Mach number
P	reflection point, pressure
P_i	pressure in state (i)
q_{sn}	normal velocity component of moving shock wave
q_{in}	velocity component normal to oblique shock wave in state (i)
q_{it}	velocity component tangential to oblique shock wave in state (i)
R	reflected shock wave, gas constant
R'	second reflected shock wave
RR	regular reflection
S, S'	slipstreams
SMR	single Mach reflection
T	temperature, first triple point
T'	second triple point
t	time, traverse time of the incident shock wave from the leading edge of the cylinder
u_i	flow velocity in state (i) with respect to pseudo-stationary coordinates
u	absolute velocity component along x-axis
V	absolute flow velocity
V_R	speed of reflected Mach stem

Notation (continued)

v	absolute velocity component along y-axis
x	x-coordinate in physical plane
y	y-coordinate in physical plane
γ	ratio of specific heats
Δ	difference between successive values
δ	angle between incident and reflected shock waves
Θ	flow deflection angle with respect to pseudo-stationary coordinates, angle in polar coordinate system
Θ_w	actual wedge angle
Θ'_w	$\Theta_w + \chi$, effective wedge angle
λ	wavelength
ρ	density
ϕ	incident shock wave angle between flow and shock wave
χ	first triple-point-trajectory angle
ω'	angle of reflection

Subscripts

0--4	thermodynamic states
T	with respect to first triple point
i	parameters ahead of shock wave
j	parameters after shock wave

1 INTRODUCTION

The study of shock wave diffraction dates back to the late forties and early fifties. During this period Prof. Walker Bleakney and his students at Princeton University, Refs. [1-4], investigated shock wave diffraction over a number of models, such as, rectangular blocks, triangular blocks, rectangular blocks with rounded corners, semicylinders and airfoils. They used infinite and finite fringe techniques to evaluate the isopycnic and isobaric contours over the flow field and the pressures on the various model surfaces.

They regretted the fact that there were no solutions to such complex flow problems. However, it is possible today to numerically simulate shock wave diffraction over obstacles [5-9]. Although it would be of much interest to simulate numerically Walker Bleakney and his co-workers' investigations, it was decided to study shock wave diffraction over a semicircular cylinder [10] and over a half-diamond cylinder. The reason for this decision was based on the fact that much more is known today about regular, single Mach, complex Mach, and double Mach reflections, than in the late forties or early fifties. These reflections occur only on the front face of a half-diamond cylinder. In addition, it was of interest to study the flow patterns at subsonic, transonic and supersonic speeds behind the initial shock wave. The interferograms and isopycnics presented herein should provide an excellent basis for simulating them numerically and critically evaluate the comparisons with experiments.

2 CLASSIFICATION OF TYPES OF SHOCK WAVE REFLECTIONS

When a planar moving incident shock encounters the wedge of a half-diamond cylinder, four different types of shock reflections may appear depending on the wedge angle and initial shock Mach number M_s, such as, regular reflection (RR), single Mach reflection (SMR), complex Mach reflection (CMR) and double Mach reflection (DMR). The latter three reflections as a group are called Mach reflection (MR).

As far as their discovery and research history is concerned, Mach [11] investigated various shock wave phenomena and was the first to observe RR and MR. However, detailed experimental and analytical programs [23] to study oblique shock wave reflection did not begin in earnest until the 1940's. Smith [12] at Princeton University conducted an extensive experimental investigation providing a firm foundation for later study. In the course of this work complex Mach reflection (CMR) was discovered. Subsequently White [13], at Princeton University, conducted experiments and was able to identify double Mach reflection. The four types of reflections are illustrated schematically in Figs. 1-a, b, c and d. In these figures the detailed flow parameters are also presented.

2.1 Regular Reflection (RR)

A RR consists of a two-shock configuration, i.e., the incident shock wave I and the reflected shock wave R, as shown in Fig. 1-a. When the shock wave angle ϕ_0 is sufficiently small, the intersection point P, the incident shock wave I and the reflected shock wave R occurs on the wall, and moves along the wall surface. In a frame of reference attached to P, the initial flow u_0 along the wall is deflected toward the wall by the incident shock wave, and the deflected flow u_1 generates the reflected shock wave R, which turns the flow u_1, so that u_2 is again parallel to the wall. Except for one particular value of ϕ_0, the angle of reflection ω' is not equal to the shock wave angle ϕ_0 [14].

In the frame of reference attached to the reflection point P (the intersection point of the two shock waves at the wall), the flow configuration is made stationary, so that two-shock theory may be used to find the flow properties of the angular regions around P [15, 16]. Since the velocity with which P moves along the wall is very high for small values of shock wave angle ϕ_0, the flow u_2 behind the reflected shock wave R is in general supersonic relative to P.

2.2 Single Mach Reflection (SMR)

A SMR configuration has an additional third shock wave M, referred to as a Mach stem and a slipstream S, as shown in Fig. 1-b. It occurs when the flow u_2 behind the reflected shock wave R is subsonic relative to the triple point T and is identified by the curved reflected shock wave over its entire length up to T. This configuration is always observed when the incidence is near glancing ($\theta_W \to 0°$). In general, in the case of SMR, the flow angles θ_1 and θ_3 to the incident shock wave and the Mach stem differ only slightly, and hence the reflected shock wave is weak. As a result, it is difficult to pinpoint the triple point T exactly and to determine the shock angles at T.

With the frame of reference attached to the triple point T the flow configuration becomes stationary and three-shock theory may be used to find the flow properties around the triple point T [15, 16].

2.3 Complex Mach Reflection (CMR)

The CMR shock system is characterized by a kinked reflected shock wave K, as shown in Fig. 1-c. When the flow u_2 behind the reflected shock wave R is supersonic relative to the triple point T, R is straight at T. The resultant Mach reflection configuration, see Fig. 1-c, with a straight reflected shock wave R at the triple point T and the kink K caused by a band of compression waves is referred to as complex Mach reflection to distinguish it from single Mach reflection which has a curved reflected shock over its entire length. The remaining reflected shock R' is still curved [17, 18].

2.4 Double Mach Reflection (DMR)

The DMR configuration has two reflected shock waves R and R', two Mach stems M and M', and two slipstreams S and S', as shown in Fig. 1-d. When the band of compression wave at the kink K of a complex Mach reflection converges to form a new shock stem M', the kink becomes the second triple point T' and the flow u_2 behind the reflected shock wave R, in a frame of reference attached to the second triple point T', is supersonic. Consequently, two systems of three shock interactions exist in the flow. This configuration is termed double Mach reflection, see Fig. 1-d. In the second three shock interaction system, the flow states (4) and (5) behind the second triple point T' can be obtained from state (1) by passing through either the second reflected shock wave R' or through the reflected shock wave R and second Mach stem M'. A second slipstream S' is formed at the second triple point T' and the second triple point trajectory angle χ' is defined as the angle between the wedge surface and the line extending from the wedge corner to the triple point T'. The method of calculations used for SMR applies to the first triple point of DMR. Since an analogy can be made between the first and second triple points, three-shock theory may also be used to find the flow properties around the second triple point T' [19, 20]. A fifth type of reflection is also possible and is known as terminal double Mach reflection (TDMR) [28, 5, 42]. However, this type of reflection is not possible in air, unless γ is very low at high temperature.

The different types of reflections depend on the incident shock Mach number M_s and wedge angle θ_w for a frozen test gas and also on the initial thermodynamic states for an equilibrium test gas [21, 22]. The reflected shock R and R' may be attached to or detached from the wedge tip [19]. The line separating the detached shock wave in a diatomic perfect gas from the attached shock wave is shown in the $(M\text{-}\theta_w)$ plane, (Fig. 2), where the flow Mach number behind the planar shock wave $M_1' \gtrless 1$ is also shown.

3 TRANSITION CRITERIA

The transition criteria of the various types of oblique shock-wave reflections have been proposed by a number of researchers in order to define their transition boundaries and domains. A schematic graph of the transition criteria in the $(M_s\text{-}\theta_w)$ plane is shown in Fig. 2. An analytical transition criterion for the termination of RR in an inviscid perfect gas was suggested by von Neumann [23] and is called "the detachment criterion", which states that the transition from RR to MR occurs when the wedge angle decreases to the value at which the flow deflection angle through the incident shock wave exceeds in magnitude the maximum flow deflection angle through the reflected shock wave .

Henderson and Lozzi [24] proposed an alternative criterion for the transition from RR to MR, which is refferred to as the "the mechanical equilibrium criterion". However, their criterion is accepted as a correct transition criterion only for the steady flow. Then, Hornung and Kychakoff

[25] suggested another criterion called "the sonic criterion". Since the transition boundaries predicted by the sonic and the detachment criterion are almost identical, it is difficult to resolve them experimentally.

The criterion for the transition from SMR to CMR and from CMR to DMR, which were initiated by Law and Glass [26], were established by Ben-Dor and Glass [21, 22]. They proposed the transition from SMR to CMR occurred when the flow behind the reflected shock wave was sonic with respect to the first triple point and from CMR to DMR when the flow behind the reflected shock was sonic with respect to the second triple point. A new additional and necessary criterion of SMR termination was proposed by Shirouzu and Glass [27]. They showed that the angle between the incident and reflected shock wave at the first triple point should be larger than 90° when CMR occurs. Lee and Glass [28] calculated the transition bundaries between the various types of shock reflection for both perfect and imperfect air up to $M_s = 20$ and for perfect gases with different specific heat ratios.

Recently, the experimental results obtained by Deschambault [29] and Hu [30] showed experimentally that the transition boundary from CMR to DMR met the boundary from SMR to CMR at a single point on the RR termination boundary. Ando and Glass [31] computed the transition boundaries in carbon dioxide and concluded that the perfect gas model can be used to predict the transition boundaries and the properties in the vicinity of the triple point. However, Shirouzu and Glass [27] showed that carbon dioxide and air should be treated as an equilibrium gas with vibration at shock Mach numbers higher than 3 and 6, respectively.

4 EXPERIMENTAL INVESTIGATIONS

4.1 Experimental Instrumentation

The simplest laboratory experiments designed to study diffraction can be conducted in a shock tube using optical methods [32]. The UTIAS 10 cm x 18 cm Hypervelocity Shock Tube [33] was used to perform the present experiments. Bristow [34] reported on further modifications and improvements. An updated and detailed documentation of the shock tube and the other associated facilities as well as their maintenance and operation procedures can be found in Ben-Dor and Whitten [35]. Therefore, only a brief discussion of the facilities relevant to the present study will be given.

The UTIAS 10 cm x 18 cm Hypervelocity Shock Tube is a large well constructed facility, approximately 15 meters in length, for generating gas flows of very short duration. It consists of two tubes, in which a diaphragm initially separates the two sections called the driver chamber and the channel, respectively. They can be filled with the same gas or different gases at different pressures. The incident shock wave is generated by rupturing the diaphragm with the high-pressure driver gas. The present diaphragm is composed of several layers of Mylar polyester films. A schematic overview of the shock tube facility in its present form is shown in Fig. 3.

Initially, the channel and driver chamber were evacuated by vacuum pumps. Medical grade air was used as the test gas in the channel. Pure cold helium at high pressure was used in the driver chamber. The initial pressure was monitored by pressure gauges. The initial temperature of the test gas was assumed to reach a thermal equilibium state within 5 minutes after gas admission. The temperature was measured by a mercury bulb thermometer, which was embedded in the midsection of the channel.

The shock speed was calculated from the measured traverse time interval between several stations in the channel (Fig. 4). Several piezoelectric pressure transducers flush mounted in the wall of the channel provided the velocity signals. Five digital counters with microsecond resolution were used to record the time intervals. When the incident shock arrived at the station D (5.7 meters upstream of the centre of the window of the test section) (Fig. 4), all of the five counters were triggered simultaneously. Each counter was then stopped in succession as the shock travelled past subsequent transducers at stations F G, H, I and J. The absolute error in calculating the incident shock Mach number can be estimated by means of a procedure outlined by Ben-Dor and Whitten [35]. For air the absolute error is 0.016 at $M_s = 1.35$, 0.019 at $M_s = 1.60$, 0.025 at $M_s = 2.02$, 0.032 at $M_s = 2.45$, 0.038 at $M_s = 2.82$.

To investigate the diffraction processes over the half-diamond cylinder, a 23 cm diam field-of-view Mach-Zehnder interferometer in an infinite fringe mode was used to study the density field of the diffraction pattern. Its basic construction is shown in Fig. 5. Details of the design and operation of this interferometer are given by Hall [36]. A detailed description of the special research resolution and alignment of the interferometer can be found in Ben-Dor and Whitten [35]. The infinite fringe interferometric technique provides excellent isopycnic contours, and is a very sensitive method of measuring density, However, the adjustments for an infinite-fringe interferograms were difficult in order to obtain just one fringe over the entire no flow field-of-view. Fortunately, only a few residual fringes remained far from the model surface and their effects on the quality of the infinite-fringe interferograms were negligible. The initial setup was almost identical before each run and all the photographs were taken under similar conditions.

The interferometric light source used was a giant-pulse ruby-laser consisting of a TRG model 104A laser head and power supply, and an integrated TRG model 2113-1 harmonic generator and TRG Pockels Q-switch. It was found experimentally that the Pockels cell opened after a time of 890 microseconds, the flash lamp pumping cycle gave an output pulse width of 15 nanoseconds, which was sufficiently fast to freeze the shock motion during the recording of the interferograms. The laser pulse provided monochromatic light at a wavelength of 6943.0 Å (first harmonic) and 3471.5 Å (second harmonic). The control of the laser light source operation is shown in Fig. 4. The laser flash lamp capacitor bank was triggered by the shock arrival at station F, correctly delayed by an oscilloscope to get 890 microseconds of the energy pumping by the time Pockels cell shutter opened. The Pockels cell Q-switch was triggered from station I, and suitably delayed in a delay unit to take the interferogram of the shock wave at a desired location with respect to station I.

4.2 Model Design

In order to study the diffraction of a planar shock wave over a half-diamond cylinder a test model was used, Fig. 6. The models were made of steel and extended over the full width of the shock tube from one window to the other. To investigate the diffraction process over the initial half-diamond cylinder for the four different types of reflection, the base angle of 45° was chosen for our experimental purposes. Five different incident shock numbers were chosen, $M_s = 1.35$, 1.60, 2.02, 2.45 and 2.82, to obtain the four types of reflections. Since all of the Mach numbers were $M_s < 3.00$, the test gas can be considered a perfect gas, with $\gamma = 1.4$.

For long-duration phenomena of interest, a small half-diamond model (half size of the original model) was also constructed for this purpose. The small model had to be carefully mounted in the test section. Any misalignment caused a deformation of the interferometric fringes.

Since there are many different types of coarse materials to be used to cover the front and rear faces of the model to observe the effects of surface roughness, two types were selected, a plastic spongy material, 5 mm thick, Airguard Industries, washable foam filter media, which has a completely open pore construction of 30 pores per inch and sandpaper with the most coarse grain, 3M Company. Garnet paper #TA2-36 grit. These roughness materials were attached with glue, rubber cement and epoxy-patch, so that they would not detach during an experiment, especially at high shock Mach number. In addition, the half-diamond cylinder shape must remain unchanged, as the roughness materials are attached.

4.3 Run Conditions

In order to study the interaction with the half-diamond cylinder, five different incident shock Mach numbers were chosen to acquire RR, SMR, CMR and DMR in air. For shock Mach number $M_s = 1.35$ and 1.60, the flow Mach number behind the incident shock, $M_1' < 1$, so that the induced flow was subsonic. For $M_s = 2.02$, then $M_1' \simeq 1$, the induced flow was transonic. For $M_s = 2.45$ and 2.82, $M_1' > 1$, the induced flow was supersonic. At the different Mach numbers, the flowfield had completely different isopycnic patterns.

For the various Mach numbers the corresponding initial test gas pressures were about 80.3 Kpa (605 torr) for $M_s = 1.35$; 32.66 Kpa (245 torr) for $M_s = 1.60$; 20.27 Kpa (152 torr) for $M_s = 2.02$; 10.53 Kpa (79 torr) for $M_s = 2.45$; 6.67 Kpa (50 torr) for $M_s = 2.82$, respectively. It was sufficient to get quite clear interferograms under these conditions. The initial temperatures of the driver and test gas were assumed to be at room temperature.

It is useful to investigate the diffraction processe by taking a series of interferograms with different time delays at identical run conditions. Unfortunately, it is difficult in practice to generate exactly the same incident shock Mach number owing to the non-repeatability of the bursting pressures of the diaphragms. In the present experiments the scatter of the incident shock Mach numbers ranged from 1.34 to 1.36 for RR; from 1.57 to 1.61 for SMR; from 1.98 to 2.03 for SMR ($M_1' \simeq 1.00$); from 2.43 to 2.47 for CMR; from 2.80 to 2.85 for DMR.

5 EVALUATION OF THE FLOWFIELDS

The phenomena are assumed to be pseudo-stationary and all the velocities in the equations below are those relative to a frame of reference attached to a point that moves at constant velocity. The reference point is the reflection point P in RR and the triple point T in MR, respectively. Each region which is divided by shocks and a slipstream is designated by 0 to 3. The physical quantities on both sides of each shock wave in the vicinity of the reference point satisfy the following equations:

Conservation of tangential velocity:

$$\rho_i \tan \phi_i = \rho_j \tan (\phi_i - \Theta_j)$$

Continuity:

$$\rho_i u_i \sin \phi_i = \rho_j u_j \sin (\phi_i - \Theta_j)$$

Normal momentum:

$$p_i + \rho_i u_i^2 \sin^2 \phi_i = p_j + \rho_j u_j^2 \sin^2 (\phi_i - \Theta_j)$$

Energy:

$$h_i + \frac{1}{2} u_i^2 \sin^2 \phi_i = h_j + \frac{1}{2} u_j^2 \sin^2 (\phi_i - \Theta_j)$$

where i and j are the upstream and downstream values, respectively. The basic equations and the computer program used here are the same as those used by Hu and Shirouzu [20]. In the case of regular reflection, with two shock waves, two sets of equations for i = 0, j = 1 and i = 1, j = 2 are solved under the boundary condition $\Theta_1 = \Theta_2$. this means that the direction of the flow behind the reflected shock wave is along the surface. In the case of Mach reflection, with three shock waves, three sets of equations for i = 0, j = 1; i = 1, j = 2 and i = 0, j = 3 (ϕ_j is called ϕ_3 in this case) are solved under the boundary conditions $\Theta_3 = \Theta_1 - \Theta_2$ and $p_2 = p_3$, which means that the flow is parallel and the pressure is idendical on both sides of the slipstream. In the case of MR, it is also assumed that the Mach stem from the triple point is perpendicular to the wedge surface, which is reasonable, but not precise experimentally. The Mach stem may be curved outward or inward in practice.

Infinite fringe interferometric techniques can be used to record small density changes in the flowfield. The density difference $\Delta\rho$ between any two adjacent lines of constant density (isopycnics) is expressed by the relation [31]:

$$\Delta\rho = \lambda/K\ L$$

where λ is the wavelength of the light source and L is the width of the test section. For the present experiments, $\lambda = 6943$ Å and $L = 10.16$ cm. In this relation K is the Gladstone-Dale constant. The values of K are related to the nature of the test gas and the wavelength of the light source. K for air is $2.258 \times 10^{-4}\ m^3/\ kg$ at $\lambda = 6440$ Å [32]. Since the values of K vary very little with wavelength, the above mentioned value of K was used in the present experiments.

Depending on the analytical considerations discussed in the foregoing the values of the density can be evaluated in several states near the first triple point. Just after the collision of the incident shock wave or the Mach stem with the cylinder, the density behind a regular reflected shock wave or a normally reflected Mach stem can also be given. The density in these particular states were used as starting points to evaluate the isopycnics. Ideally, only experimental results should be used obtained from white light fringes. However, this has been done by many experimenters verifying the correctness of the calculated results for the flow properties behind shock waves of known Mach number.

6 EXPERIMENTAL RESULTS

6.1 General Description

In this study an experimental investigation was performed in the 10 cm x 18 cm UTIAS Hypervelocity Shock Tube in air at initial pressures ranging from 6.67 Kpa to 80.3 Kpa (50 torr to 605 torr), at initial temperatures near 300°K in all cases and at initial Mach numbers of $1.35 < M_s < 2.82$. A detailed description of the initial conditions and evaluated properties in these regions are listed in Tables 1-5.

All of the infinite fringe interferograms are presented in Figs. 7-11 along with the tabulated evaluations of the density fields to illustrate the processes of diffraction in the cases of RR SMR, CMR and DMR in air over a half-diamond cylinder.

In some experiments three coarse materials were used to cover over the cylinder surface with a plastic spongy material and sandpaper and using a saw-tooth model to observe roughness effects on the flowfield, see Figs. 12-17. The flowfields of long-duration were researched and are shown in Figs. 18 and 19.

It can be clearly observed from the above noted figures that the main physical processes of the diffraction over the cylinder are as follows:

As soon as the incident shock wave collides with the cylinder, a regular reflected shock wave or a Mach reflected shock wave will be formed. It can be seen that the interferometric photographs consist of the incident shock wave I, reflected shock wave R, Mach stem M, triple point T and slipstream S, as pointed out in Ref. [37]. As the incident shock diffracts over the apex of the cylinder, an expansion wave occurs followed by a vortex, a slipstream and the curved diffracted shock wave along the rear face of the cylinder. Since the reflected pressure on the front face is much greater than that behind the incident shock wave, a large expansion (angle about 90°) takes place and I and R are weakened. However, from Figs. 7-11 it is clear that the curved portion of the incident shock wave (now a Mach stem) is still perpendicular to the rear face of the cylinder. A triple point is generated between the incident shock wave, reflected shock wave and curved Mach stem that gives rise to a slipstream. The expansion wave moves from the rear face to the front face of the cylinder and it causes the pressure of the flowfield to decrease. The expansion wave weakens the reflected shock wave. The induced boundary layer behind the shock waves separates at the model apex and gives rise to a vortex which is clearly shown on the photographs.

As time goes on, the vortex moves forward and grows and interacts with the slipstream. When the curved bow shock wave passes down the rear face and reaches the wall of the shock tube, it reflects as a regular or as a Mach reflection, as shown in Figs. 18 and 19. Finally, by the time the shock has travelled further (a few cylinder diameters - referred to as the long-duration stage), the reflected shock from the floor becomes a Mach reflection and interacts with the original slipstream and the flowfield, Figs. 18 and 19.

It should be emphasized that the flow behind the incident shock wave can be subsonic or supersonic and the flow characteristics are different in the two cases. As shown in the interferograms, at the tail of the reflected shock wave or bow shock wave ahead of the cylinder there exists a shock bifurcation or λ-shock-wave system, caused by the interaction with the wall boundary layer.

Between the front face of the cylinder and the bow shock wave a stagnant region exists, in which the density, pressure and temperature come to their highest values in the whole flowfield.

6.2 Analysis of the Flowfield for Various Reflected Shock Waves

6.2.1 Regular Reflection

For regular reflection the diffracted shock configurations over the cylinder are shown in Figs. 7-a, b, c, d and e, in which the shock Mach number is 1.35. As soon as the shock wave turns round the apex, the reflected shock configuration becomes similar to Mach reflection, although at $M_s = 1.35$ the initial reflected shock is regular. The Mach stem is convex and the slipstream is also clearly seen.

The expansion wave propagates from the rear to the front face. Since the flow behind the incident shock wave is subsonic, the incident shock wave and the reflected shock wave are weakened. However, due to the wall-boundary layer effects when the incident shock wave diffracts over the apex, a vortex is formed near the rear face of the cylinder and it moves close to the rear face. In the vortex region the gas has a very strong rotational motion.

Finally, it should be noted that there is a dark area before the curved incident Mach stem, which is not clearly understood.

6.2.2 Single Mach Reflection

In Figs. 8-a, b, c, d and e a single Mach reflection is presented at $M_s = 1.60$. The Mach stem is very short and unclear, but it exists at the front face. The slipstream is also visible close to surface. The reflected shock wave is weakened by the expansion wave. In this case a bifurcation of the detached reflected shock wave does not appear. However, the interaction of the vortex with the slipstream is more pronounced than in the previous case of section 6.2.1. The triangular dark area ahead of the curved Mach stem is still visible.

6.2.3 Single Mach Reflection ($M_1' \simeq 1.00$)

The single Mach reflection at $M_s = 2.02$ is shown in Figs. 9-a, b, c, d and e. The Mach stem and the slipstream can be clearly seen, even though the stem is short. After the incident shock wave passes over the apex of the cylinder, the vortex develops further and interacts strongly with the slipstream. A second vortex lying above the main one appears to be formed in the slipstream region. Since the flow behind the incident shock wave has reached a critical state of $M_1' \simeq 1.00$, the reflected shock is weakened less than in the previous cases, so that a λ-shock-wave starts to appear at the head of the cylinder. Since the bow shock bifurcation is close to the corner of the cylinder, the stagnaion region is narrower than that in sections 6.2.1 and 6.2.2. The detachment distance increases with time. Finally, the detached shock wave tends to a stationary position. Morever, there is also evidence of recompression at the tail of the expansion wave. The shock thickness appears to change with curvature as a result of diffraction effects. There is still evidence of a dark triangular region at the curved Mach stem on the rear face in Fig. 9-d, but is not seen in Fig. 9-e.

6.2.4 Complex Mach Reflection

The diffracted configurations of complex Mach reflection at $M_s = 2.45$ are shown in Fig. 10-a, b, c, d and e. From the interferograms it is clear that a kink exists in the reflected shock wave. As described above, as soon as the incident shock wave passes over the apex of the cylinder, the expansion wave propagates ahead and a vortex is formed. An expansion wave goes back as it encounters a higher pressure region. The interaction of the vortex with the slipstream is strong. A compression wave is formed at the tail of the expansion wave and around the vortex. The reflected shock interacts with the induced boundary layer to produce a λ-shock system. The slipstream is too weak to be noted here. In Fig. 10-d, the curved bow shock wave on the rear face has formed a Mach stem.

6.2.5 Double Mach Reflection

At $M_s = 2.82$, double Mach reflection is formed, see Figs. 11-a, b, c, d and e. The first and second Mach stems can be seen in Fig. 11-a. However, the second slipstream is weak and does not appear. The second Mach stem appears to consist of a compression wave. As the main shock wave propagates over the apex, the second Mach stem is absorbed by the expansion wave and nearly vanishes, leaving a weak remnant in Figs. 11-c and d. The interaction of the vortex with the slipstream is more severe. A compression wave and shock wave appear at the tail of the expansion wave and around the vortex to provide recompression. The reflected bow shock wave is bifurcated owing to its interaction with the wall boundary layer and it lies close to the base. A slipstream is not evident in the λ-shock configuration.

6.3 Effects of Model Surface Roughness on the Flowfield

In order to investigate the roughness effect, two Mach numbers were chosen, $M_s = 1.60$ and $M_s = 2.45$, to provide subsonic and supersonic flow behind the shock wave, respectively.

6.3.1 Effects of Plastic Spongy Material

The roughness effects caused by the covering spongy material over the half-diamond cylinder are shown in Figs. 12-a, b, c and d at $M_s = 1.60$ for the subsonic case, and in Figs. 13-a, b, c and d at $M_s = 2.45$ for the supersonic case.

It has been found that the density distributions are entirely different from the smooth surface cases. The fringes in the roughness case arise from the local surface roughness elements. As time goes on and the induced boundary layer becomes thicker, they appear to smooth. It can be found from the photographs that there is a two-shock-structure. The disturbance behind the reflected shock wave is present even after interacting with the expansion wave in Figs. 12-c and d. No slipstream is generated from either reflected wave interacting with the incident shock wave.

6.3.2 Effects of Sandpaper Roughness

The flowfield generated by the covering sandpaper are shown in Figs. 14-a, b, c and d and 15-a, b, c and d. The roughness affects the shape and distribution of the isopycnics, but it is not as severe as in the case of the spongy mesh, for the single Mach reflection at $M_s = 1.60$ or the complex Mach reflection at $M_s = 2.45$. Otherwise, at later times the flow looks similar to the interferogroms for the smooth surfaces of the half-diamond cylinder.

6.3.3 Flowfield Over Saw-Tooth Model

The effects of the saw-tooth model on the flowfield are shown in Figs. 16-a, b and c at $M_s = 1.60$ and 17-a, b, c and d at $M_s = 2.45$, which have particular important phenomena. The density distribution is severely disturbed and the fringes are intermingled. An apparently thick boundary layer is generated by the saw teeth as well as disturbances that affect the flow and the reflected shock wave in Fig. 16-a. As the incident shock turns around the apex of the cylinder, there are many vortices at the rear face. The disturbances generated by the rough teeth affect the entire flowfield.

When the flow behind the incident shock wave at $M_s = 2.45$ is supersonic, Fig. 17, the flow patterns are similar to the subsonic case, Fig. 16. The flow on the front face behind the reflected shock wave is more disturbed than the one on the rear face after expansion around the apex.

6.4 Long-Duration Flowfields

The long-duration flowfields at $M_s = 1.60$ are shown in Figs. 18-a, b, c, d and e and at $M_s = 2.45$ in Figs. 19-a, b, c, d and e.

From the configurations it is found that the main characteristics of the long-duration effect is the reflection of the incident shock wave from the wall of the shock tube. At first, it is a regular reflection and then a single Mach reflection. The reflected shock wave from the wall interacts with the slipstream and the main vortex to make the flowfield more complex. Many small vortices appear behind the major vortex and the slipstream is deflected towards the vortex. The flowfield does not satisfy self-similarity. For $M_s = 2.45$ all these effects are enhanced.

7 ANALYSES AND DISCUSSIONS

7.1 Some Flowfield Similarity Features

As noted in [37, 38], before the incident shock wave turns around the apex of the cylinder, in all cases of RR, SMR, CMR and DMR the flowfields are self-similar. The trace of the triple-point trajectory is basically a straight line. However, after the shock wave turns over the apex, the flowfield becomes rather complex because of the interaction of the expansion wave with the incident shock wave. It is verified from the present experiments that, even after the shock turns over the apex, the traces of the triple points remain close to straight lines, as shown in Figs. 20-a and b. Figure 20-a is the trace of triple points for SMR case ($M_s = 1.60$). Since the Mach stem is very short. it can been shown that the trace emanates from the sharp apex of the half-diamond cylinder like the RR case and is inclined at 29.5°. However, it is found that in Fig. 20-b for MR the trace of the triple point, which is inclined at 30.5°, emanates from a position above the apex of the cylinder, at which the initial height is equal to that of the Mach stem when the stem reaches the apex of the cylinder for SMR, CMR and DMR. Consequently, even after the shock wave turns over the apex, there appears to be some remnant of self-similarity. It is surprising that the new triple point in RR and the existing triple point in MR have traces that are inclined at nearly the same angle. This fact might be useful and convenient for further analysis of the flowfield. It can only be substantiated further by numerical simulation.

7.2 Vortex Formation and Development

As the incident shock wave diffracts over the apex of the cylinder and passes down along the rear face of the cylinder a vortex is produced which rolls up in the form of a spiral with one end remaining in contact with the model. The opposing velocities set up by the incident and reflected shock waves and the separated boundary layer produce the shear layer, that gives rise to the vortex [39]. In fact, from the interferograms (even better from shadowgrams) it can be observed that the induced boundary layer separates at the apex, rolls up and forms a vortex. The shape of the vortex core is different with increasing Mach number M_s For $M_s = 1.35$ the vortex core appears to be perfectly circular. However, as M_s increases, the shape of the vortex departs progressively from circular. The first revolution of the gas around the core should depend on the contour of the half-diamond cylinder, on Mach number M_s, and the kinematic viscosity of the gas [40].

The vortex continues to move down the rear face of the cylinder. The trace of the moving vortex core can be measured from the interferograms. According to the measurements the trace of the vortex core is nearly a straight line and the angle between the vortex trace and the rear face is near 23°. As noted previously, this angle has somewhat different values for $M_1' < 1$ or $M_1' \geq 1$, but the trace remains a straight line before the incident shock wave reaches the wall of the shock tube. Consequently, the vortex motion also has certain self-similarity features along the rear face of the cylinder. As soon as the incident shock wave reaches the wall, a new reflected shock system is formed, which interacts with the slipstream and the vortex. The flowfield becomes more complex and the self-similarity features are destroyed.

7.3 Distribution of the Density and Pressure

A series of infinite fringe interferograms are shown in Figs. 7-11 along with a tabulated evaluation of the density field to illustrate the process of the collision of all reflection cases RR, SMR, CMR and DMR with the half-diamond cylinder. From the interferograms it is seen that the highest density is located at the head of the front face of the cylinder to form a stagnation region, where the flow velocity is zero. Here, the stagnation pressure and temperature also have the greatest values. On the contrary, in the region near the vortex core along the rear face of the cylinder the density, temperature and pressure have their lower values. However, at the vortex core the flow velocity has a high value.

On both sides of the slipstream the density and temperature are different at the same position, but the pressure and flow inclination are the same.

Comparing the different Mach numbers, it is seen that at $M_s = 1.35$ and 1.60, in which $M_1' < 1$, the density distributions are similar. Whereas, when M_s is 2.05, in which $M_1' \approx 1$, and when M_s is 2.45 and 2.80, where $M_1' > 1$, the fringe distributions tend to be more and more complex, and the vortex interacts strongly with the slipstream.

At a later time when the incident shock wave reaches the wall of the shock tube and reflects as a regular or Mach reflection, this flowfield is further compressed. From the long-duration experiments it is found that the new reflected shock system at the wall moves ahead along the wall. The new reflected shock system will continue to develop into a new simple Mach reflection, which interacts with the curved incident shock wave and reforms it into a planar shock wave (Fig. 21).

It should be pointed out that before and after the incident shock wave turns over the apex of the cylinder, the triple point trajectories have two different slopes. Hence, in the flowfield behind the apex of the cylinder the method of calculating the density distribution around the triple point in Ref. [20] could not be used. Fortunately, the triple point trace is a straight line, so that the flowfield in the rear region may be equivalent to one produced by an incident shock wave diffracting over another imaginary wedge of unknown wedge angle.

In order to determine the flowfield density distribution it was neccessary to measure the angle δ between the incident and reflected shock waves (Fig. 1-b). Then according to the M_s and δ values the parameters of states (1), (2) and (3) in the neighbourhood of the reference point can be calculated using three-shock theory, as described in section 3. From these parameters the fringe density distribution could be determined.

From the calculated results for $M_1' < 1$ and $M_1' \geqslant 1$ good agreement was obtained from the measureed angle χ with the calculated angle χ.

It is possible to evaluate the density contours or isopycnics at any instant of time by obtaining interferograms. When considering the forces or pressures exerted on the cylinder, the pressure is a more important parameter than the density and a method to determine the pressure from the density distribution is required. It is not easy to calculate P/P_0 from the diffraction pattern, but fortunately, it may be assumed that all changes are isentropic in states (2) and (3) of the flowfield. Making use of this assumption:

$$P/\rho^{\gamma} = P_2/\rho_2^{\gamma}$$

and

$$P/P_0 = (P_2/P_0)(\rho_0/\rho_2)^{\gamma}(\rho/\rho_0)^{\gamma}$$

Here P_2 and ρ_2 are the pressure and density behind the reflected shock wave, which are obtained from a knowledge of the strength of the incident shock wave, as described previously. The data given on each of the interferograms together with above equations permits the computation of the pressure distribution for any contour in the flowfield.

7.4 Comparison of the Density Distribution with Bleakney's Results for $M_s = 1.35$

In order to check our evaluated density distribution with that of Bleakney [3], inteferogram (No. 42), the RR case with $M_s = 1.36$, t = 138 μs was used to compare with Bleakney's experimental result of the RR case with $M_s = 1.35$, t = 136 μs (Figs. 22-a and b).

A comparison shows that the two methods yield essentially the same values for the density distribution. Especially, white fringe 1 in experiment No. 42 and fringe No. 12 in Bleakney's experiment are in good agreement and the density distribution behind the expansion wave also is similar. From this, it can be concluded that the present method is quite reasonable. However, it is found that the density values in the expansion region are somewhat different by 2 or 3 fringe values. It will be settled by computational simulations.

7.5 Characteristics of the Reflected Shock

As the incident shock wave impinges on the cylinder, a reflected shock wave is formed. These shock waves diffract over the apex of the cylinder and the shock system becomes more complex owing to the corner expansion wave, which interacts with the reflected shock wave, the vortex and the slipstream. When the flow behind the incident shock is subsonic, the expansion wave turns the reflected shock wave into compression waves, as shown in Figs. 7 and 8. When the flow behind the incident shock wave is transonic, this effect does not appear to be so strong. As noted above, when $M_1' > 1$, the counterflow keeps the reflected bow shock wave close to the head of the cylinder, where it becomes a λ-shock-wave.

As shown from the interferograms, the bifurcation of the reflected shock wave at the head of the cylinder is caused by its interaction with the boundary layer on the wall. When the incident shock wave impinges on the cylinder, the flowfield behind the reflected shock wave is not uniform and the boundary layer properties are more complex, such problem has been studied in steady supersonic flow [41], but it has not been investigated in nonstationary flow. When $M_1' < 1$, this bifurcation phenomenon is not present.

7.6 Apparent Change of the Shock Thickness

From the interferograms it can be seen that owing to diffraction effects the shock waves have apparently different thicknesses in the diffracted regions of the flowfield. For example, the incident and reflected shock waves near the triple point have the largest thicknesses. The incident shock thickness becomes thinner as it approaches the shock tube wall. Undoubtedly, the expansion wave contributes much to the apparent shock thickness of the reflected shock wave by turning it into a compression wave.

7.7 Evaluation of the Shock Detachement Distance

By the time the incident shock wave has travelled a few cylinder lengths, the reflected shock wave takes up a stationary position for $M_1' > 1$. However, for $M_1' < 1$, the bow portion of the reflected shock wave can move upstream without achieving a stationary position [38].

For $M_1' \geqslant 1$, in the case of present study, the shock detachment distances (δ/d), where d is the half-diamond cylinder base, are as follows [43]:

For $M_s = 2.45$ $M_1' = 1.15$ $\delta/d = 0.65$
For $M_s = 2.82$ $M_1' = 1.35$ $\delta/d = 0.54$

7.8 Characteristics of Roughness Effects

Generally speaking, the density distributions with the variously covered roughness elements are similar to that without roughness for both $M_1' < 1$ and $M_1' \geqslant 1$. However, the size of the roughness element will control the size of the flow disturbance. For example, the disturbances caused by the sandpaper are much less than those caused by the saw-tooth model. A thick turbulent boundary layer on the wall results from the saw-tooth model and the disturbances from the teeth propagate thoughout the region behind the reflected shock wave.

In the case of the plastic spongy material, a second reflected shock wave forms from a strong disturbance behind the main reflected shock. This second reflected shock wave maintains itself through the expansion wave. The reflected shock wave becomes so weak that no clear triple point or slipsteam is in evidence.

8 CONCLUSIONS

Infinite fringe interferograms and isopycnics have been obtained of the diffraction of planar shock waves over a half-diamond cylinder for RR, SMR, CMR and DMR for $M_1' \gtrless 1$. The effects of roughness and of the long-duration flow characteristics at $M_s = 1.60$ and $M_s = 2.45$ have also been investigated briefly.

It should be noted that the flow Mach number is a very important parameter for the flow characteristics. The isopycnic shapes and distributions are completely different for $M_1' \gtrless 1$. The other differences are as follows:

No.	Case	$M_1' < 1$	$M_1' \geqslant 1$
1.	density distribution	simple	more complex
2.	reflected shock	detached shock with strong expansion effect	detached shock with weak expansion effect
3.	detachment distance	increases with time	almost stationary
4.	stagnation region	large	small
5.	bifurcation	none	λ-shock-wave
6.	apparent shock thickness change	weak	strong
7.	roughness effect	weak	strong

From the comparison with Bleakney's experiment it can be concluded that the present method of evaluation is quite reasonable.

As noted previously, as the incident shock wave travels on the rear face of the cylinder, a dark triangular area precedes it especially when $M_1' < 1$. However, when $M_1' \geqslant 1$, this triangular area is not apparent. As yet, a satisfactory explanation has not been found.

It should be emphasized that the size of a roughness element plays an important role in disturbing the flowfield. Consequently, roughness effects are important in the study of shock wave loading of structures.

Although detailed values of the flowfield densities are provided, their accuracy will not be known untill complete numerical simulations have been made. This will also shed much more light on what has been to date mainly an empirical description of the diffraction phenomena, although the isopycnics and isobars are exact.

It is hoped that the numerical simulations will appear in a separate report in the near future, from which temperature, velocity, internal energy and other flow quantities will add to the interpretations of the present research.

REFERENCES

1. Walker Bleakney, White, D. R., Griffith, W. C. and Priceton, N. J., "Measurements of Diffraction of Shock Waves and Resulting Loading of Structures", J. of Applied Mechanics, Vol. 17, No. 4, pp. 430-445, December 1950.

2. Walker Bleakney, "The Diffraction of Shock Waves Around Obstacles and Transient Loading of Structures", Techn. Report II-3, Dept. of Phys., Princeton University, 1950.

3. White, D. R., Weimer, D. K. and Walker Bleakney, "The Diffraction of Shock Waves Around Obstacles and the Resulting Transient Loading of Structures", Tech. Report II-6, Dept. of Phys., Princeton University, 1950.

4. Walker Bleakney, "Shock Loading of Rectangular Structures", Tech. Report II-11, Dept. of Phys., Princeton University, 1952.

5. Glass, I. I., "Some Aspects of Shock Wave Research", Dryden Lecture in Research, AIAA J. Vol. 25, No. 2, pp. 214-229, February 1987.

6. Glaz, H. M., Colella, P., Glass, I. I. and Deschambault, R. L., "A Numerical Study of Oblique Shock Wave Reflections with Experimental Comparisons", Proc. Roy. Soc. Lond. A 398, pp. 117-140, 1985.

7. Glaz, H. M., Glass, I. I., Li, J. C. and Walter, P. A., "Interaction of Oblique Shock Waves Reflections in Air and CO_2 with Downstream Obstacles"Proc. of 15th Int. Symp. Shock Tubes and Waves, pp. 219-225, 1986.

8. Booen, W. B. and Needham, C. E.,"Two Dimensional HULL code Simulation of Complex and Double Mach Reflections", AFWL Tech. Report No. NTE TN-81-001, 1981.

9. Fry, M., et al., "Shock Capturing Using Flux-Corrected Transport Algorithms with adaptive Gridding", Proc. 13th Int. Symp. of Shock Tubes and Shock Waves, pp. 376-384, 1981.

10. Kaca, J. and Glass, I. I., "An Interferometric Investigation of the Diffraction of a Planar Shock Wave Over a Semicircular Cylinder", UTIAS Report (to be published), 1988.

11. Mach, E.,, "Uber der Verlauf des Funkenwellen in der Ebene und in Raume", Oesterreichische Akademie der Wissenschaften, Matematisch-naturwissenschaftliche Klasse, Sitzungsbechichrte, Abt II, V. pp. 819-838, 1878.

12. Smith, L. G., "Photographic Investigation of the Reflection of Plane Shocks in Air, "OSRD Report No. 6271, or NDRC Report No. A-350, 1945.

13. White, D. R., "An Experimental Survey of the Mach Reflection of Shock Waves", Tech. Report II-10, Dept. of Phys. Princeton University, 1951.

14. Polachek, H. and Seeger, R. J., "On Shock Wave Phenomena: Interaction of Shock Waves in Gases", Proc. 1st Symp. Appl. Math. p. 119, 1949.

15. von Neumann, J., "Oblique Reflection of Shocks", Explosives Research Report No. 12, Navy Dept., Bureau of Ordnance, 1943.

16. Bleakney, W. and Taub, A. H., "Interaction of Shock Waves", Rev. Mod. Phys., Vol. 21, No. 4, pp. 584-605, 1949.

17. Kawamura, R., "On the Mach Reflection of a Shock Wave", J. Phys. Soc. Japan 6, p. 533, 1951.

18. Gvozdeva, L. G., Bazhenova, T. V., Predvoditeleva, O. A. and Fokeev, V. P., "Mach Reflection of Shock Waves in Real Gases", Astronautica Acta, 14, p. 503, 1969.

19. Ben-Dor, G., "Regions and Transitions of Nonstationary Oblique Shock Wave Diffractions in Perfact and Imperfact Gases", UTIAS Report No. 232, 1978.

20. Hu, T. C. J. and Shirouzu, M., "Tabular and Graphical Solutions of Regular and Mach Reflections In Pseudo-Stationary Frozen and Vibrational Equilibrium Flows", UTIAS Report No. 283, Parts 1 and 2, 1985.

21. Ben-Dor, G. and Glass, I. I., "Domains and Boundaries of Non-stationary Oblique Shock Wave Reflection 1. Diatomic Gas", J. Fluid Mech. Vol. 92, Part 3, pp. 459-496, 1979.

22. Ben-Dor, G. and Glass, I. I., "Domain and Boundaries of Non-Stationary Oblique Shock Wave Reflection 2. Monoatomic Gas " J. Fluid Mech. Vol. 96, part 4, pp. 735-756, 1980.

23. Von Neumann J., "Refraction, Intersection and Reflection of Shock Waves", NAVORD Report 203-245, Navy Dept. Bureau of Ordinance, Washington D.C., 1945.

24. Henderson, L. F. and Lozzi, A., "Experiments on Transition of Mach Reflection" J. Fluid Mech. Vol. 68, p. 139, 1975.

25. Hornung, H. G. and Kychakoff, G., "Transition from Regular to Mach Reflection of Shock Waves in Relaxing Gases " Proc. of 11th Int. Symp. on Shock Tubes and Waves, pp. 296-302, 1977.

26. Law, C. K. and Glass, I. I., "Diffraction of Strong Shock Waves by Sharp Compressive Cornner", CASI Trans. Vol. 4, pp. 2-12, 1971.

27. Shirouzu, M and Glass, I. I., "An Assessment of Recent Results on Pseudo-Stationary Oblique Shock Wave Reflection", UTIAS Report No. 264, 1982, see also Proc. Roy. Soc. Lond. A 406, pp. 75-92, 1986.

28. Lee, J. H. and Glass, I. I., "Pseudo-Stationary Oblique Shock Wave Reflections in Frozen and Equilibrium Air", Progress in Aero. Sci. Vol. 21, No. 1, pp. 33-80, 1984.

29. Deschambault R. L., "Non-Stationary Oblique Shock Wave Reflections in Air", UTIAS Report No. 270, 1984, see also J. Fluid Mech. Vol. 131, pp. 27-57, 1983.

30. Hu, T. C. J. and Glass, I. I., "An Interferometric and Numerical Study of Pseudo-Stationary Oblique Shock Waves Reflections in Sulfur Hexafluoride (SF_6)", Proc. of 15th Int. Symp. on Shock Waves and Shock Tubes, pp. 227-234, 1985, see also Proc. Roy. Soc. A 408, pp. 321-344. 1986.

31. Ando, S. and Glass, I. I., "Domains and Boundaries of Pseudo-Stationary Oblique Shock Wave Reflections in Carbon Dioxide", Proc. 7th Int. Symp. on MABS,pp. 13-17, 1981.

32. Glass, I. I. and Hall, J. G., "Shock Tubes ", Handbook of Supersonic Aerodynamics, NAVORD report 1488, Vol. 6, Sec. 18, 1959.

33. Boyer, A. G., "Design Instrumentation and performance of the UTIAS 4 in x 7 in Hypersonic Shock Tube", UTIAS Report No. 99, 1964.

34. Bristow, M. P. F., " An Experimental Determination of the Polarizality for Singly Ionized Argon", UTIAS Report No. 158, 1971.

35. Ben-Dor, G. and Whitten, B. T., "Interferometric Techniques and Data Evaluation Methods for the UTIAS 10 cm x 8 cm Hypervelocity Shock Tube" UTIAS Tech. Note No. 208, 1979.

36. Hall, J. G., "The Design and Performance of a 9-Inch Plate Mach-Zehnder Interferometer", UTIAS Report No. 27, 1954.

37. Jones, D. M., Martin, P. E. and Thornhill, C. K., "A Note on the Pseudo-Stationary Flow Behind a Strong Shock Diffracted or Reflected at a corner " Proc. Roy. Soc. sec. A, Vol. 209, p. 238, 1951.

38. Li, J. C. and Glass, I. I., " Collision of Mach Reflection with a 90° Ramp in Air and CO_2", UTIAS Report No. 290, see also 1985, Int. Symp. on Shock Waves and Shock Tubes, pp. 105-112, 1985.

39. Waldron, H. F., "An Experimental Study of a Spiral Vortex Formed by Shock Wave Diffraction", UTIAS Tech. Note No. 2. 1954.

40. Emrich, R. J. and Reichenbach, H., "Photographic Study of Early Stages of Vortex Formation Behind an Edge", Proc. of 7th Int. Symp. on Shock Tubes and Waves, pp. 740-747, 1970.

41. Delery, J. and Marvin, J. G., "Shock Wave Boundary Layer Interactions", AGARD-AG-280, 1986.

42. Urbanowicz, J. T. and Glass, I. I., "Pseudo-stationary Oblique Shock Wave Reflections in Low Gamma Gases Isobutane and Sulphur Hexafluovide" UTIAS Tech. Note No. 267, 1987.

43. Liepmann, H. W. and Roshko, A., "Elements of Gasdynamics", Wiley, London, 1957.

INITIAL CONDITIONS AND EVALUATED PROPERTIES FOR EXPERIMENTS

Table 1: RR Case

Expt. No.	M_s	M_1'	t μs	p_0 KPa	T_0 °K	ρ_0 $10^{-5}g/cm^3$	$\Delta\rho/\rho_0$	P_{10}	T_{10}	ρ_{10}	$P_{20}=P_{30}$	T_{20}	ρ_{20}	T_{30}	ρ_{30}	Fig. No.
38	1.35	0.46	26	80.65	297.7	94.50	0.032	1.96	1.23	1.60	3.74	1.49	2.52			7(a)
40	1.35	0.46	58	80.51	297.7	94.33	0.032	1.96	1.23	1.60	3.74	1.49	2.52			(b)
39	1.35	0.46	68	80.51	297.7	94.33	0.032	1.96	1.23	1.60						(c)
41	1.36	0.47	110	80.25	298.2	93.87	0.032	1.99	1.24	1.63						(d)
42	1.36	0.47	138	80.51	298.5	94.08	0.032	1.99	1.24	1.63						(e)

Table 2: SMR Case

Expt. No.	M_s	M_1'	t μs	p_0 KPa	T_0 °K	ρ_0 $10^{-5}g/cm^3$	$\Delta\rho/\rho_0$	P_{10}	T_{10}	ρ_{10}	$P_{20}=P_{30}$	T_{20}	ρ_{20}	T_{30}	ρ_{30}	Fig. No.
48	1.59	0.68	18	32.66	298.5	38.16	0.079	2.80	1.39	2.01	6.17	1.77	3.49	1.98	3.11	8(a)
45	1.60	0.69	52	32.66	298.4	38.17	0.079	2.84	1.40	2.03	6.26	1.78	3.52	2.00	3.13	(b)
50	1.59	0.68	77	32.53	298.7	37.98	0.079	2.80	1.39	2.01						(c)
51	1.59	0.68	85	32.66	298.2	38.20	0.079	2.80	1.39	2.01						(d)
52	1.60	0.69	111	32.66	298.2	38.20	0.079	2.84	1.40	2.03						(e)

Table 3: SMR ($M_1' = 1.00$) Case

Expt. No.	M_s	M_1'	t μs	p_0 KPa	T_0 °K	ρ_0 10^{-5}g/cm^3	$\Delta\rho/\rho_0$	P_{10}	T_{10}	ρ_{10}	$p_{20}=P_{30}$	T_{20}	ρ_{20}	T_{30}	ρ_{30}	Fig. No.
32	2.00	0.96	27	19.86	299.0	23.17	0.13	4.50	1.69	2.67	10.11	2.16	4.68	2.65	3.83	9(a)
31	2.01	0.97	37	19.86	298.4	23.21	0.13	4.55	1.70	2.68	10.23	2.18	4.71	2.68	3.84	(b)
30	2.01	0.97	59	19.86	298.4	23.22	0.13	4.55	1.70	2.68						(c)
29	2.03	0.98	76	19.86	298.0	23.48	0.13	4.66	1.72	2.71						(d)
28	2.02	0.97	97	19.86	298.0	23.25	0.13	4.60	1.71	2.69						(e)

Table 4: CMR Case

Expt. No.	M_s	M_1'	t μs	p_0 KPa	T_0 °K	ρ_0 10^{-5}g/cm^3	$\Delta\rho/\rho_0$	P_{10}	T_{10}	ρ_{10}	$p_{20}=P_{30}$	T_{20}	ρ_{20}	T_{30}	ρ_{30}	Fig. No.
64	2.44	1.16	20	10.66	297.6	12.49	0.24	6.81	2.10	3.25	15.50	2.70	5.76	3.57	4.21	10(a)
63	2.45	1.17	36	10.66	297.8	12.49	0.24	6.86	2.11	3.27	15.63	2.71	5.79	3.59	4.22	(b)
57	2.45	1.17	47	10.40	298.5	12.15	0.25	6.86	2.11	3.27						(c)
56	2.44	1.16	60	10.40	298.5	12.15	0.25	6.81	2.10	3.25						(d)
53	2.44	1.16	87	10.40	298.3	12.16	0.25	6.81	2.10	3.25						(e)

Table 5: DMR Case

Expt. No.	M_s	M_1'	t μs	p_0 KPa	T_0 °K	ρ_0 10^{-5}g/cm^3	$\Delta\rho/\rho_0$	P_{10}	T_{10}	ρ_{10}	$p_{20}=P_{30}$	T_{20}	ρ_{20}	T_{30}	ρ_{30}	Fig. No.
15	2.81	1.30	18	6.67	297.5	7.81	0.38	9.12	2.49	3.66	20.91	3.21	6.51	4.48	4.67	11(a)
25	2.84	1.32	31	6.67	297.5	7.81	0.38	9.30	2.52	3.69	21.33	3.25	6.56	4.56	4.70	(b)
18	2.81	1.30	39	6.67	296.9	7.83	0.38	9.12	2.49	3.66						(c)
21	2.81	1.30	101	6.67	296.6	7.84	0.38	9.12	2.49	3.66						(d)
22	2.85	1.33	96	6.67	296.6	7.84	0.38	9.36	2.54	3.70						(e)

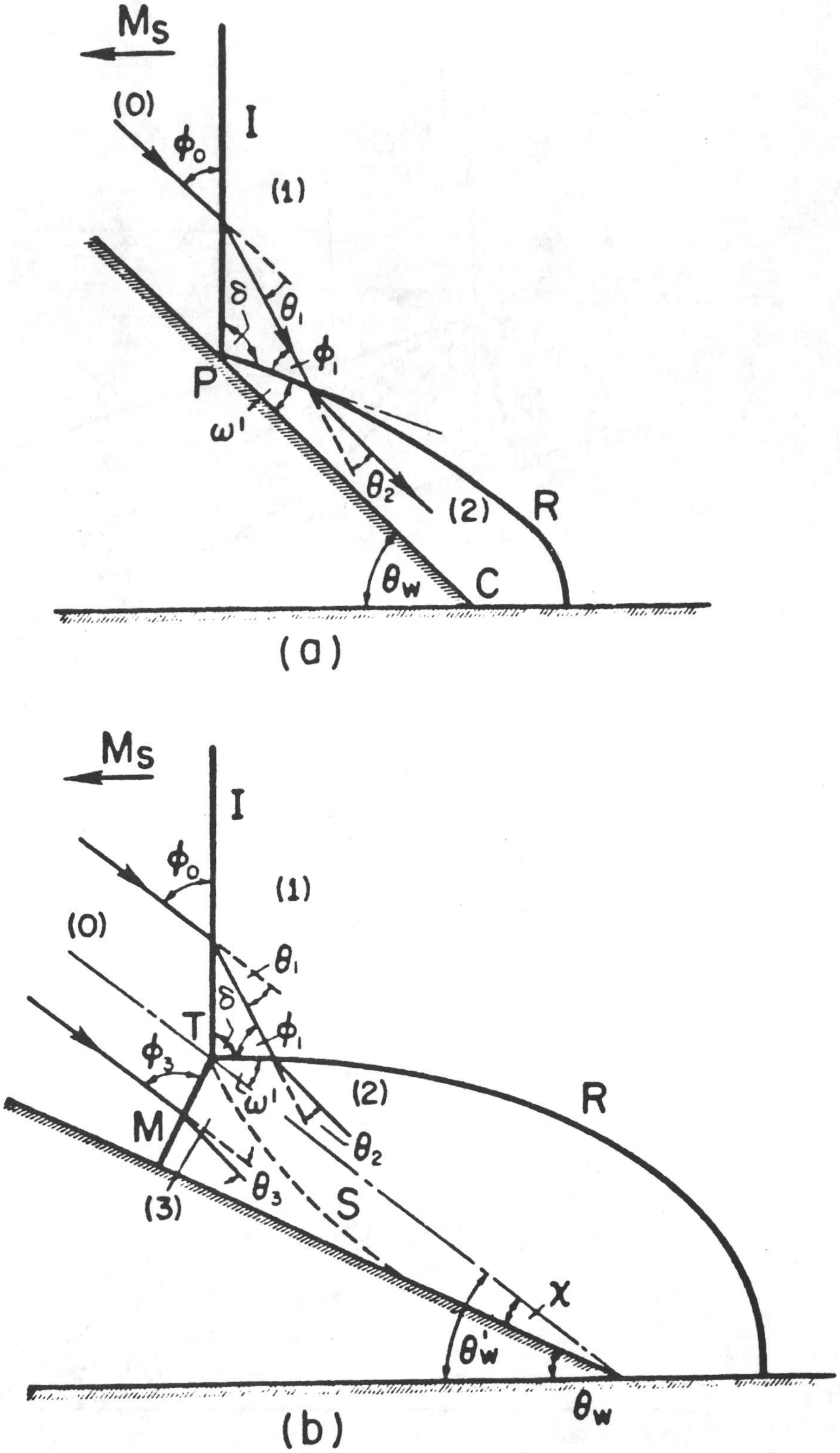

FIG. 1 TYPES OF OBLIQUE SHOCK-WAVE REFLECTIONS IN PSEUDOSTATIONARY FLOW. (a) RR, (b) SMR. I - INCIDENT SHOCK WAVE, R - REFLECTED SHOCK WAVE, M_S - INCIDENT SHOCK-WAVE MACH NUMBER, θ_W - WEDGE ANGLE, C - WEDGE CORNER, (0) - INITIAL STATE, (1), (2), (3) - SUBSEQUENT STATES, ϕ - WAVE ANGLE, θ - FLOW ANGLE, δ - ANGLE BETWEEN I AND R, ω' - ANGLE BETWEEN R AND WALL IN RR, AND BETWEEN R AND χ IN MR, χ - TRIPLE POINT TRAJECTORY ANGLE, T - TRIPLE POINT, M - MACH STEM, S - SLIPSTREAM, $\theta'_W = \theta_W + \chi$ - EFFECTIVE WEDGE ANGLE IN MR.

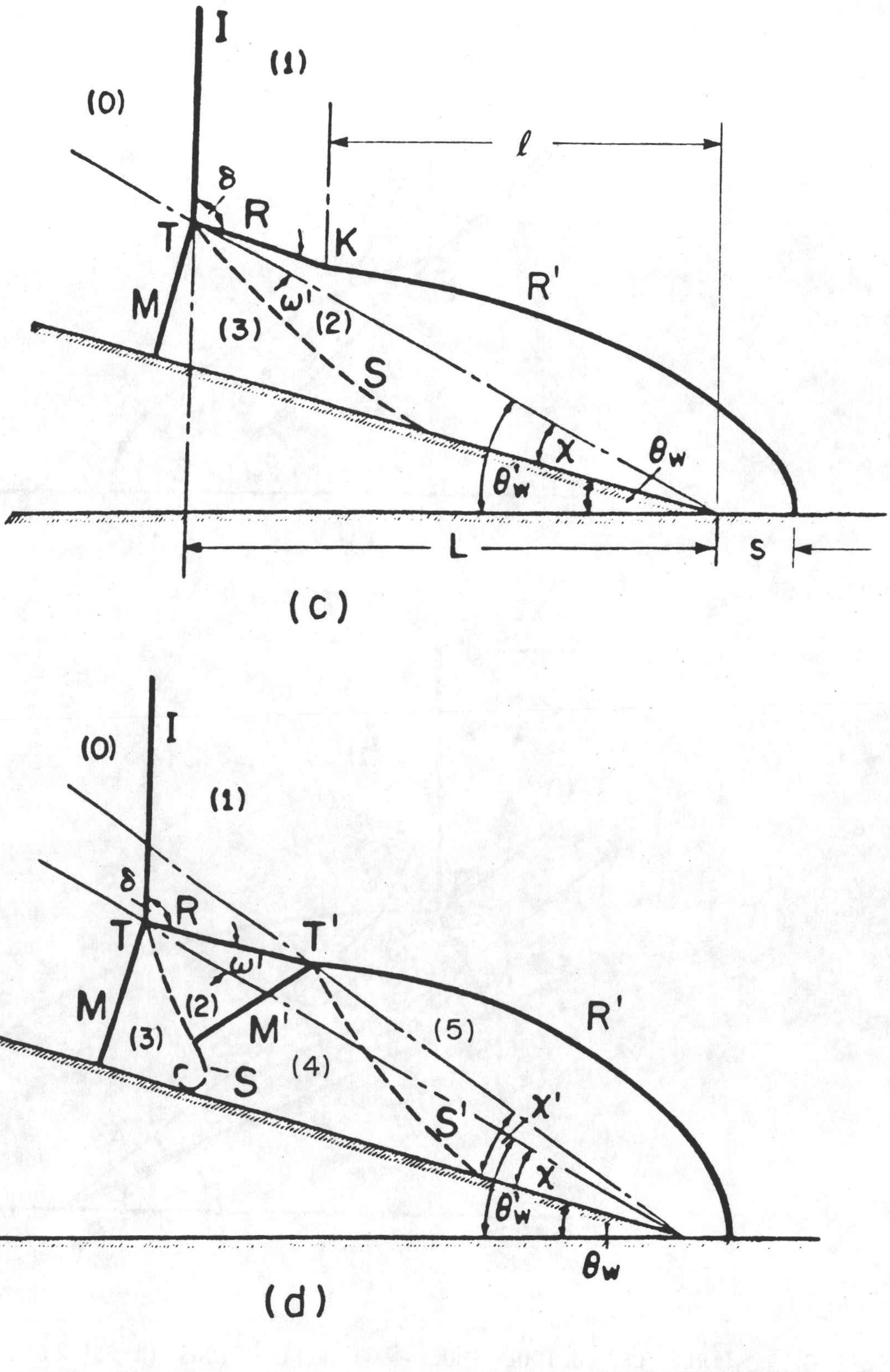

FIG. 1 TYPES OF OBLIQUE SHOCK-WAVE REFLECTIONS IN PSEUDOSTATIONARY FLOW. (c) CMR, (d) DMR. K - KINK, ℓ - DISTANCE BETWEEN K AND C, T' - SECOND TRIPLE POINT, M' - SECOND MACH SHOCK, R - STRAIGHT REFLECTED SHOCK WAVE, R' - CURVED REFLECTED SHOCK WAVE, S' - SECOND SLIPSTREAM, χ' - SECOND TRIPLE POINT TRAJECTORY ANGLE, s - STANDOFF DISTANCE, L - DISTANCE TRAVELLED BY I FROM CORNER C.

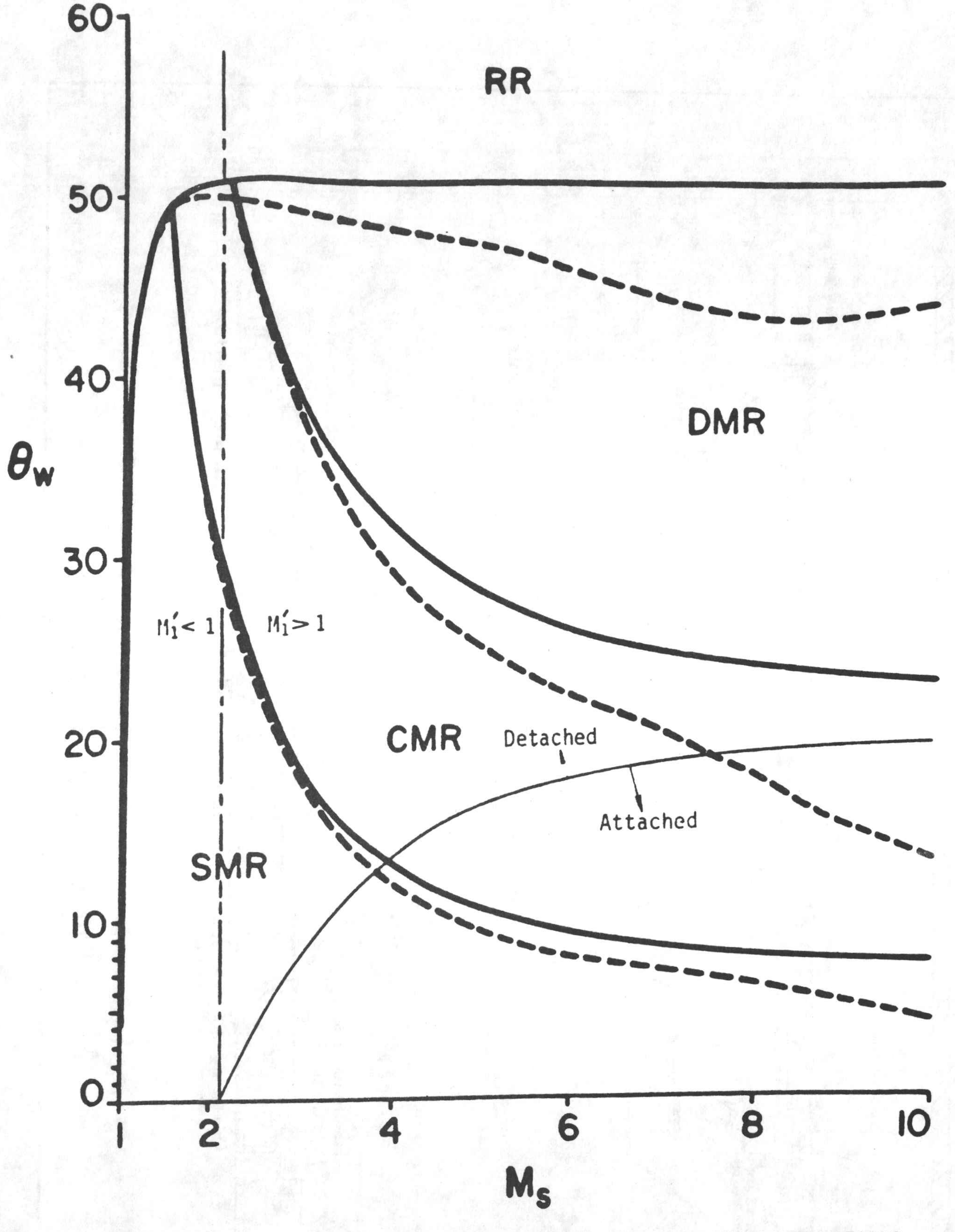

FIG. 2 REGIONS OF VARIOUS TYPES OF OBLIQUE SHOCK WAVE REFLECTIONS. SOLID LINES ARE FOR PERFECT AIR. DASHED LINE ARE FOR IMPERFECT AIR AT P_o= 2.00 KPa AND T_o= 300 K°.

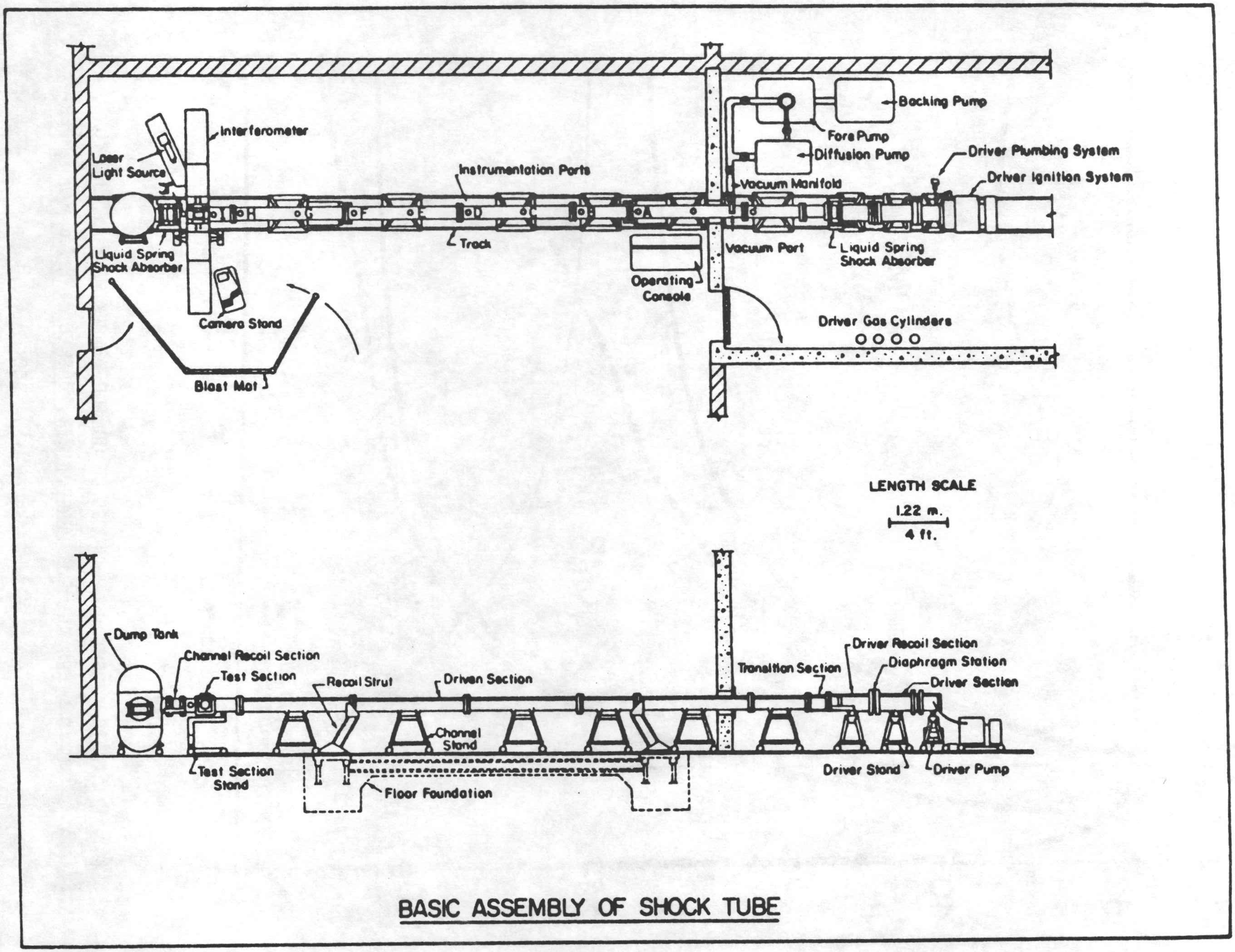

Fig. 3 GENERAL TOP AND SIDE VIEWS OF THE UTIAS 10cm x 18 cm HYPERVELOCITY SHOCK TUBE (REF. 35).

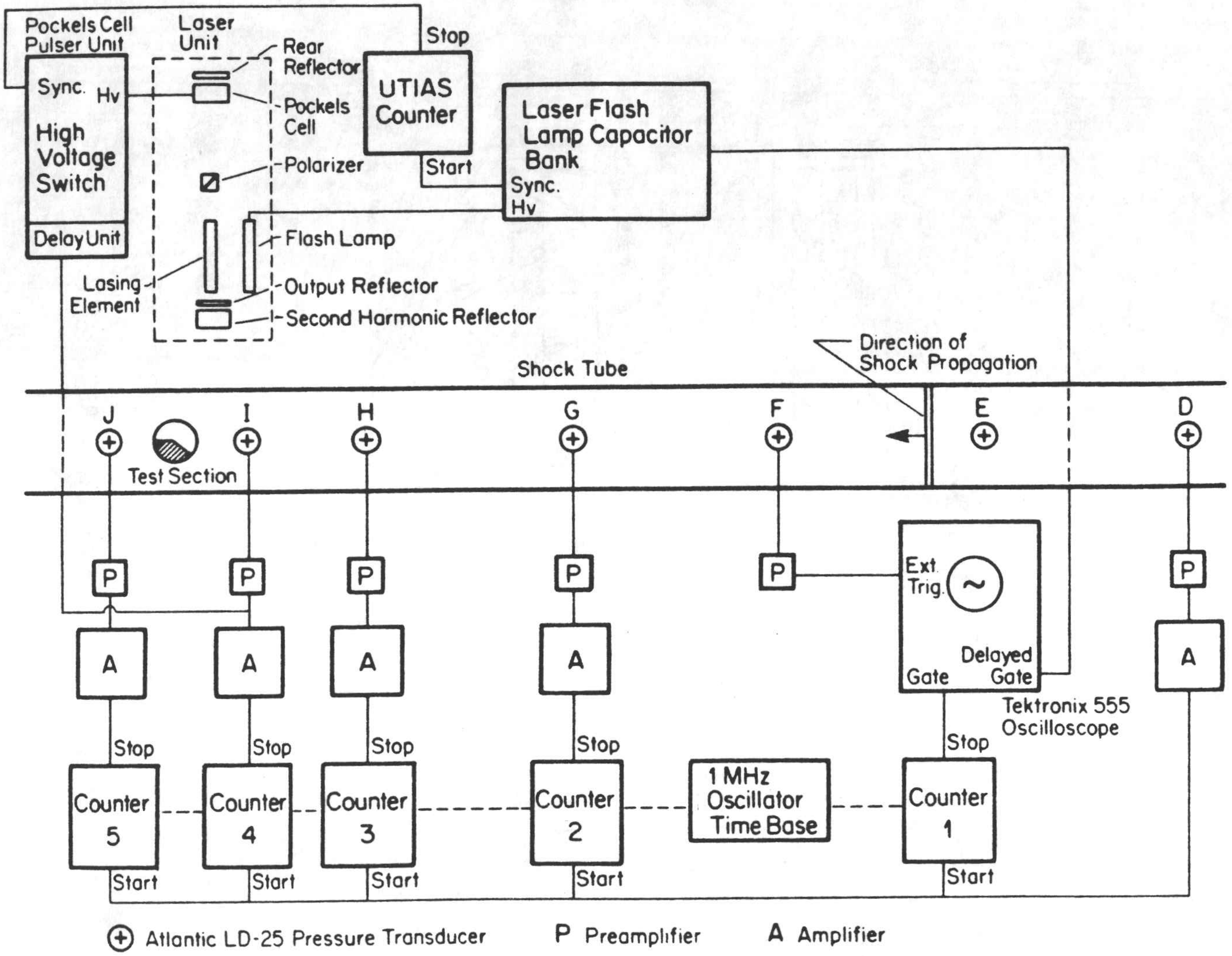

FIG. 4 BASIC INSTRUMENTATION SETUP FOR RECORDING THE SHOCK WAVE REFLECTION PROCESS. (REF. 35).

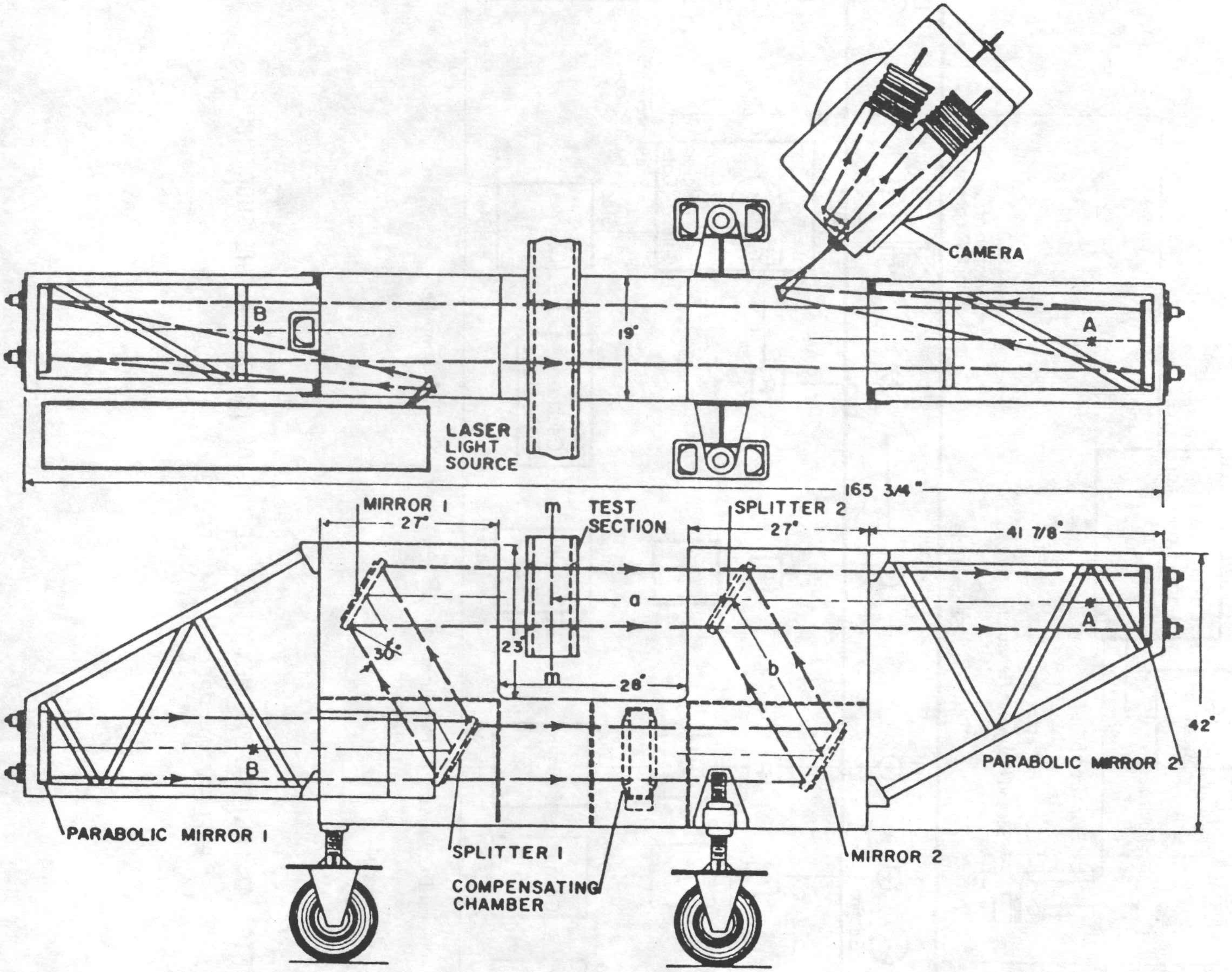

FIG. 5 GEOMETRY OF 9 INCH MACH-ZEHNDER INTERFEROMETER. (REF. 36)

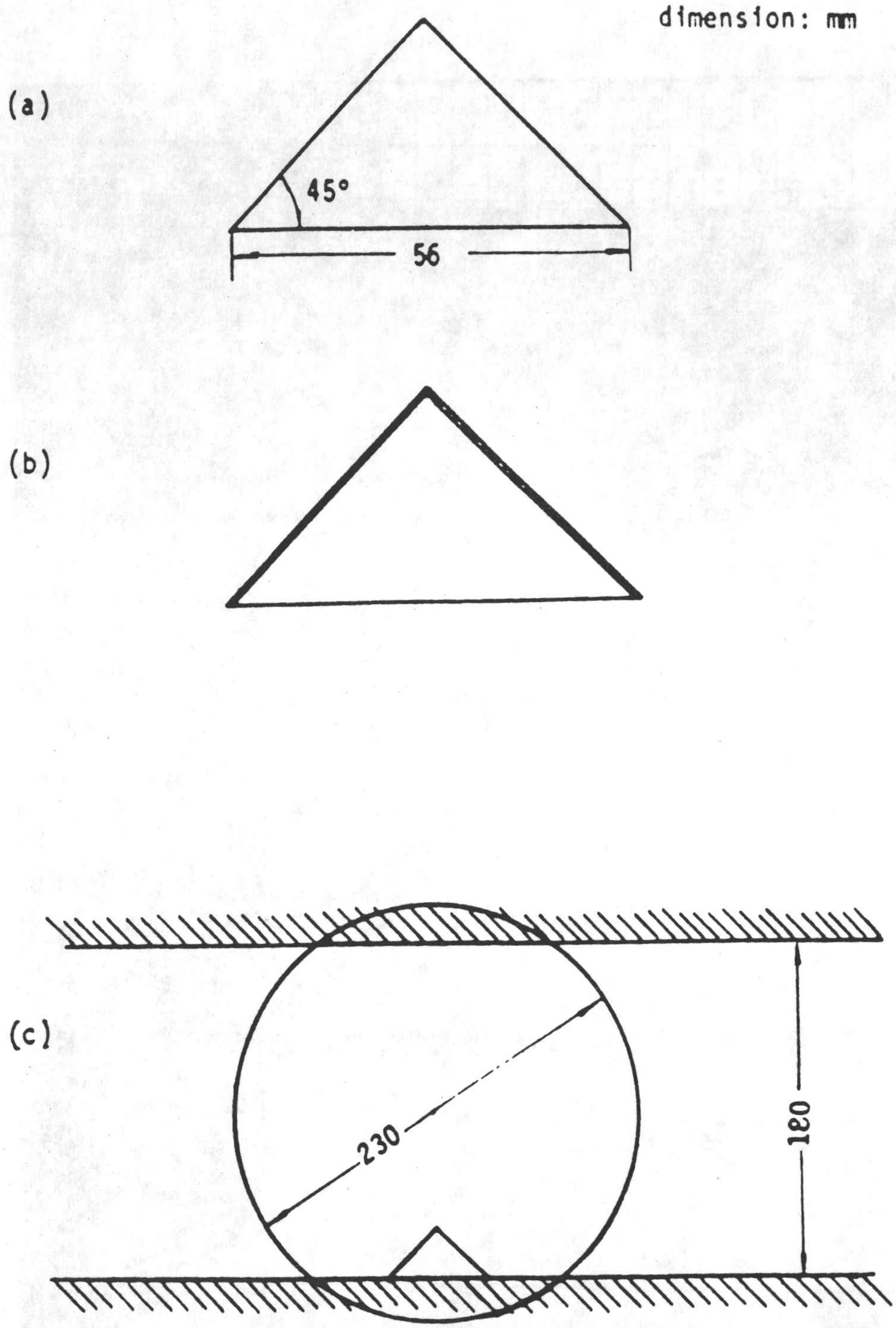

FIG. 6 SKETCH OF MODELS AND THEIR POSITIONS IN THE UTIAS 10cm x 18 cm HYPERVELOCITY SHOCK TUBE. (a) MODEL OF THE HALF-DIAMOND CYLINDER (b) MODEL WITH ROUGHNESS MATERIALS. (c) MODEL POSITION IN SHOCK TUBE.

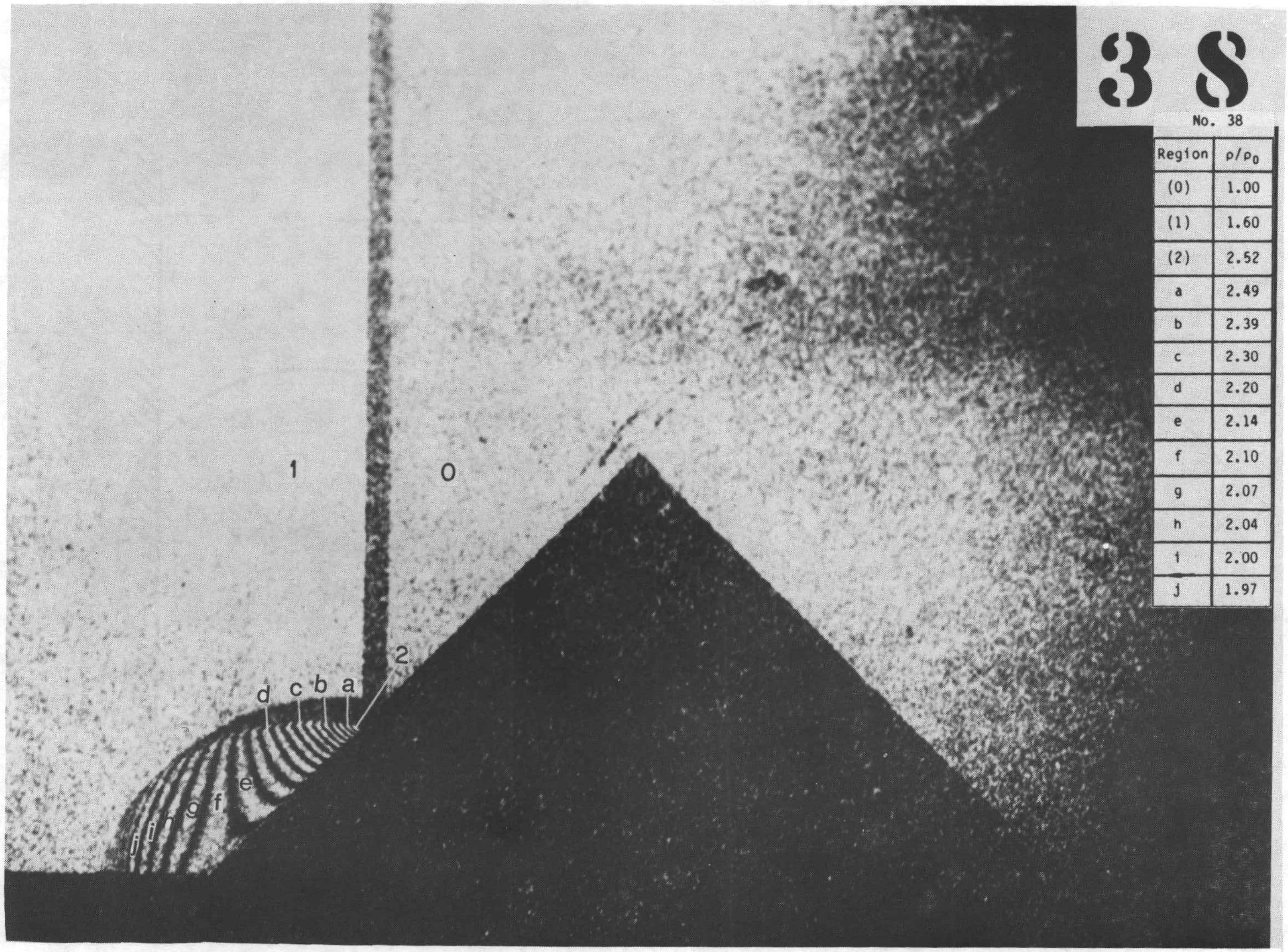

Region	ρ/ρ_0
(0)	1.00
(1)	1.60
(2)	2.52
a	2.49
b	2.39
c	2.30
d	2.20
e	2.14
f	2.10
g	2.07
h	2.04
i	2.00
j	1.97

Fig. 7 INTERFEROGRAMS OF DIFFRACTION OF PLANAR SHOCK WAVE OVER A HALF - DIAMOND CYLINDER IN AIR FOR CASE OF REGULAR REFLECTION; M_S=1.35, M_1'=0.46, SUBSONIC FLOW.

(a) AN INTERFEROGRAM (No. 38) TAKEN AT 26 μs AFTER SHOCK WAVE HITS CORNER; M_S=1.35, M_1'=0.46; P_0=80.65KPa, ρ_0=94.50x10^{-2}kg/m^3, T_0=297.7°K

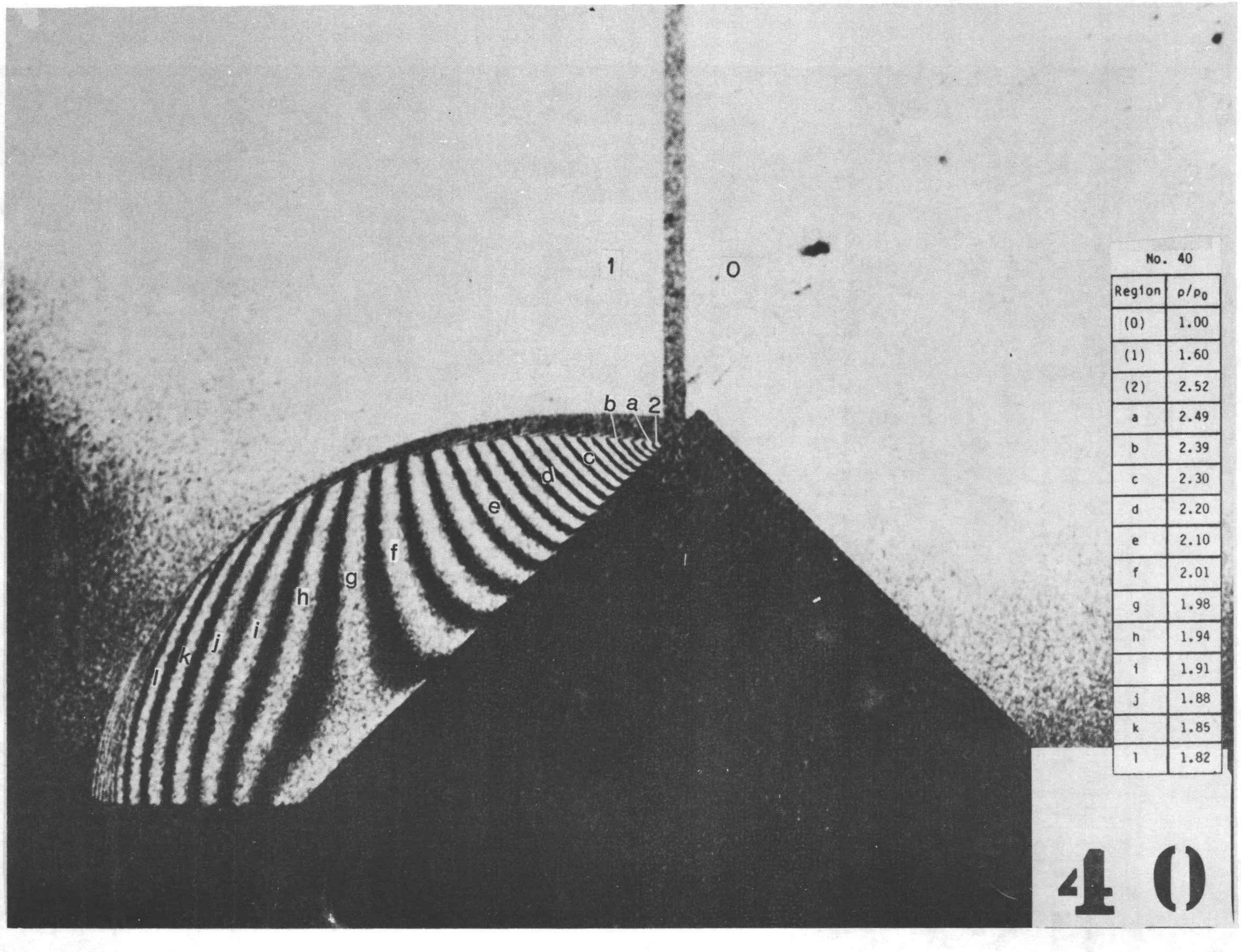

No. 40

Region	ρ/ρ_0
(0)	1.00
(1)	1.60
(2)	2.52
a	2.49
b	2.39
c	2.30
d	2.20
e	2.10
f	2.01
g	1.98
h	1.94
i	1.91
j	1.88
k	1.85
l	1.82

(b) AN INTERFEROGRAM (No. 40) TAKEN AT 58 μs AFTER SHOCK WAVE HITS CORNER; $M_S=1.35$, $M_1'=0.46$; $P_0=80.51$KPa, $\rho_0=94.33\times10^{-2}$kg/m^3, $T_0=297.7$°K

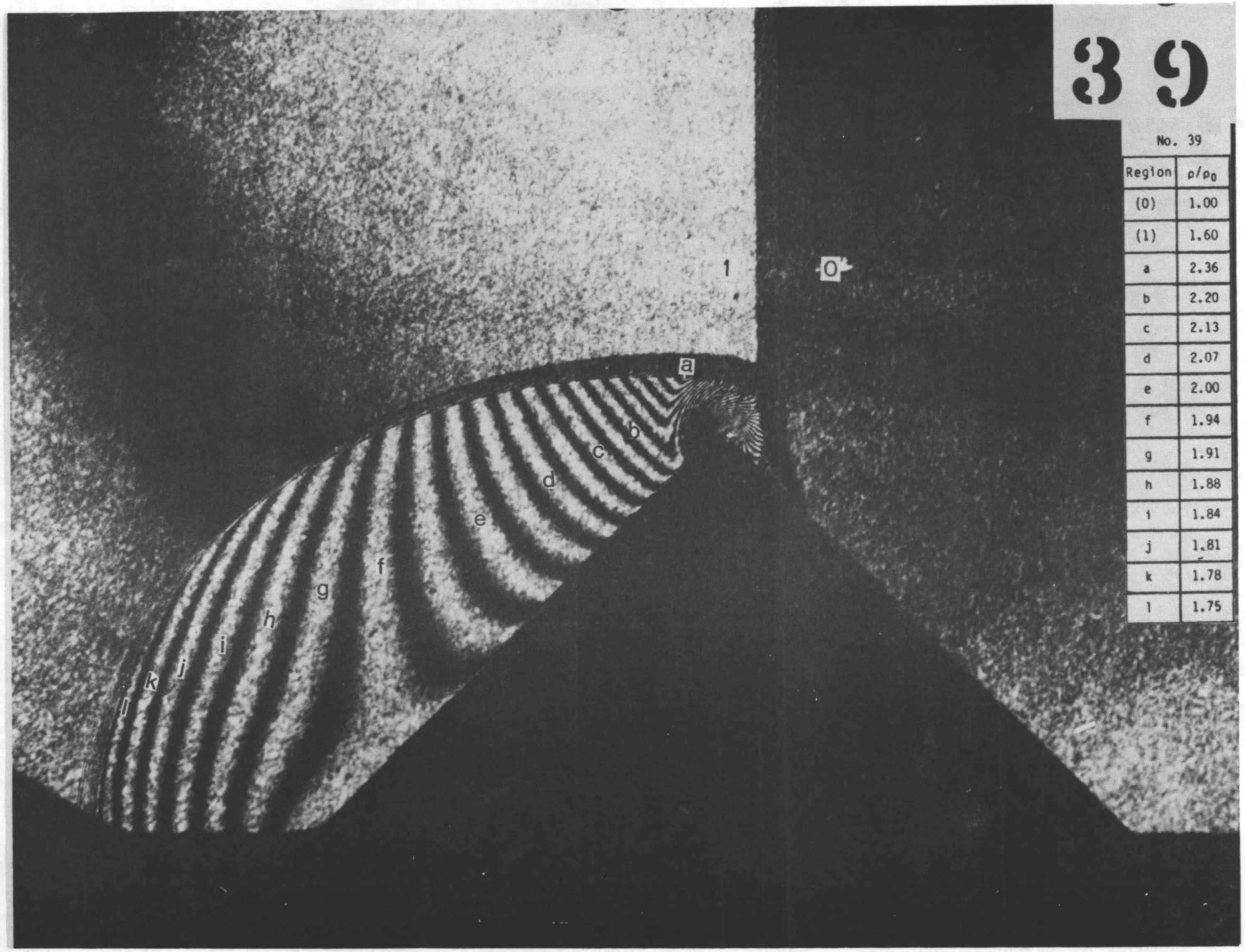

No. 39

Region	ρ/ρ_0
(0)	1.00
(1)	1.60
a	2.36
b	2.20
c	2.13
d	2.07
e	2.00
f	1.94
g	1.91
h	1.88
i	1.84
j	1.81
k	1.78
l	1.75

(c) AN INTERFEROGRAM (No. 39) TAKEN AT 68 μs AFTER SHOCK WAVE HITS CORNER; M_s=1.35, M_1'=0.46; P_0=80.51KPa, ρ_0=94.33x10^{-2}kg/m^3, T_0=297 °K

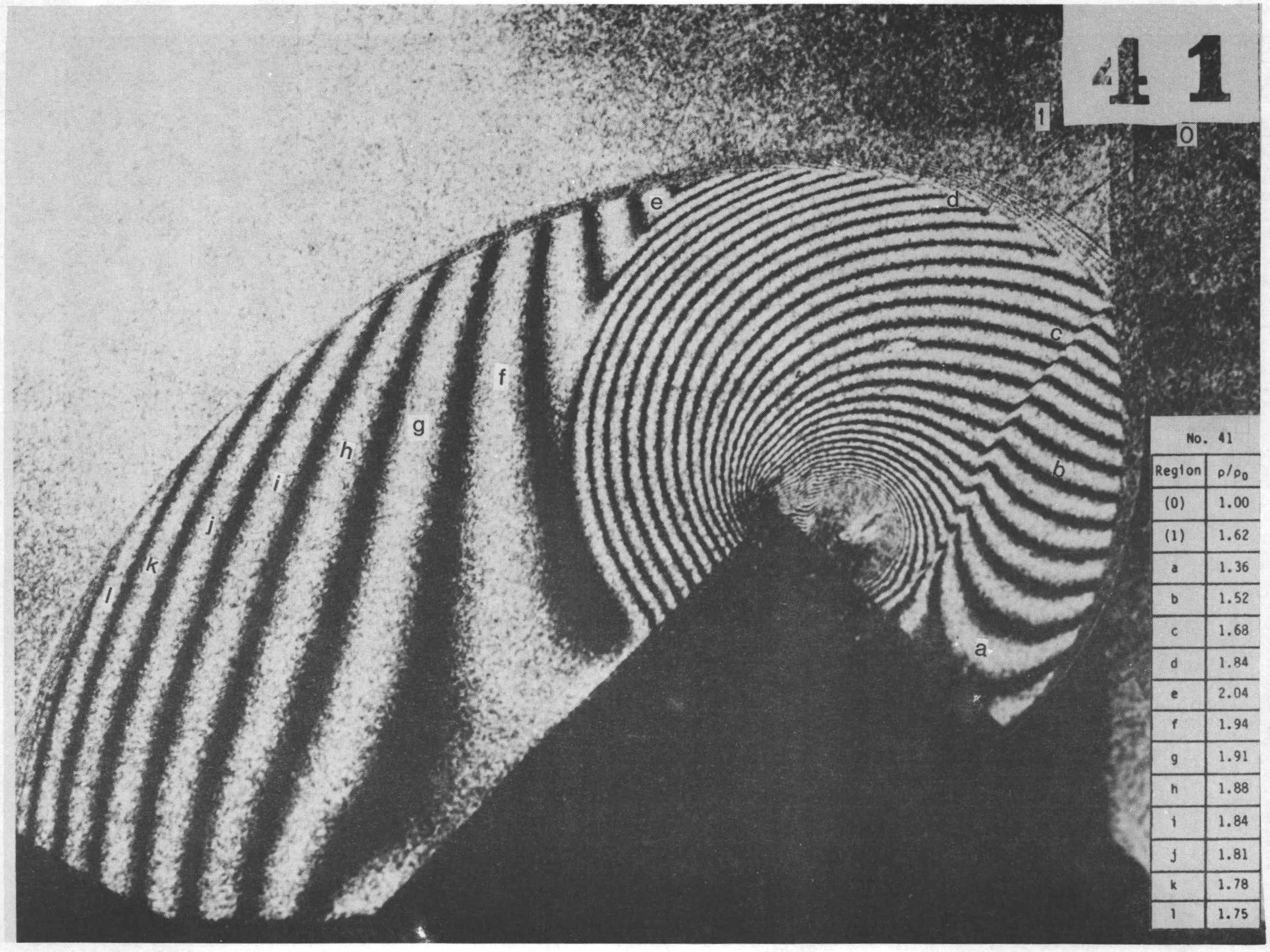

No. 41	
Region	ρ/ρ_0
(0)	1.00
(1)	1.62
a	1.36
b	1.52
c	1.68
d	1.84
e	2.04
f	1.94
g	1.91
h	1.88
i	1.84
j	1.81
k	1.78
l	1.75

(d) AN INTERFEROGRAM (No. 41) TAKEN AT 110 μs AFTER SHOCK WAVE HITS CORNER; M_S=1.36, M_1'=0.47; P_0=80.25KPa, ρ_0=93.87x10^{-2}kg/m^3, T_0=298.2°K

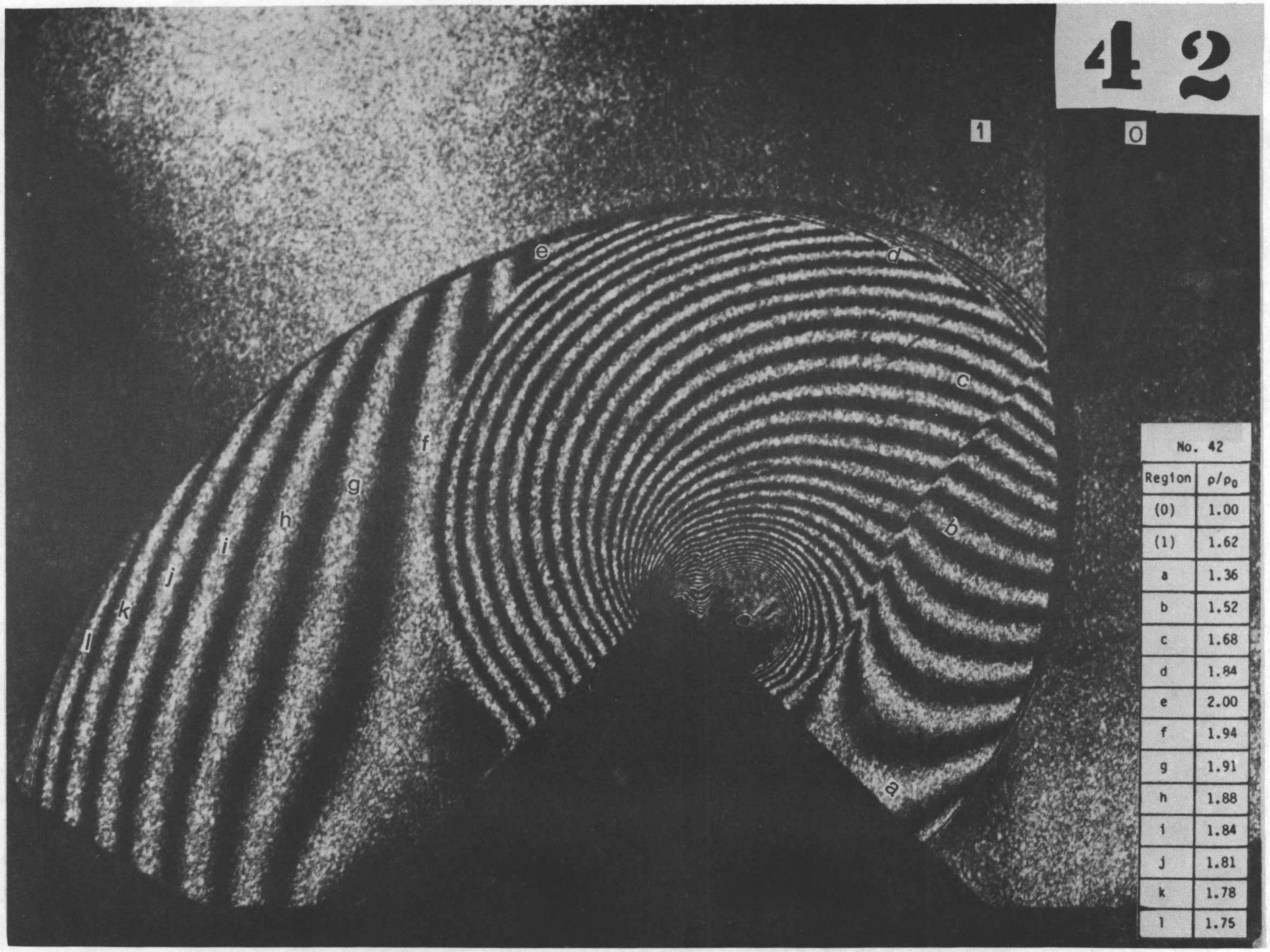

No. 42	
Region	ρ/ρ_0
(0)	1.00
(1)	1.62
a	1.36
b	1.52
c	1.68
d	1.84
e	2.00
f	1.94
g	1.91
h	1.88
i	1.84
j	1.81
k	1.78
l	1.75

(e) AN INTERFEROGRAM (No. 42) TAKEN AT 138 μs AFTER SHOCK WAVE HITS CORNER; $M_s=1.36$, $M_1'=0.47$; $P_0=80.51$KPa, $\rho_0=94.08\times10^{-2}$kg/m^3. $T_0=298.5$°K

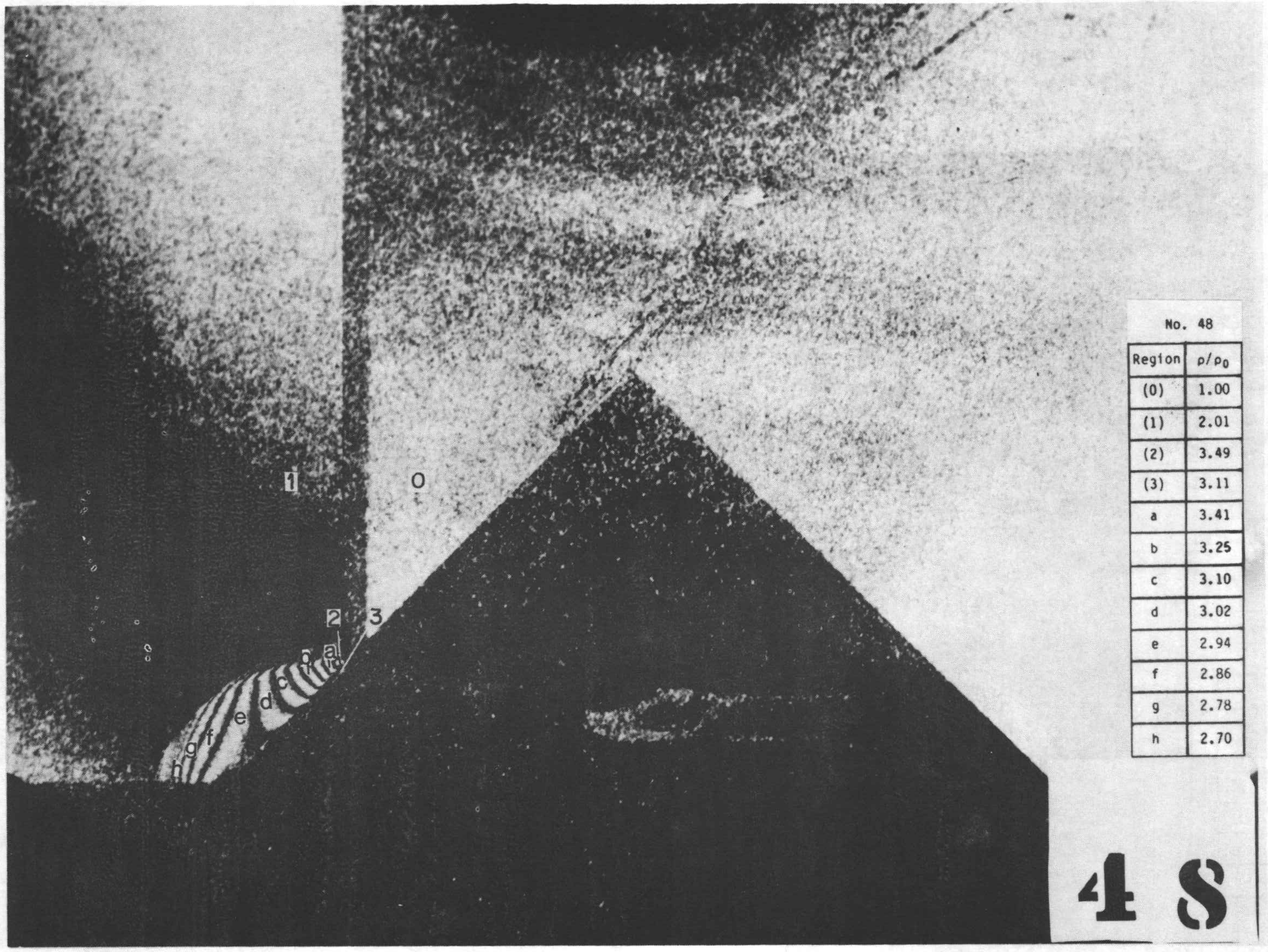

No. 48

Region	ρ/ρ_0
(0)	1.00
(1)	2.01
(2)	3.49
(3)	3.11
a	3.41
b	3.25
c	3.10
d	3.02
e	2.94
f	2.86
g	2.78
h	2.70

Fig. 8 INTERFEROGRAMS OF DIFFRACTION OF PLANAR SHOCK WAVE OVER A HALF - DIAMOND CYLINDER IN AIR FOR CASE OF SINGLE-MACH REFLECTION, M_s=1.60, M_1'=0.69, SUBSONIC FLOW.

(a) AN INTERFEROGRAM (No. 48) TAKEN AT 18 μs AFTER SHOCK WAVE HITS CORNER; M_s=1.59, M_1'=0.68; P_0=32.66KPa, ρ_0=38.16x10^{-2}kg/m^3, T_0=298.5°K

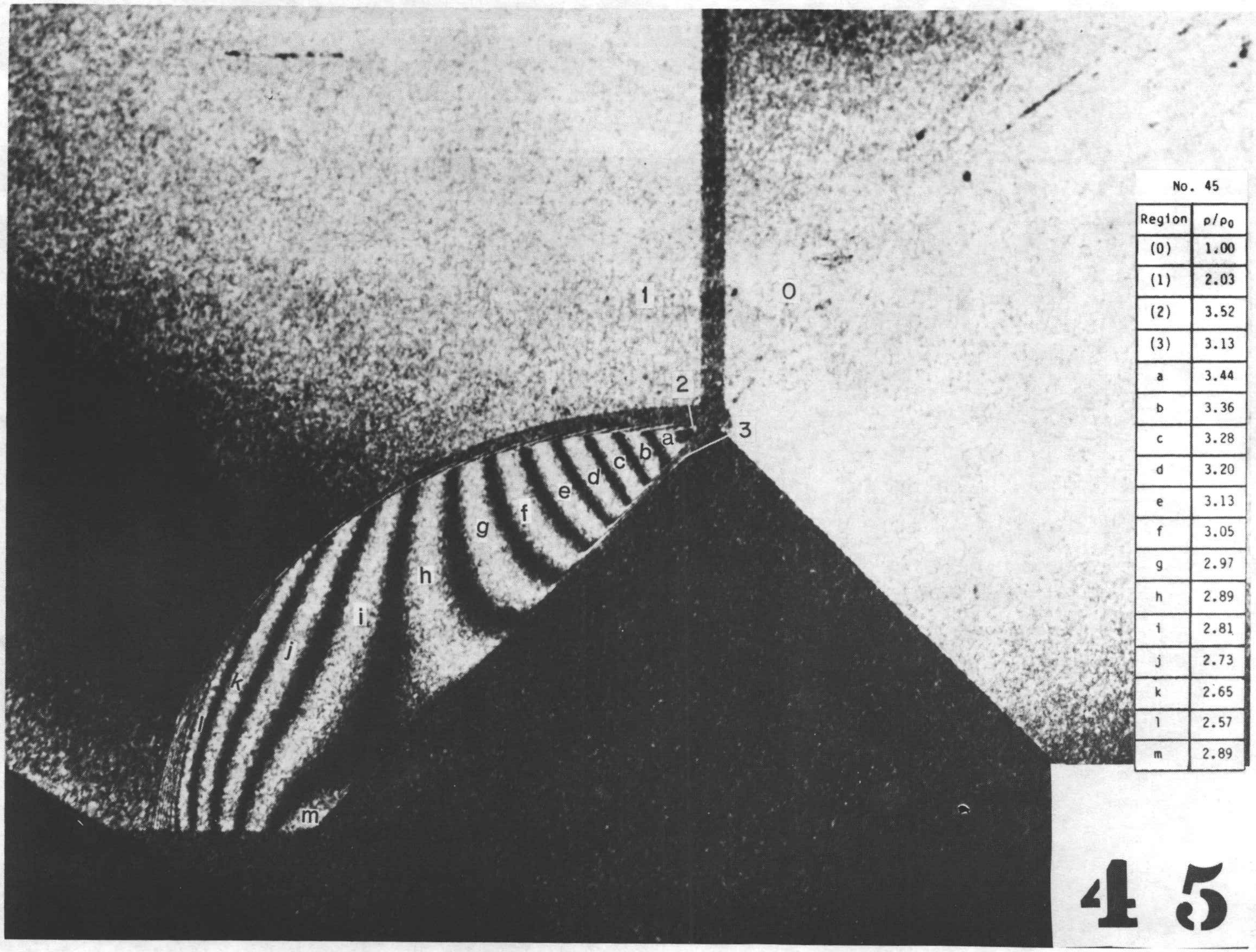

No. 45

Region	ρ/ρ_0
(0)	1.00
(1)	2.03
(2)	3.52
(3)	3.13
a	3.44
b	3.36
c	3.28
d	3.20
e	3.13
f	3.05
g	2.97
h	2.89
i	2.81
j	2.73
k	2.65
l	2.57
m	2.89

(b) AN INTERFEROGRAM (No. 45) TAKEN AT 52 μs AFTER SHOCK WAVE HITS CORNER; M_s=1.60, M_1'=0.69; P_0=32.66KPa, ρ_0=38.17x10^{-2}kg/m^3, T_0=298.4°K

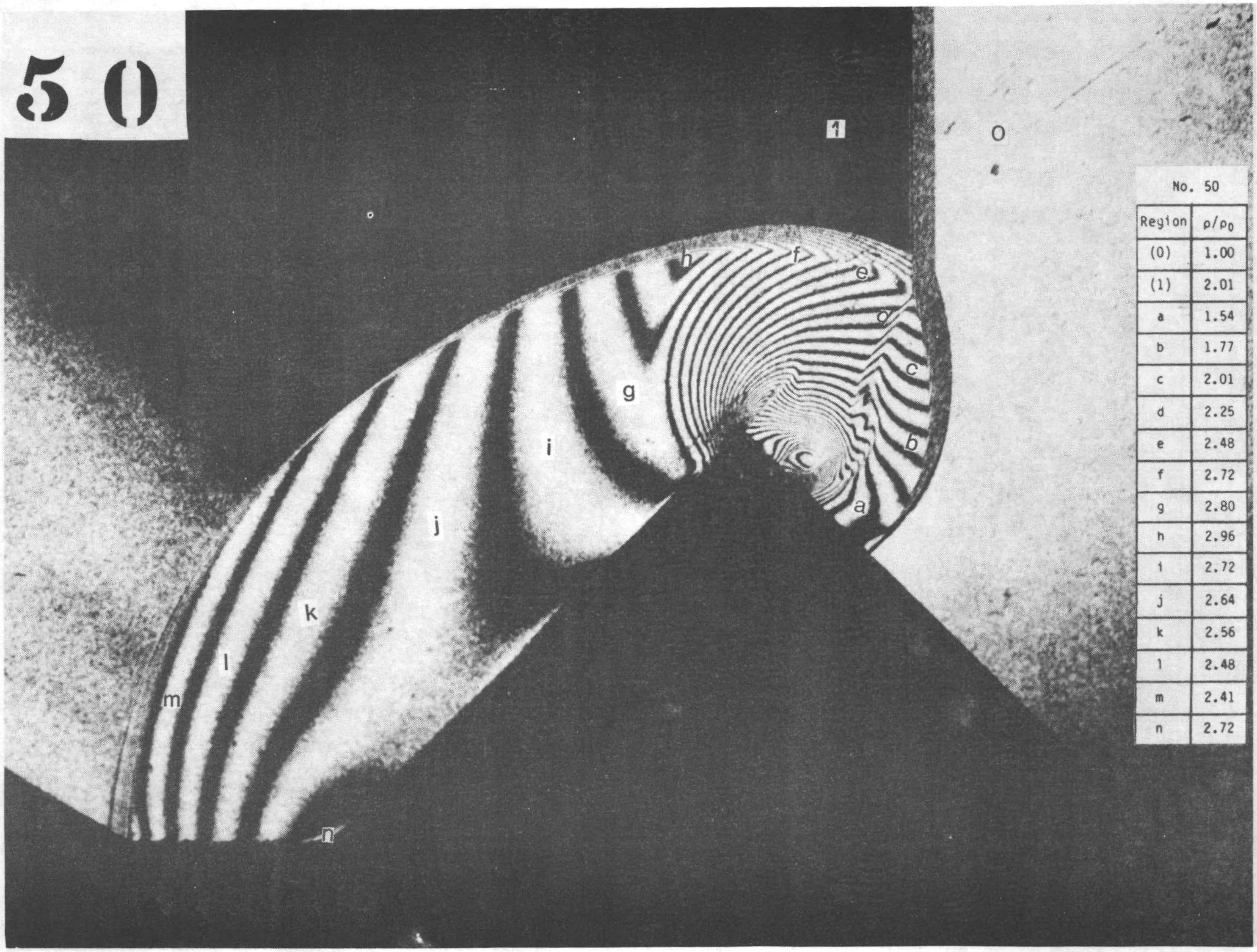

No. 50

Region	ρ/ρ_0
(0)	1.00
(1)	2.01
a	1.54
b	1.77
c	2.01
d	2.25
e	2.48
f	2.72
g	2.80
h	2.96
i	2.72
j	2.64
k	2.56
l	2.48
m	2.41
n	2.72

(c) AN INTERFEROGRAM (No. 50) TAKEN AT 77 μs AFTER SHOCK WAVE HITS CORNER; M_s=1.59, M_1'=0.68; P_0=32.52KPa, ρ_0=37.98x10^{-2}kg/m^3, T_0=298.7°K

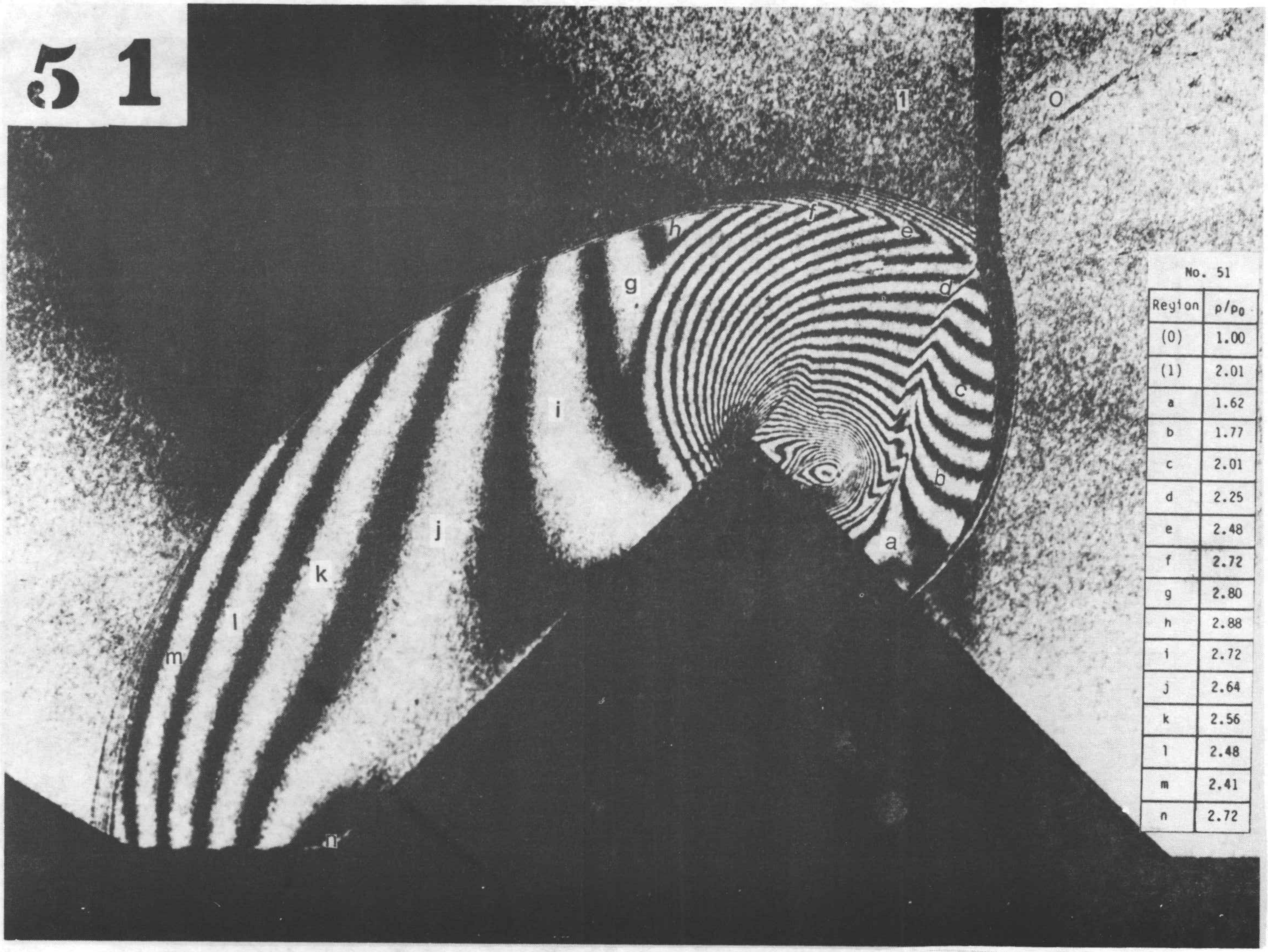

No. 51

Region	ρ/ρ_0
(0)	1.00
(1)	2.01
a	1.62
b	1.77
c	2.01
d	2.25
e	2.48
f	2.72
g	2.80
h	2.88
i	2.72
j	2.64
k	2.56
l	2.48
m	2.41
n	2.72

(d) AN INTERFEROGRAM (No. 51) TAKEN AT 85 μs AFTER SHOCK WAVE HITS CORNER; M_s=1.59, M_1'=0.68; P_0=32.66KPa, ρ_0=38.20x10^{-2}kg/m^3, T_0=298.2°K

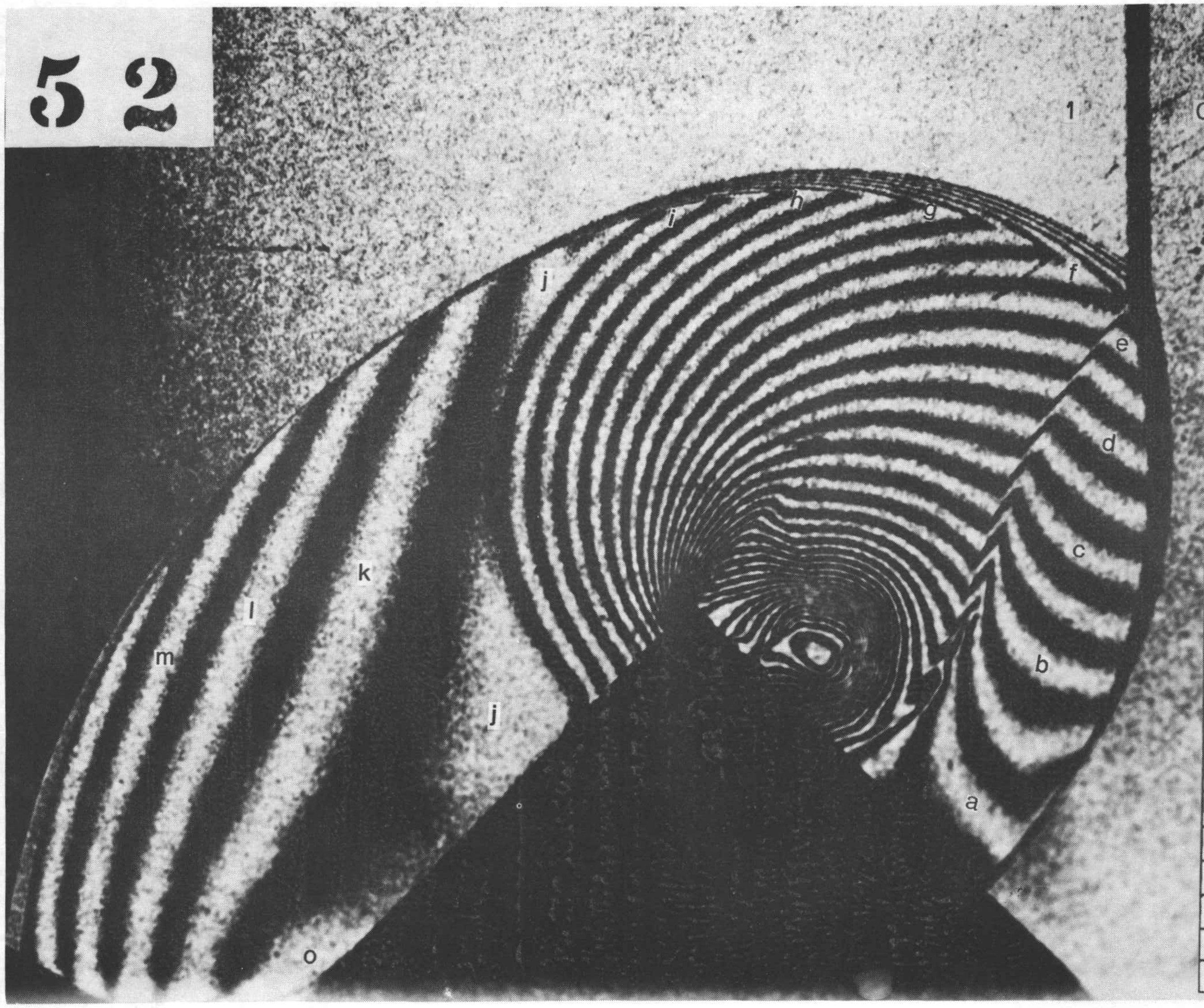

No. 52	
Region	ρ/ρ_0
(0)	1.00
(1)	2.03
a	1.56
b	1.71
c	1.87
d	2.03
e	2.19
f	2.35
g	2.50
h	2.66
i	2.82
j	2.74
k	2.66
l	2.58
m	2.50
n	2.43
o	2.74

(e) AN INTERFEROGRAM (No. 52) TAKEN AT 111 μs AFTER SHOCK WAVE HITS CORNER; M_s=1.60, M_1'=0.69; P_0=32.66KPa, ρ_0=38.20x10^{-2}kg/m^3, T_0=298.2°K

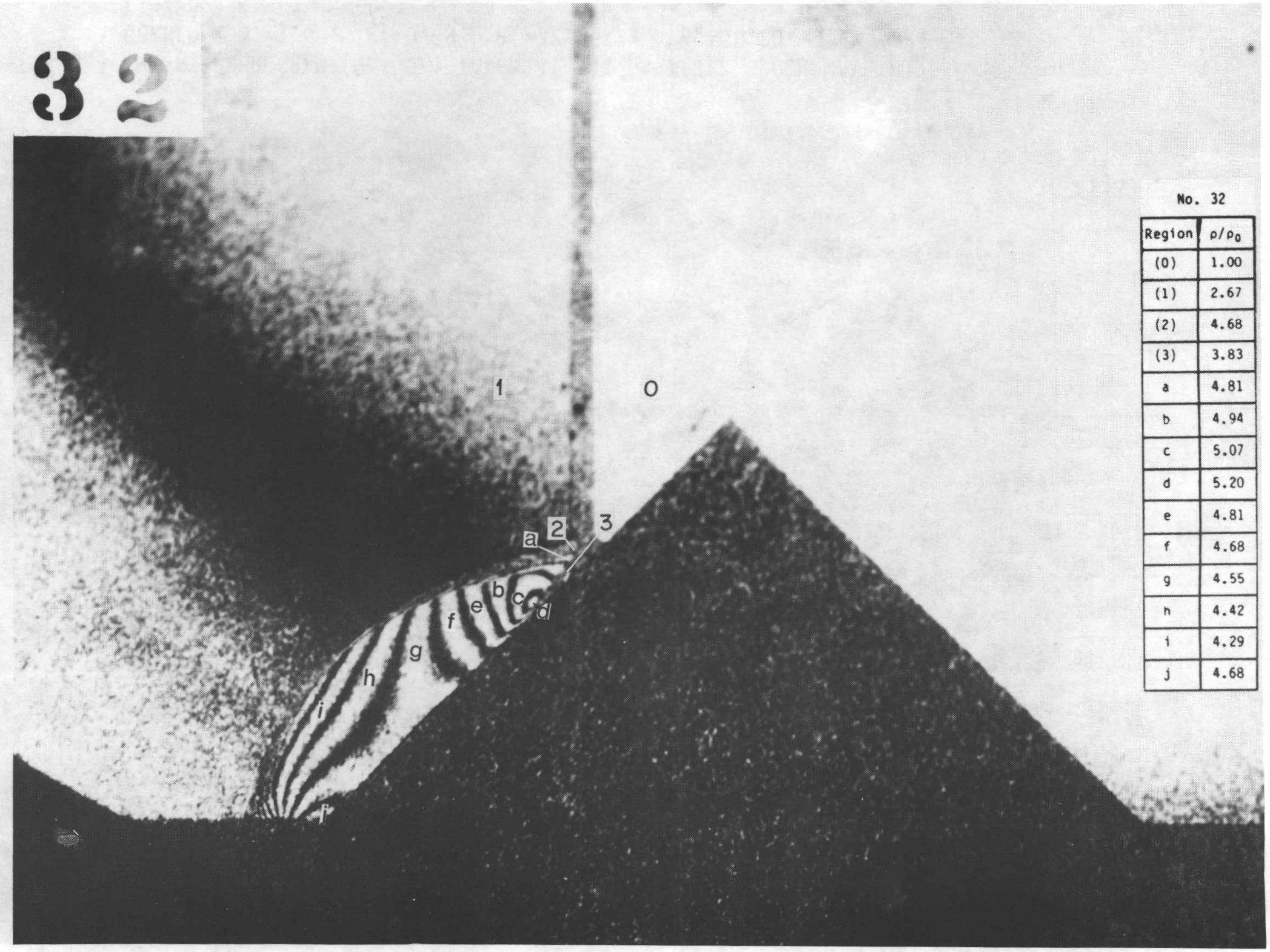

No. 32

Region	ρ/ρ_0
(0)	1.00
(1)	2.67
(2)	4.68
(3)	3.83
a	4.81
b	4.94
c	5.07
d	5.20
e	4.81
f	4.68
g	4.55
h	4.42
i	4.29
j	4.68

Fig. 9 INTERFEROGRAMS OF DIFFRACTION OF PLANAR SHOCK WAVE OVER A HALF - DIAMOND CYLINDER IN AIR FOR CASE OF SINGLE-MACH REFLECTION. $M_s=2.02$, $M_1'=0.97$, TRANSONIC FLOW.

(a) AN INTERFEROGRAM (No. 32) TAKEN AT 27 μs AFTER SHOCK WAVE HITS CORNER; $M_s=2.00$, $M_1'=0.96$; $P_0=19.86$KPa, $\rho_0=23.17\times10^{-2}$kg/m^3, $T_0=299.0$°K

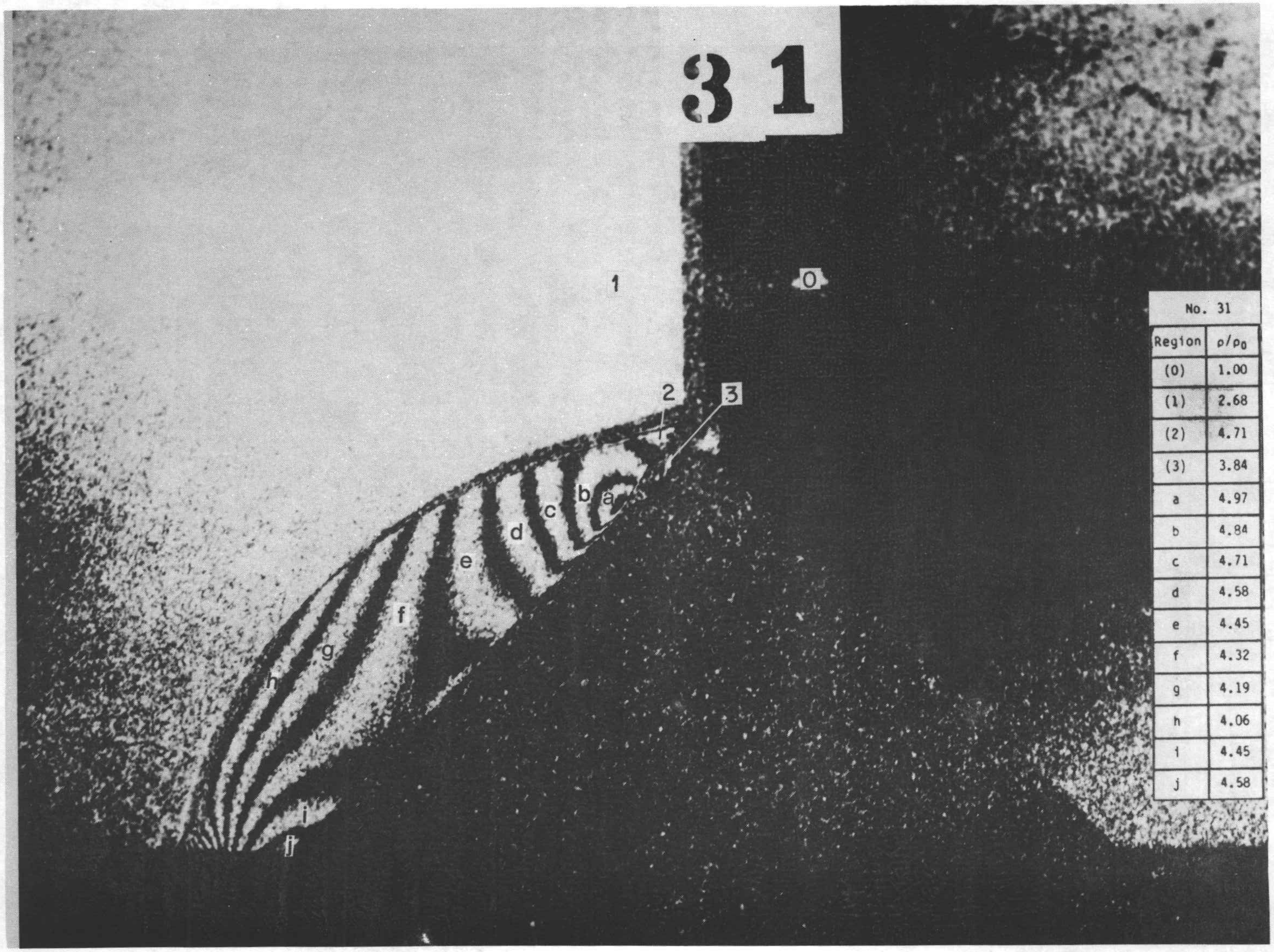

No. 31	
Region	ρ/ρ_0
(0)	1.00
(1)	2.68
(2)	4.71
(3)	3.84
a	4.97
b	4.84
c	4.71
d	4.58
e	4.45
f	4.32
g	4.19
h	4.06
i	4.45
j	4.58

(b) AN INTERFEROGRAM (No. 31) TAKEN AT 37 μs AFTER SHOCK WAVE HITS CORNER; M_s=2.01, M_1'=0.97; P_0=19.86KPa, ρ_0=23.21x10^{-2}kg/m^3, T_0=298.4°K

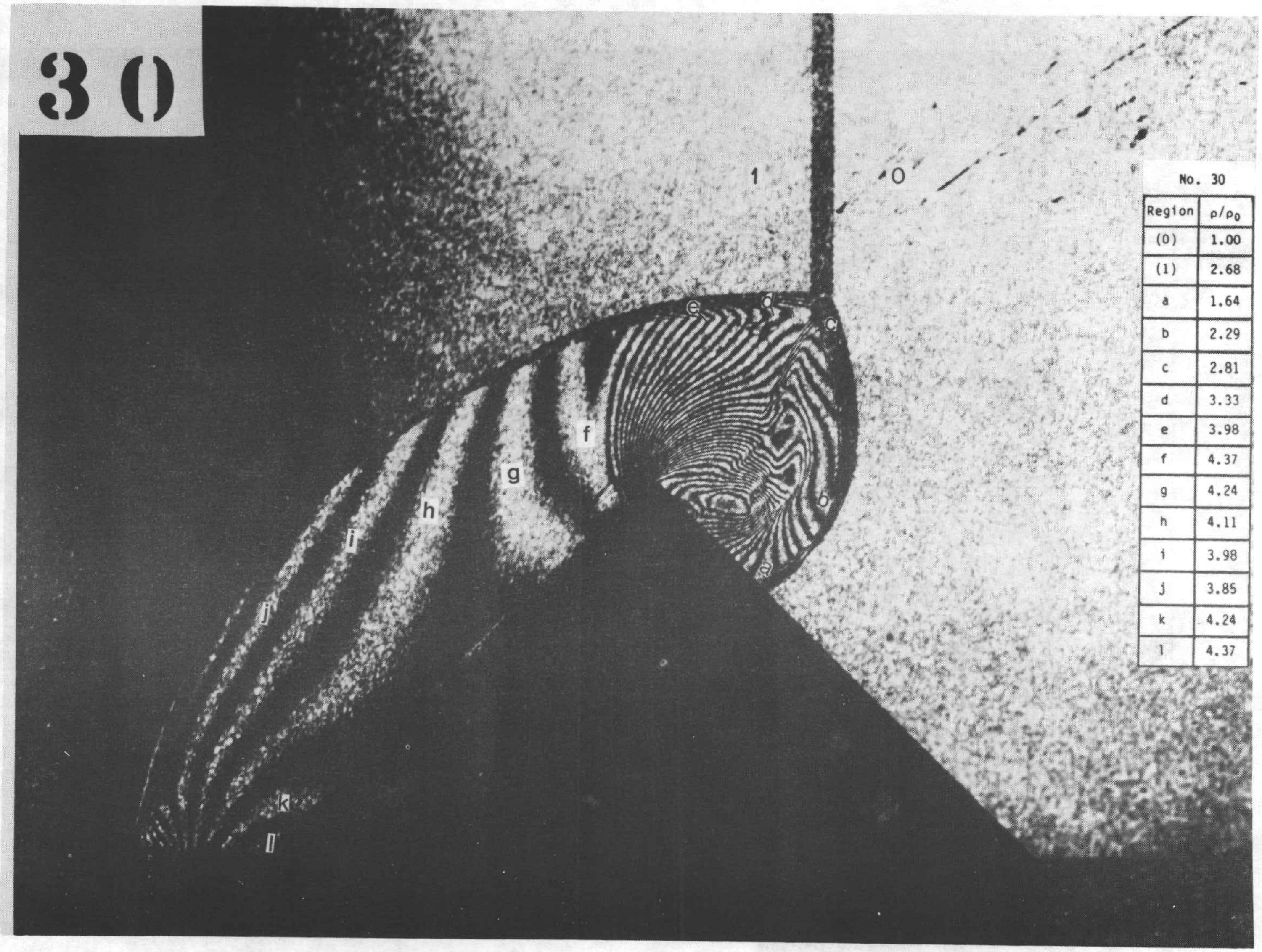

No. 30

Region	ρ/ρ_0
(0)	1.00
(1)	2.68
a	1.64
b	2.29
c	2.81
d	3.33
e	3.98
f	4.37
g	4.24
h	4.11
i	3.98
j	3.85
k	4.24
l	4.37

(c) AN INTERFEROGRAM (No. 30) TAKEN AT 59 μs AFTER SHOCK WAVE HITS CORNER; $M_S = 2.01$, $M_1' = 0.97$; $P_0 = 19.86$KPa, $\rho_0 = 23.22 \times 10^{-2}$kg/m^3, $T_0 = 298.4$°K

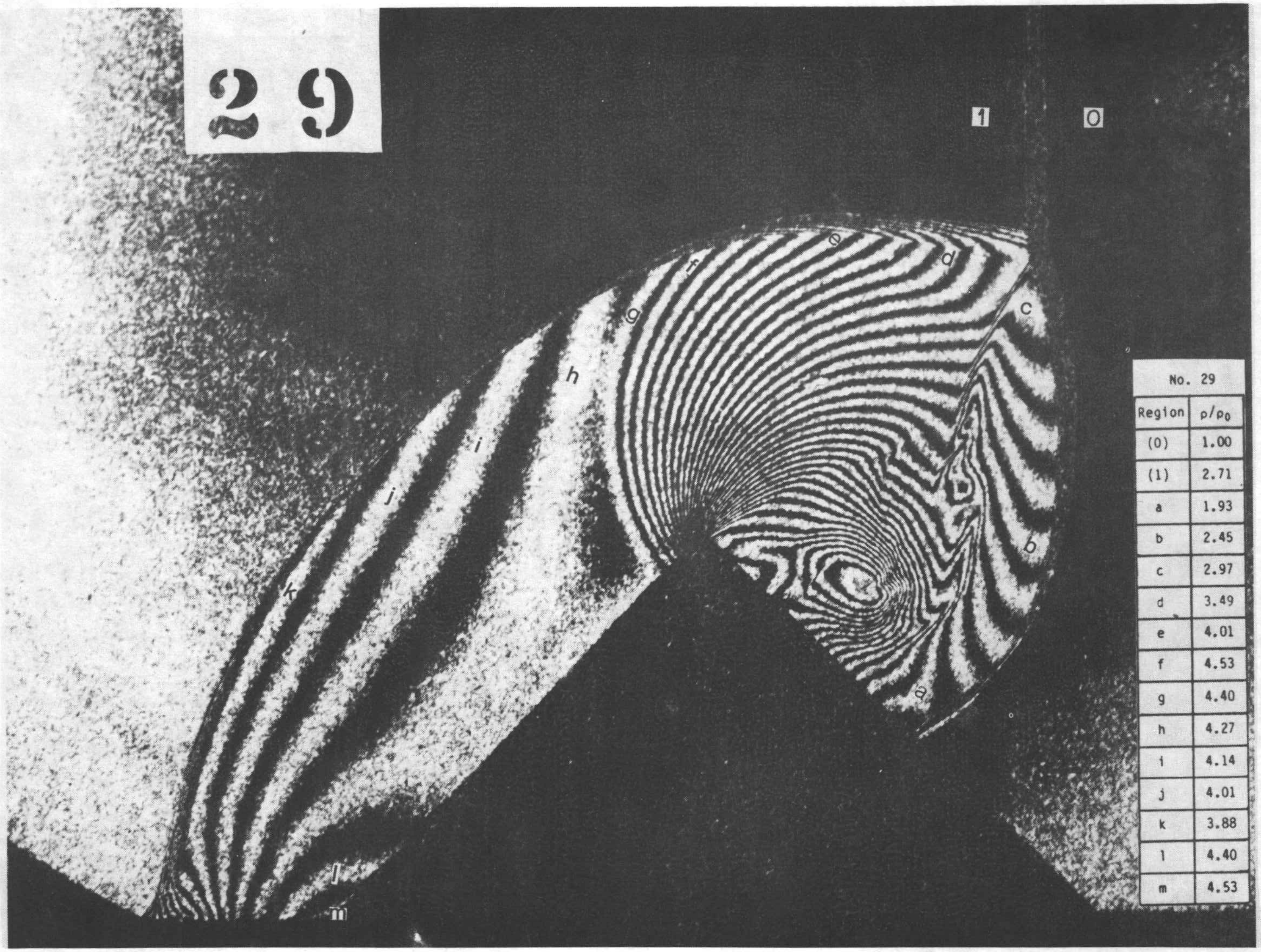

No. 29	
Region	ρ/ρ_0
(0)	1.00
(1)	2.71
a	1.93
b	2.45
c	2.97
d	3.49
e	4.01
f	4.53
g	4.40
h	4.27
i	4.14
j	4.01
k	3.88
l	4.40
m	4.53

(d) AN INTERFEROGRAM (No. 29) TAKEN AT 76 μs AFTER SHOCK WAVE HITS CORNER; M_S=2.03, M_1'=0.98; P_0=19.86KPa, ρ_0=23.48x10^{-2}kg/m^3, T_0=298.0°K

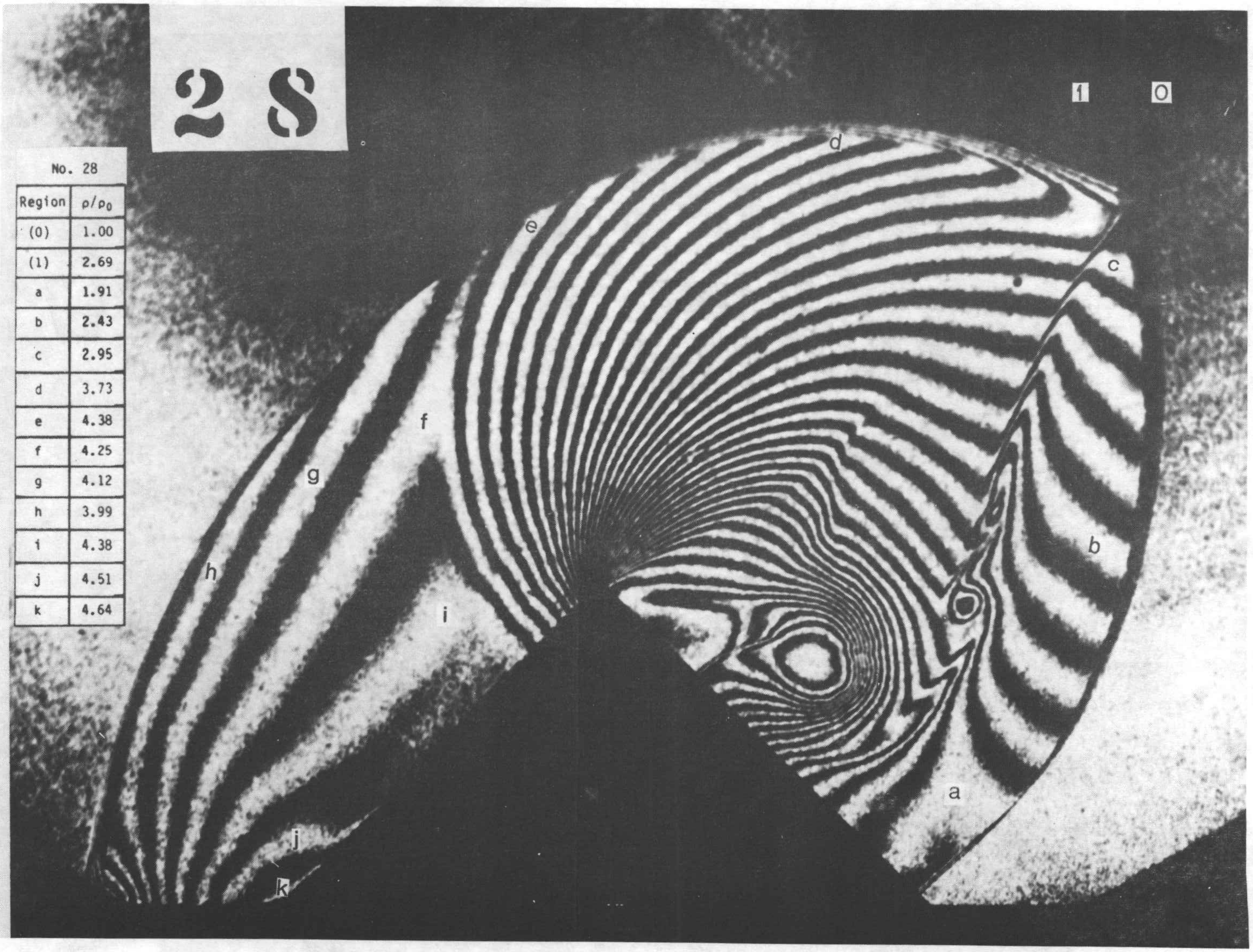

No. 28

Region	ρ/ρ_0
(0)	1.00
(1)	2.69
a	1.91
b	2.43
c	2.95
d	3.73
e	4.38
f	4.25
g	4.12
h	3.99
i	4.38
j	4.51
k	4.64

(e) AN INTERFEROGRAM (No. 28) TAKEN AT 97 μs AFTER SHOCK WAVE HITS CORNER; M_S=2.02, M_1'=0.97; P_0=19.86KPa, ρ_0=23.25x10^{-2}kg/m^3, T_0=298.0°K

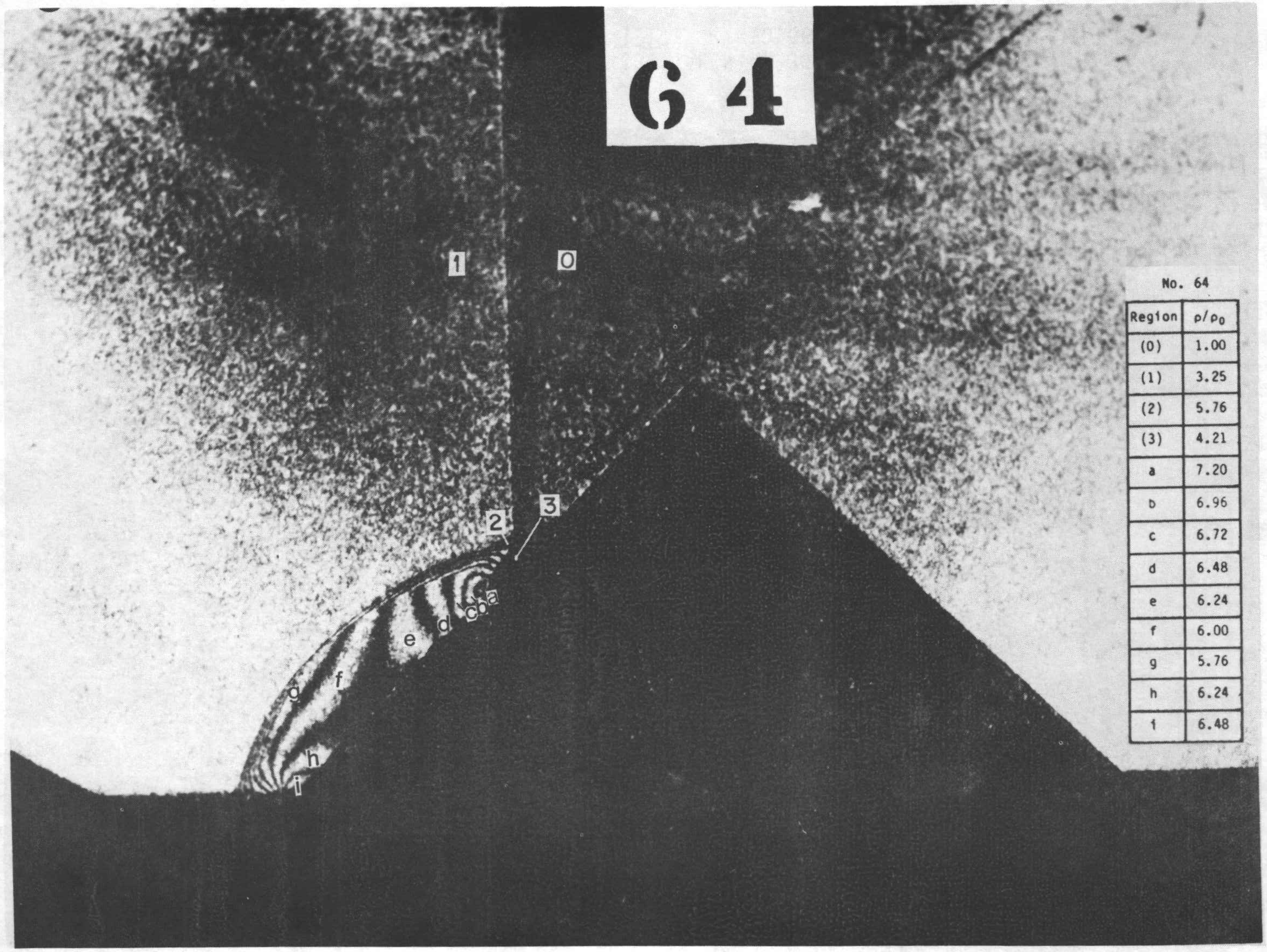

No. 64

Region	ρ/ρ_0
(0)	1.00
(1)	3.25
(2)	5.76
(3)	4.21
a	7.20
b	6.96
c	6.72
d	6.48
e	6.24
f	6.00
g	5.76
h	6.24
i	6.48

Fig. 10 INTERFEROGRAMS OF DIFRACTION OF PLANAR SHOCK WAVE OVER A HALF - DIAMOND CYLINDER IN AIR FOR CASE OF COMPLEX MACH REFLECTION. M =2.45, M'=1.17, SUPERSONIC FLOW.

(a) AN INTERFEROGRAM (No. 64) TAKEN AT 20 μs AFTER SHOCK WAVE HITS CORNER: M_s=2.44, M_1'=1.16; P_0=10.66KPa, ρ_0=12.49x10^{-2}kg/m^3, T_0=297.6°K

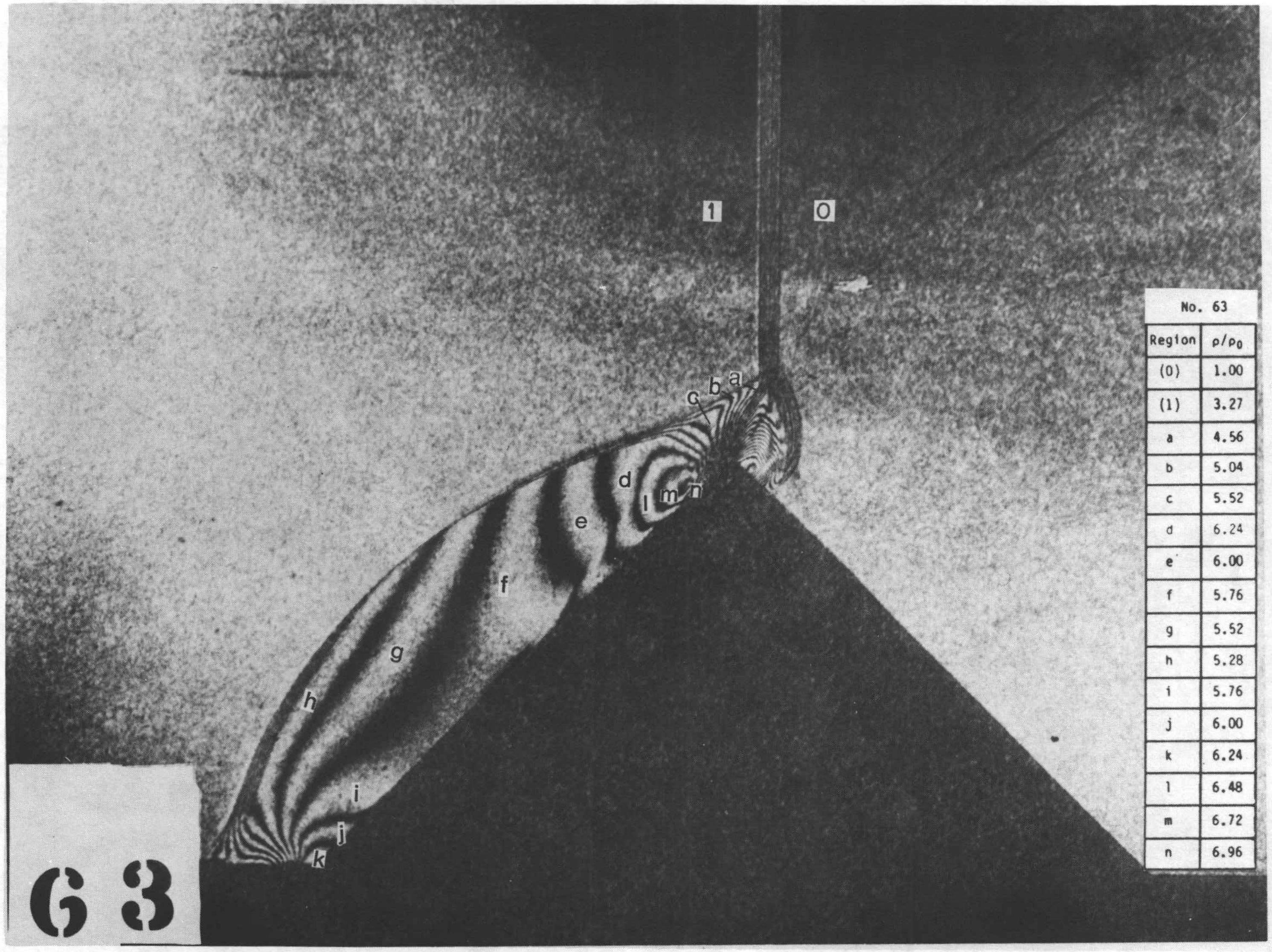

No. 63

Region	ρ/ρ_0
(0)	1.00
(1)	3.27
a	4.56
b	5.04
c	5.52
d	6.24
e	6.00
f	5.76
g	5.52
h	5.28
i	5.76
j	6.00
k	6.24
l	6.48
m	6.72
n	6.96

(b) AN INTERFEROGRAM (No. 63) TAKEN AT 36 μs AFTER SHOCK WAVE HITS CORNER; M_S=2.45, M_1'=1.17; P_0=10.66KPa, ρ_0=12.49x10^{-2}kg/m^3, T_0=297.8°K

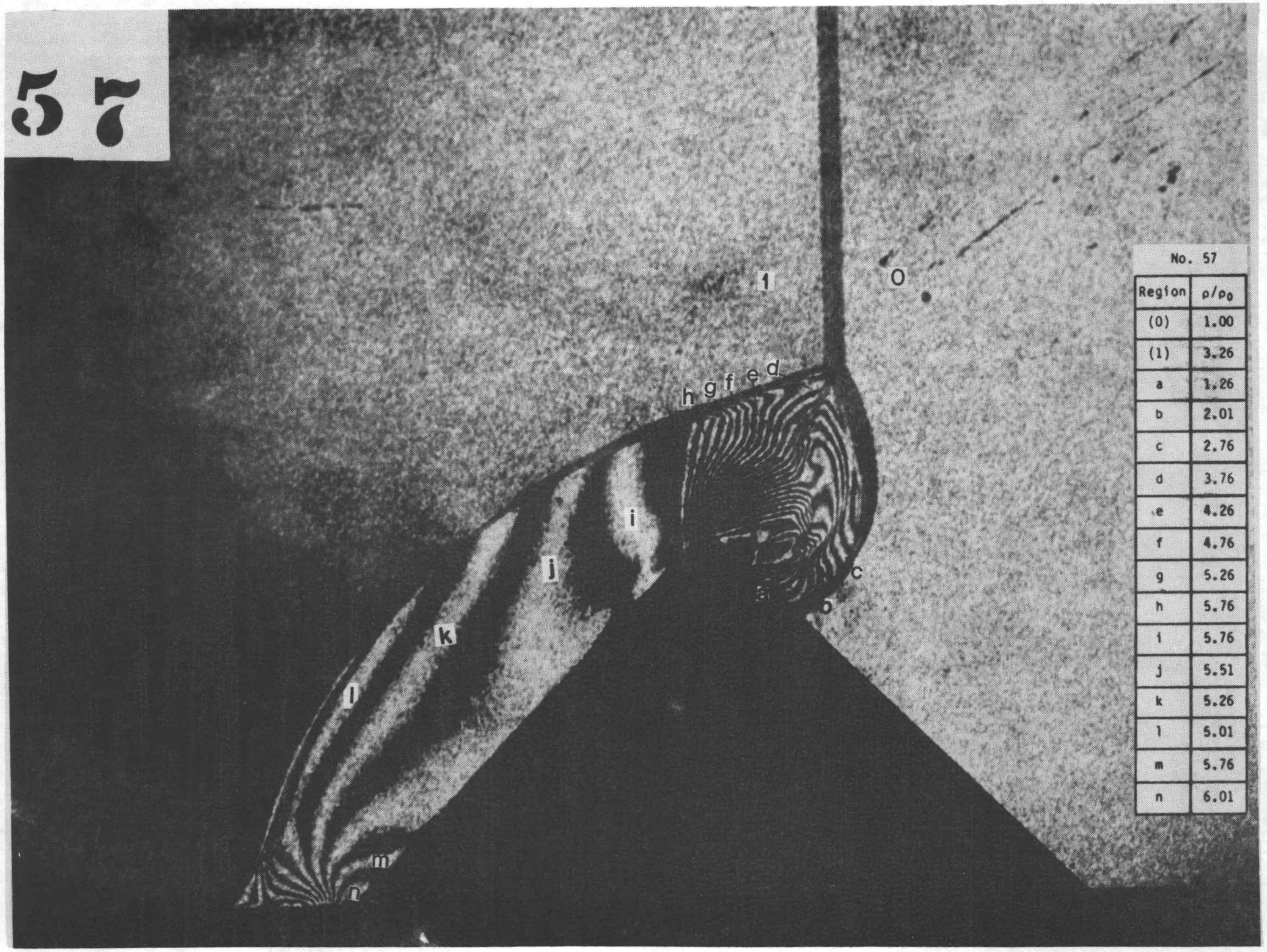

No. 57	
Region	ρ/ρ_0
(0)	1.00
(1)	3.26
a	1.26
b	2.01
c	2.76
d	3.76
e	4.26
f	4.76
g	5.26
h	5.76
i	5.76
j	5.51
k	5.26
l	5.01
m	5.76
n	6.01

(c) AN INTERFEROGRAM (No. 57) TAKEN AT 47 μs AFTER SHOCK WAVE HITS CORNER; M_s=2.45, M_1'=1.17; P_0=10.40KPa, ρ_0=12.15x10^{-2}kg/m^3, T_0=298.5°K

56

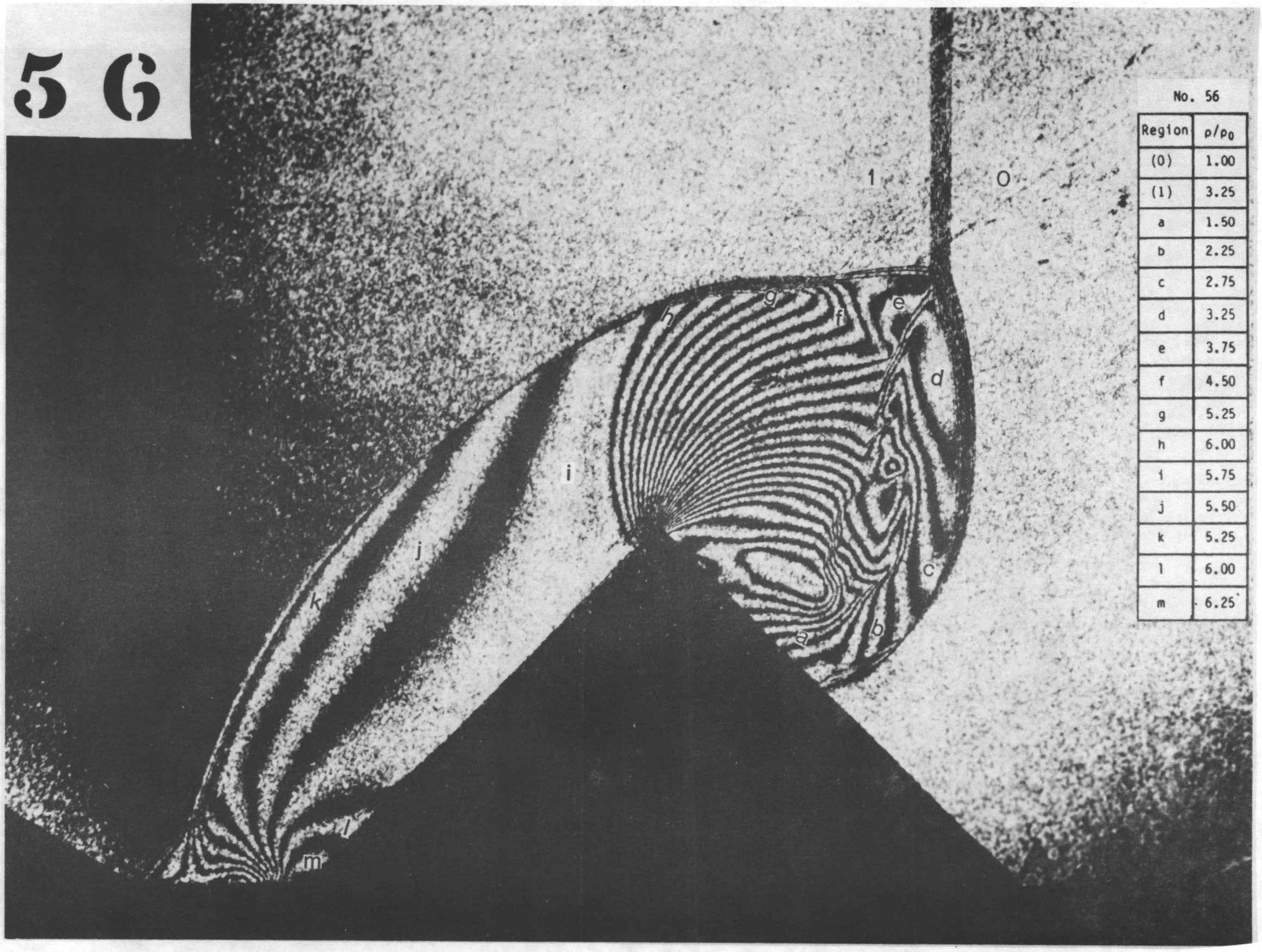

No. 56

Region	ρ/ρ_0
(0)	1.00
(1)	3.25
a	1.50
b	2.25
c	2.75
d	3.25
e	3.75
f	4.50
g	5.25
h	6.00
i	5.75
j	5.50
k	5.25
l	6.00
m	6.25

(d) AN INTERFEROGRAM (No. 56) TAKEN AT 60 μs AFTER SHOCK WAVE HITS CORNER; $M_s=2.44$, $M_1'=1.16$; $P_0=10.40$KPa, $\rho_0=12.15\times10^{-2}$kg/m^3, $T_0=298.5$°K

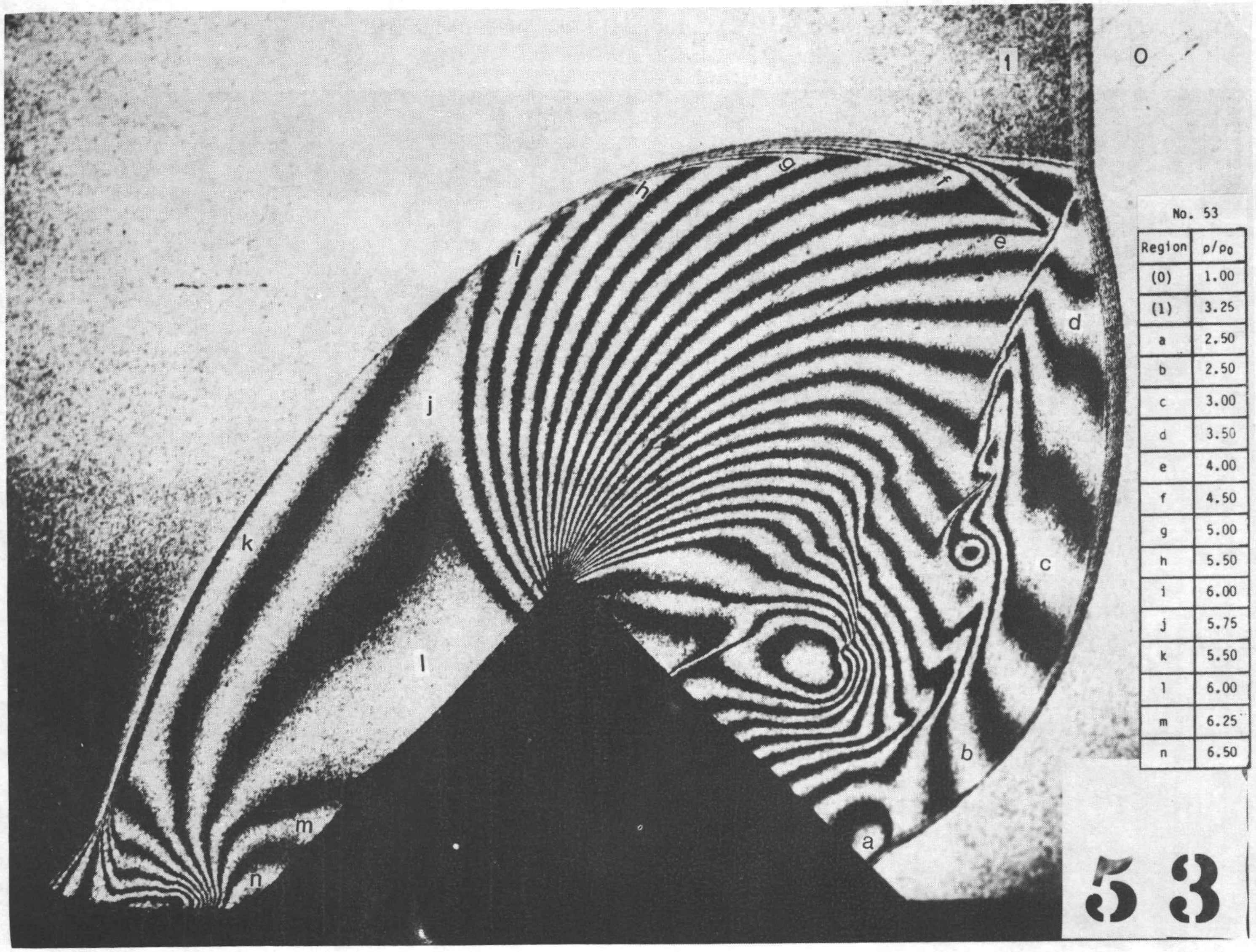

No. 53

Region	ρ/ρ_0
(0)	1.00
(1)	3.25
a	2.50
b	2.50
c	3.00
d	3.50
e	4.00
f	4.50
g	5.00
h	5.50
i	6.00
j	5.75
k	5.50
l	6.00
m	6.25
n	6.50

(e) AN INTERFEROGRAM (No. 53) TAKEN AT 87 μs AFTER SHOCK WAVE HITS CORNER; M_s=2.44, M_1'=1.16; P_0=10.40KPa, ρ_0=12.16x10^{-2}kg/m^3, T_0=298.3°K

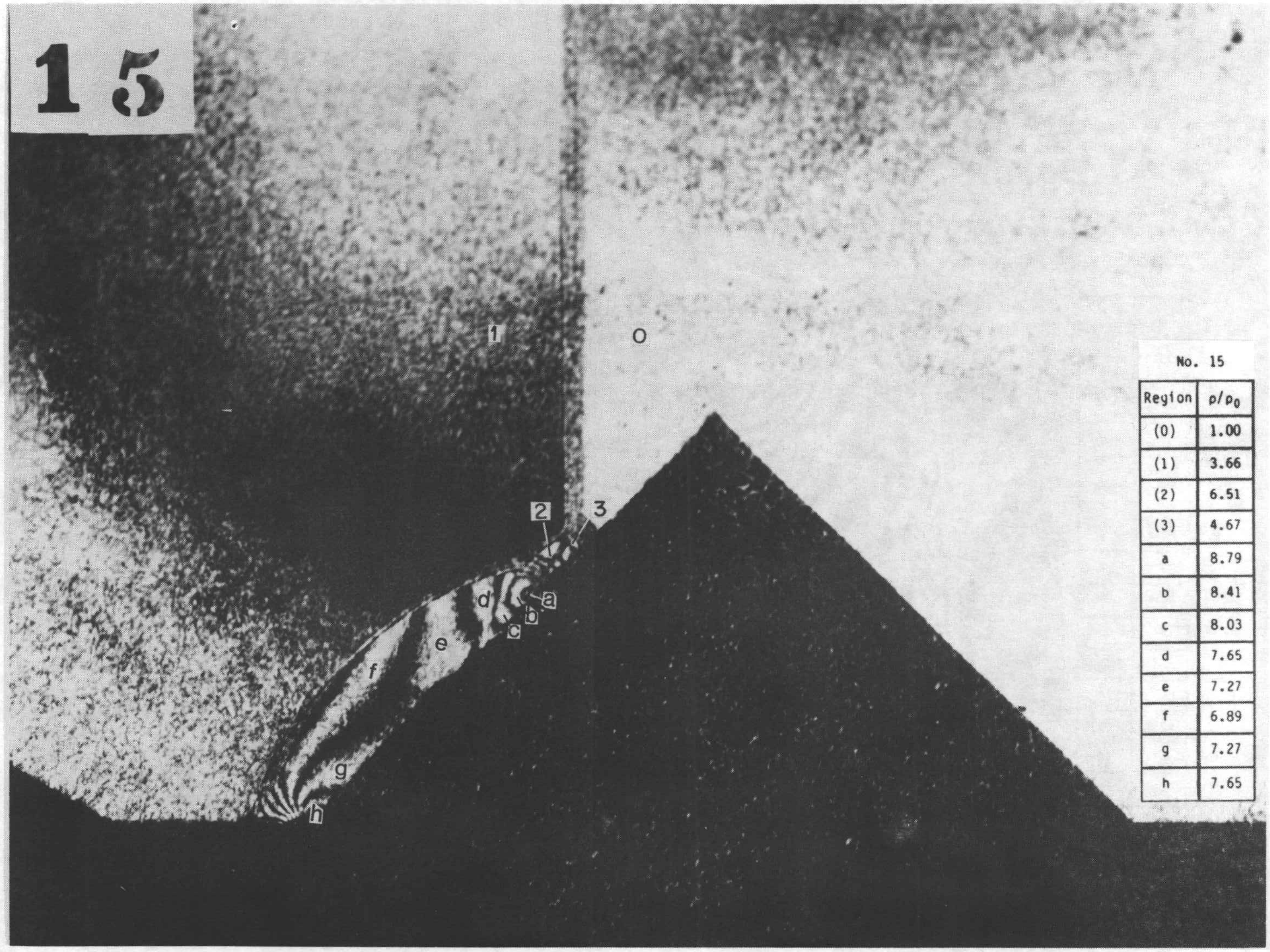

No. 15

Region	ρ/ρ_0
(0)	1.00
(1)	3.66
(2)	6.51
(3)	4.67
a	8.79
b	8.41
c	8.03
d	7.65
e	7.27
f	6.89
g	7.27
h	7.65

Fig. 11 INTERFEROGRAMS OF DIFFRACTION OF PLANAR SHOCK WAVE OVER A HALF - DIAMOND CYLINDER IN AIR FOR CASE OF DOUBLE-MACH REFLECTION. $M_S=2.82$, $M_1'=1.31$, SUPERSONIC FLOW.

(a) AN INTERFEROGRAM (No. 15) TAKEN AT 18 μs AFTER SHOCK WAVE HITS CORNER; $M_S=2.81$, $M_1'=1.30$; $P_0=6.67$KPa, $\rho_0=7.81\times10^{-2}$kg/m^3, $T_0=297.5$°K

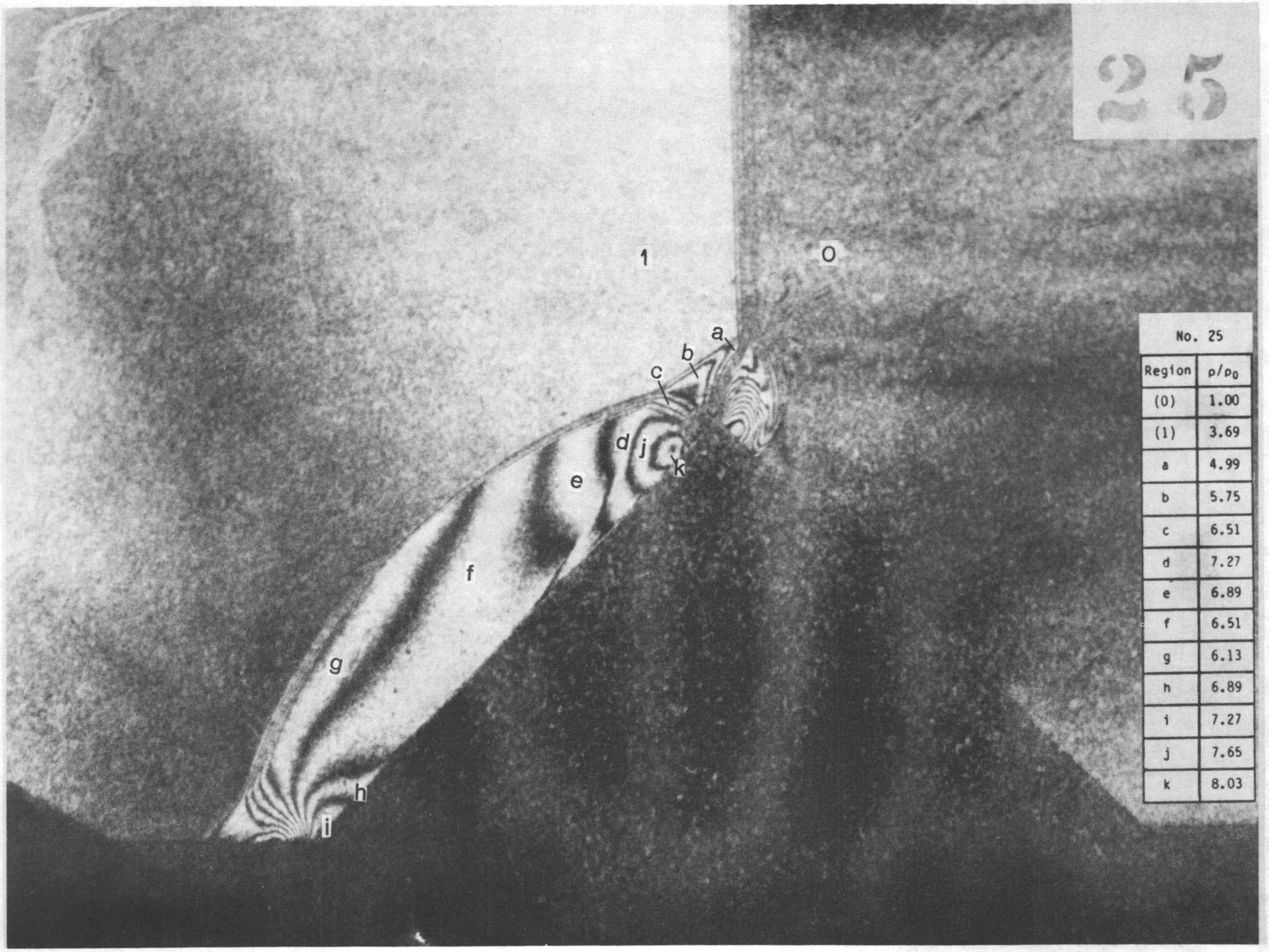

No. 25	
Region	ρ/ρ_0
(0)	1.00
(1)	3.69
a	4.99
b	5.75
c	6.51
d	7.27
e	6.89
f	6.51
g	6.13
h	6.89
i	7.27
j	7.65
k	8.03

(b) AN INTERFEROGRAM (No. 25) TAKEN AT 31 μs AFTER SHOCK WAVE HITS CORNER; $M_s=2.84$, $M_1'=1.32$; $P_0=6.67$KPa, $\rho_0=7.81\times10^{-2}$kg/m^3, $T_0=297.5$°K

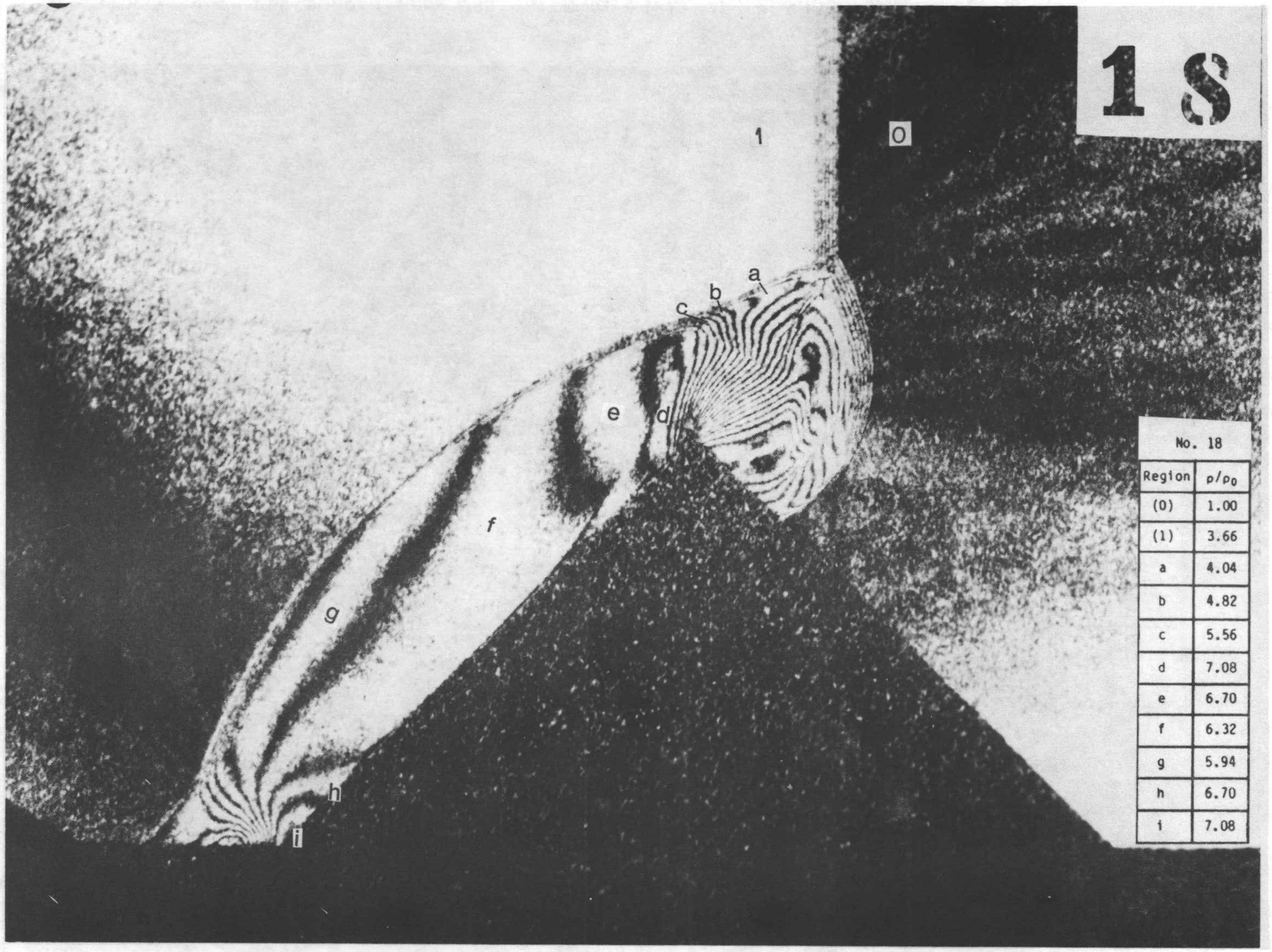

No. 18	
Region	ρ/ρ_0
(0)	1.00
(1)	3.66
a	4.04
b	4.82
c	5.56
d	7.08
e	6.70
f	6.32
g	5.94
h	6.70
i	7.08

(c) AN INTERFEROGRAM (No. 18) TAKEN AT 39 μs AFTER AHOCK WAVE HITS CORNER; M_S=2.81, M_1'=1.30; P_0=6.67Kpa, ρ_0=7.83x10^{-2}kg/m^3, T_0=296.9°K

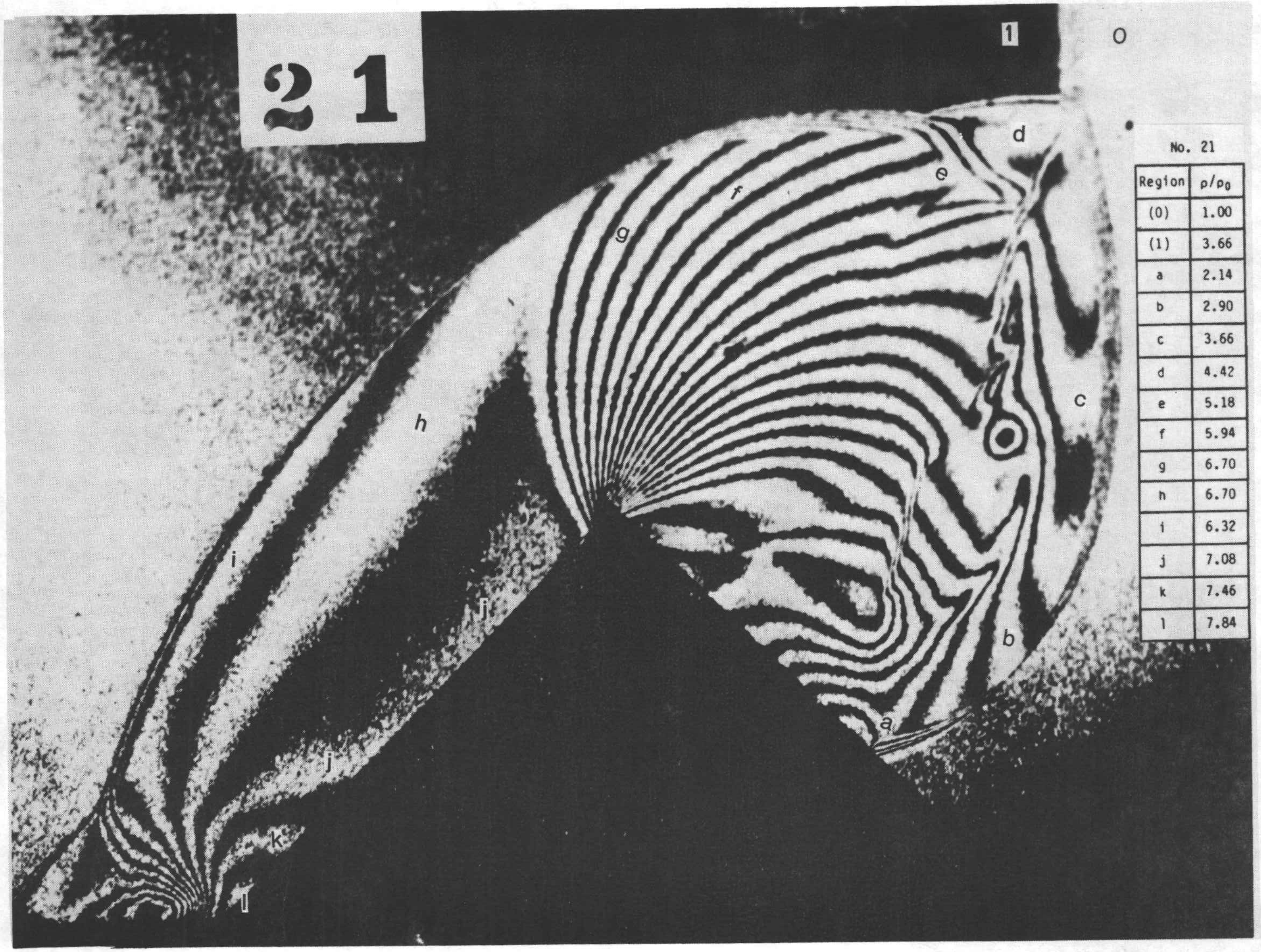

No. 21

Region	ρ/ρ_0
(0)	1.00
(1)	3.66
a	2.14
b	2.90
c	3.66
d	4.42
e	5.18
f	5.94
g	6.70
h	6.70
i	6.32
j	7.08
k	7.46
l	7.84

(d) AN INTERFEROGRAM (No. 21) TAKEN AT 101 μs AFTER SHOCK WAVE HITS CORNER; M_s=2.81, M_1'=1.30; P_0=6.67 KPa, ρ_0=7.84x10^{-2}kg/m^3, T_0=296.6°K

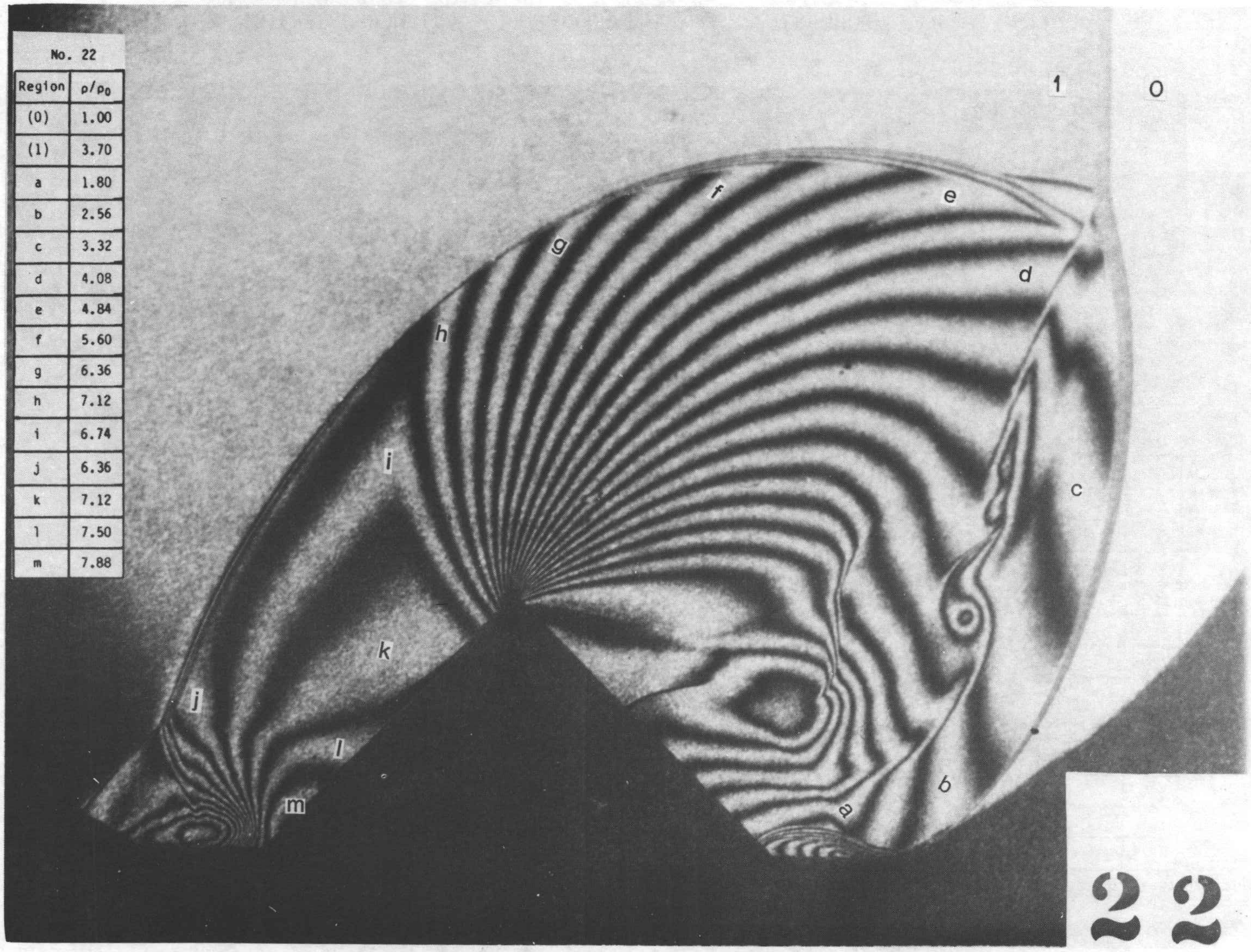

No. 22	
Region	ρ/ρ_0
(0)	1.00
(1)	3.70
a	1.80
b	2.56
c	3.32
d	4.08
e	4.84
f	5.60
g	6.36
h	7.12
i	6.74
j	6.36
k	7.12
l	7.50
m	7.88

(e) AN INTERFEROGRAM (No. 22) TAKEN AT 96 μs AFTER SHOCK WAVE HITS CORNER; M_s=2.85, M_1'=1.33; P_0=6.67KPa, ρ_0=7.84x10^{-2}kg/m^3, T_0=296.6°K

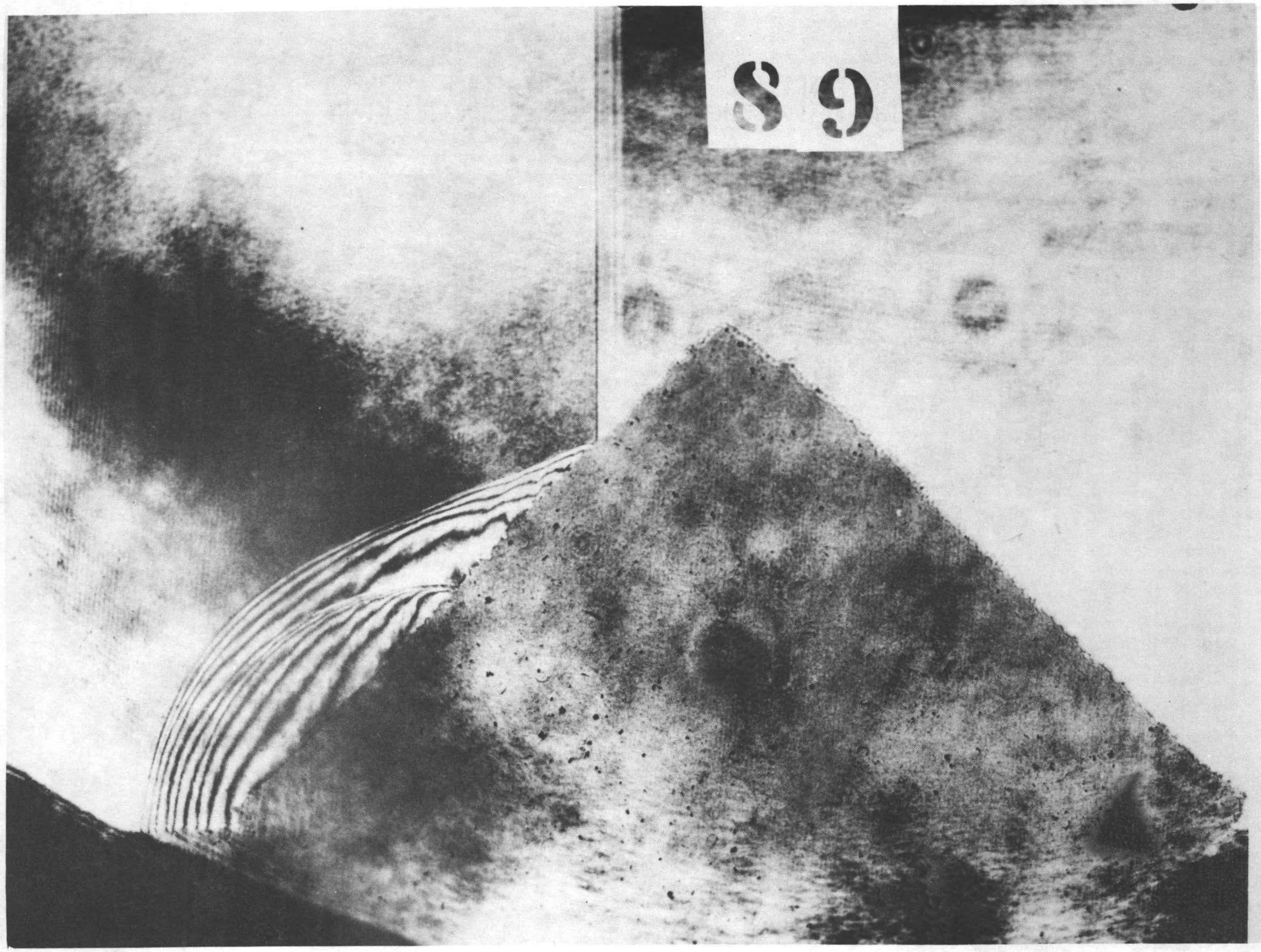

Fig. 12 INTERFEROGRAMS OF DIFFRACTION OF PLANAR SHOCK WAVE OVER A HALF - DIAMOND CYLINDER IN AIR FOR EFFECTS OF PLASTIC SPONGY MATERIAL, M_s=1.60, M_1'=0.69, SUBSONIC FLOW.

(a) AN INTERFEROGRAM (No. 89) TAKEN AT 46 μs AFTER SHOCK WAVE HITS CORNER; M_s=1.57, M_1'=0.67; P_0=32.13KPa, ρ_0=37.75x10^{-2}kg/m^3, T_0=296.9°K

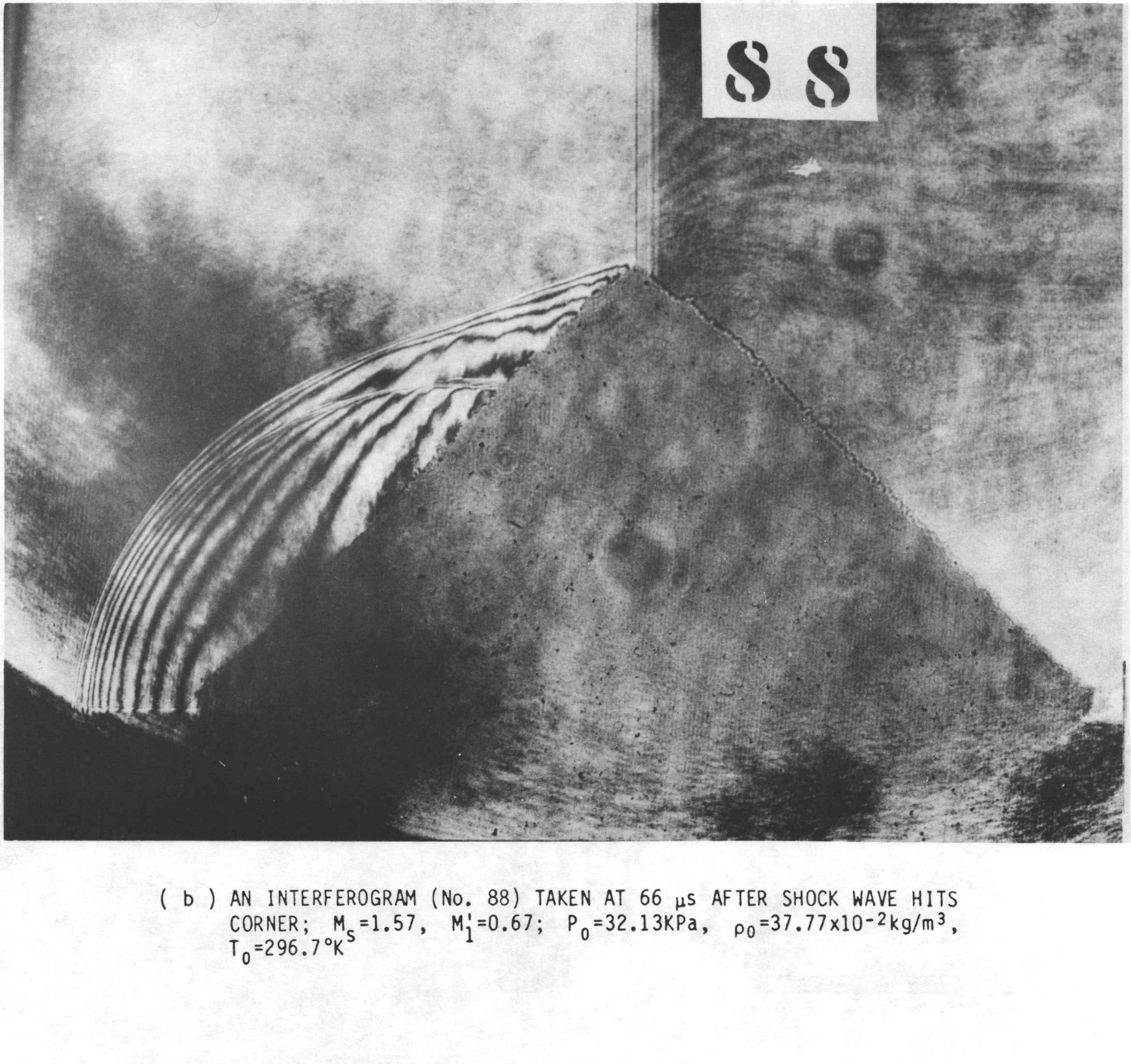

(b) AN INTERFEROGRAM (No. 88) TAKEN AT 66 μs AFTER SHOCK WAVE HITS CORNER; $M_S=1.57$, $M_1'=0.67$; $P_0=32.13$KPa, $\rho_0=37.77\text{x}10^{-2}\text{kg/m}^3$, $T_0=296.7°\text{K}$

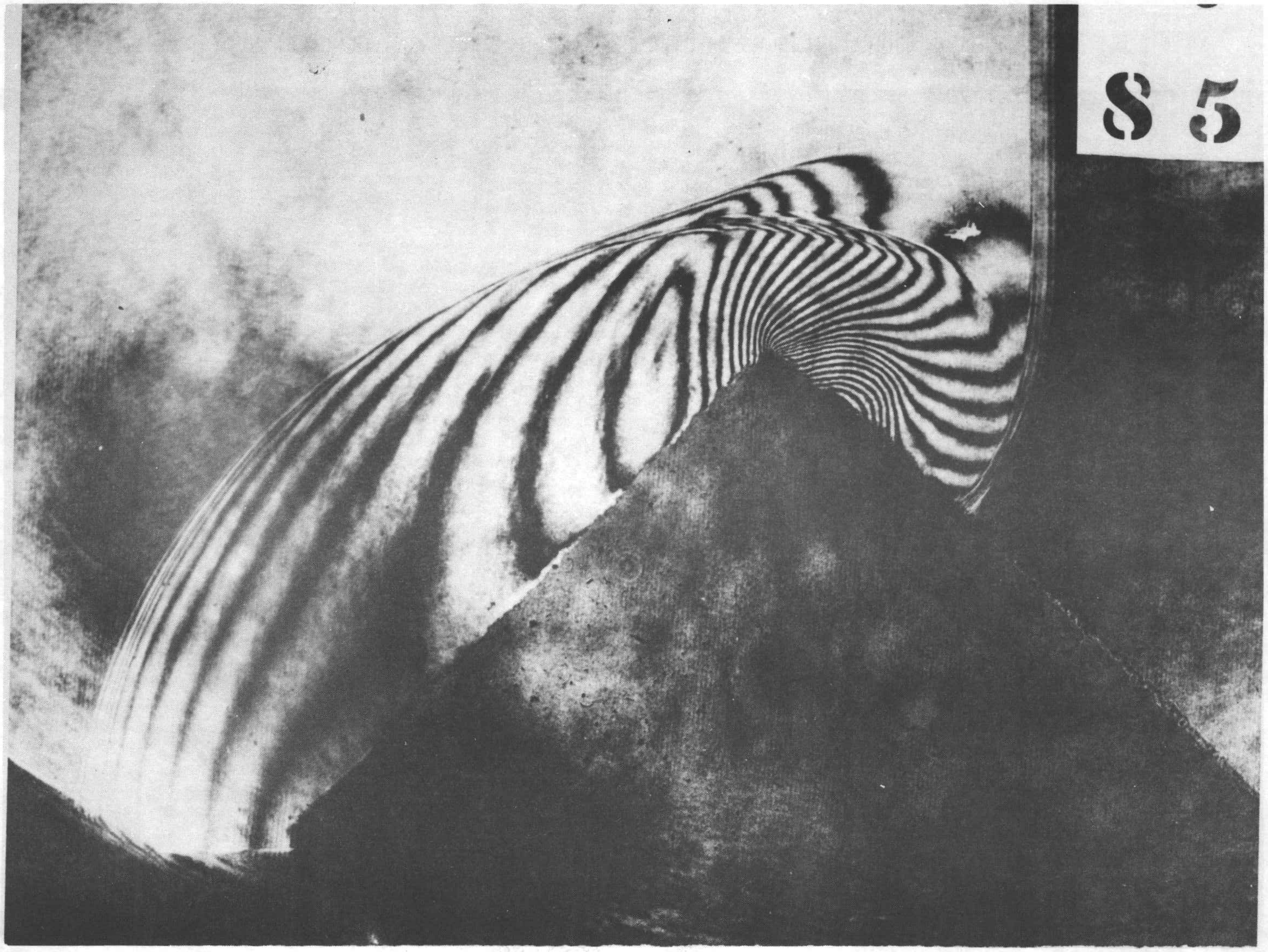

(c) AN INTERFEROGRAM (No. 85) TAKEN AT 97 μs AFTER SHOCK WAVE HITS CORNER; $M_s = 1.57$, $M_1' = 0.67$; $P_0 = 32.26$KPa, $\rho_0 = 37.98 \times 10^{-2}$kg/m^3, $T_0 = 296.3°$K

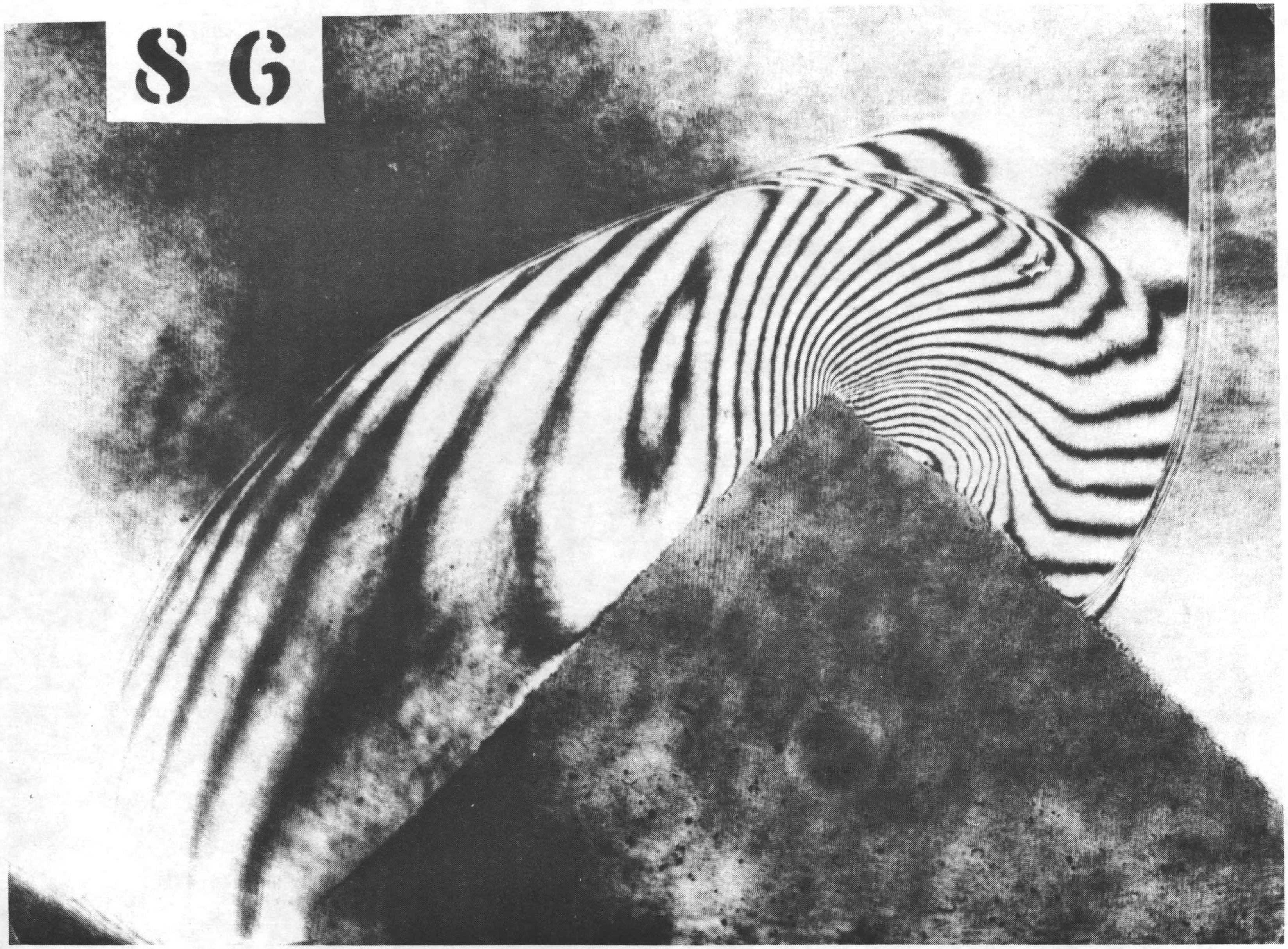

(d) AN INTERFEROGRAM (No. 86) TAKEN AT 108 μs AFTER SHOCK WAVE HITS CORNER; M_s=1.57, M'=0.67; P_0=32.13KPa, ρ_0=37.80×10^{-2} kg/m^3, T_0=296.5°K

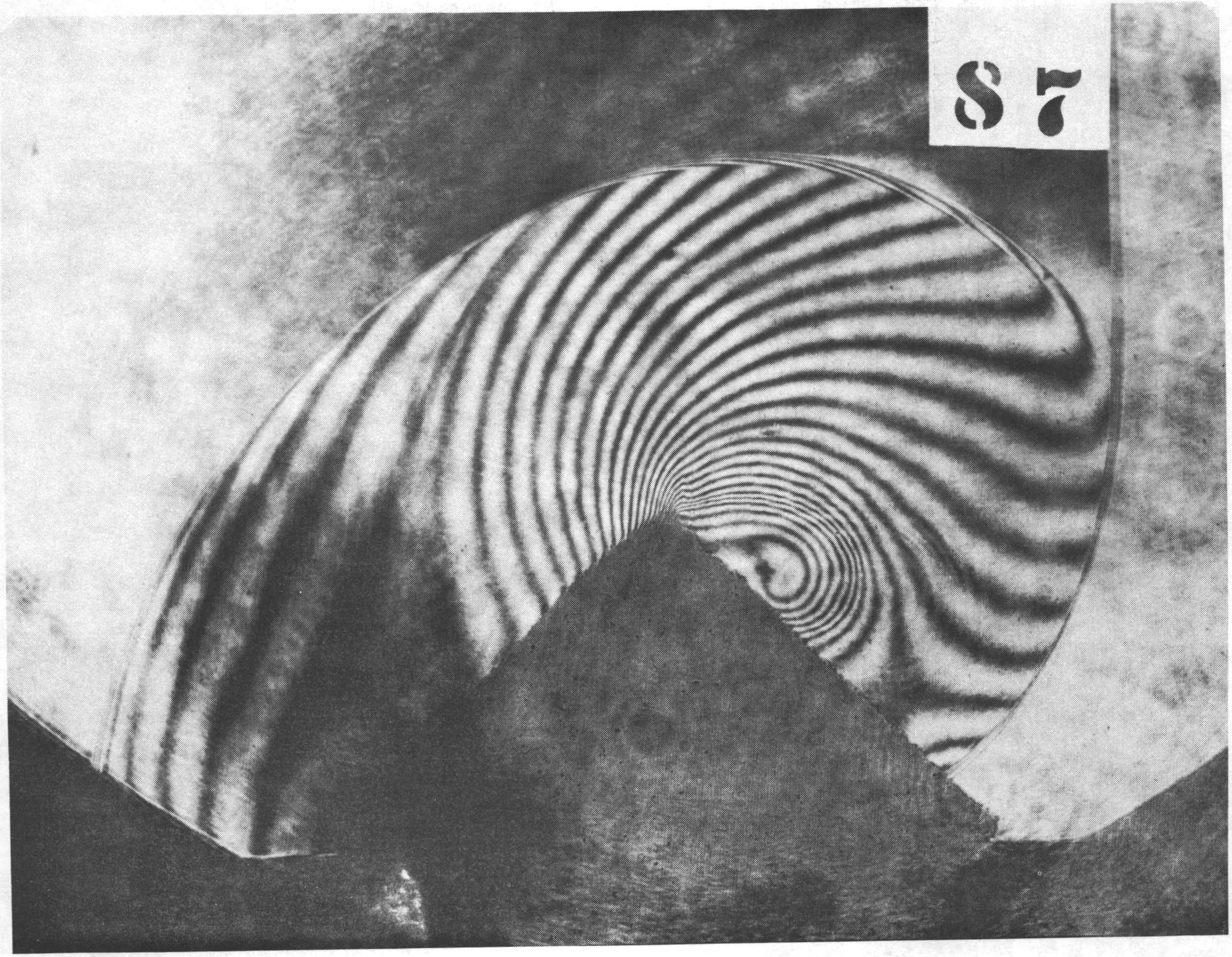

(e) AN INTERFEROGRAM (No. 87) TAKEN AT 145 μs AFTER SHOCK WAVE HITS CORNER; M_s=1.57, M_1'=0.67; P_0=32.13KPa, ρ_0=37.80x10^{-2}kg/m^3, T_0=296.5°K

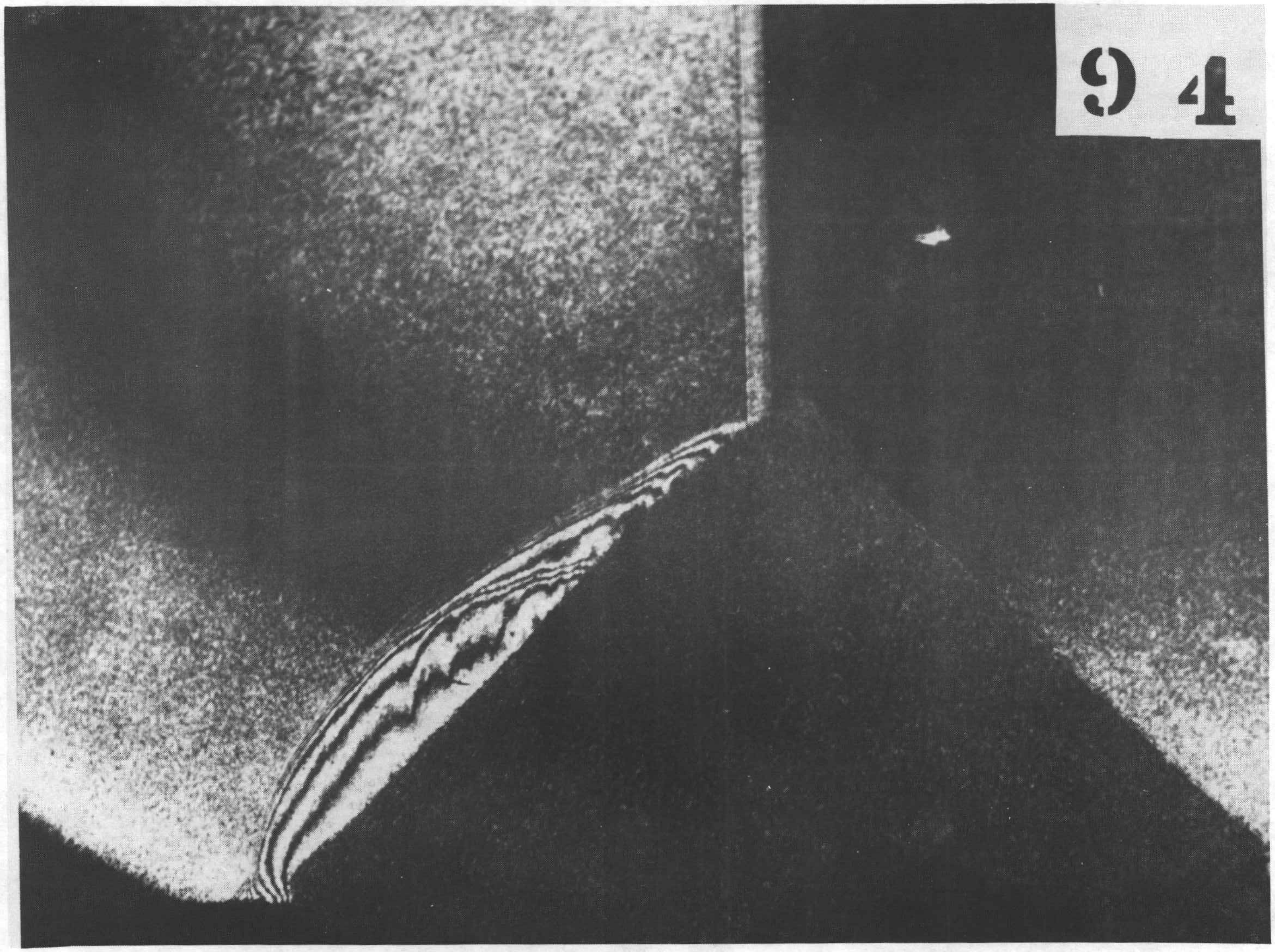

Fig. 13 INTERFEROGRAMS OF DIFFRACTION OF PLANAR SHOCK WAVE OVER A HALF - DIAMOND CYLINDER IN AIR FOR EFFECTS OF PLASTIC SPONGY MATERIAL, $M_s=2.45$, $M_1'=1.17$, SUPERSONIC FLOW.

(a) AN INTERFEROGRAM (No. 94) TAKEN AT 38 μs AFTER SHOCK WAVE HITS CORNER; $M_s=2.45$, $M_1'=1.17$; $P_0=7.46$KPa, $\rho_0=8.79\times10^{-2}$kg/m^3, $T_0=295.9$°K

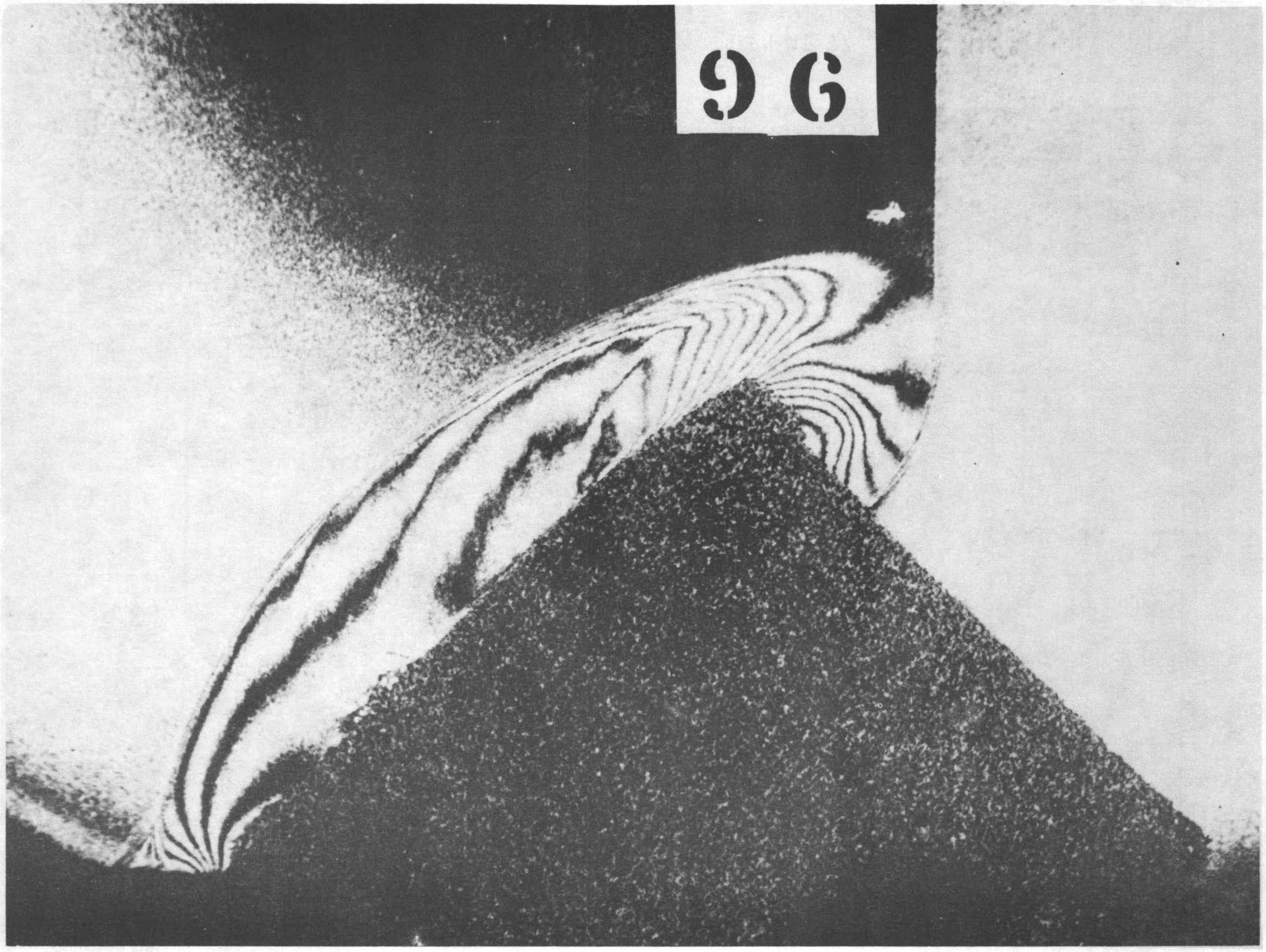

(b) AN INTERFEROGRAM (No. 96) TAKEN AT 60 μs AFTER SHOCK WAVE HITS CORNER; $M_s = 2.45$, $M_1' = 1.17$; $P_0 = 7.53$KPa, $\rho_0 = 8.88 \times 10^{-2}$kg/m^3, $T_0 = 295.8$°K

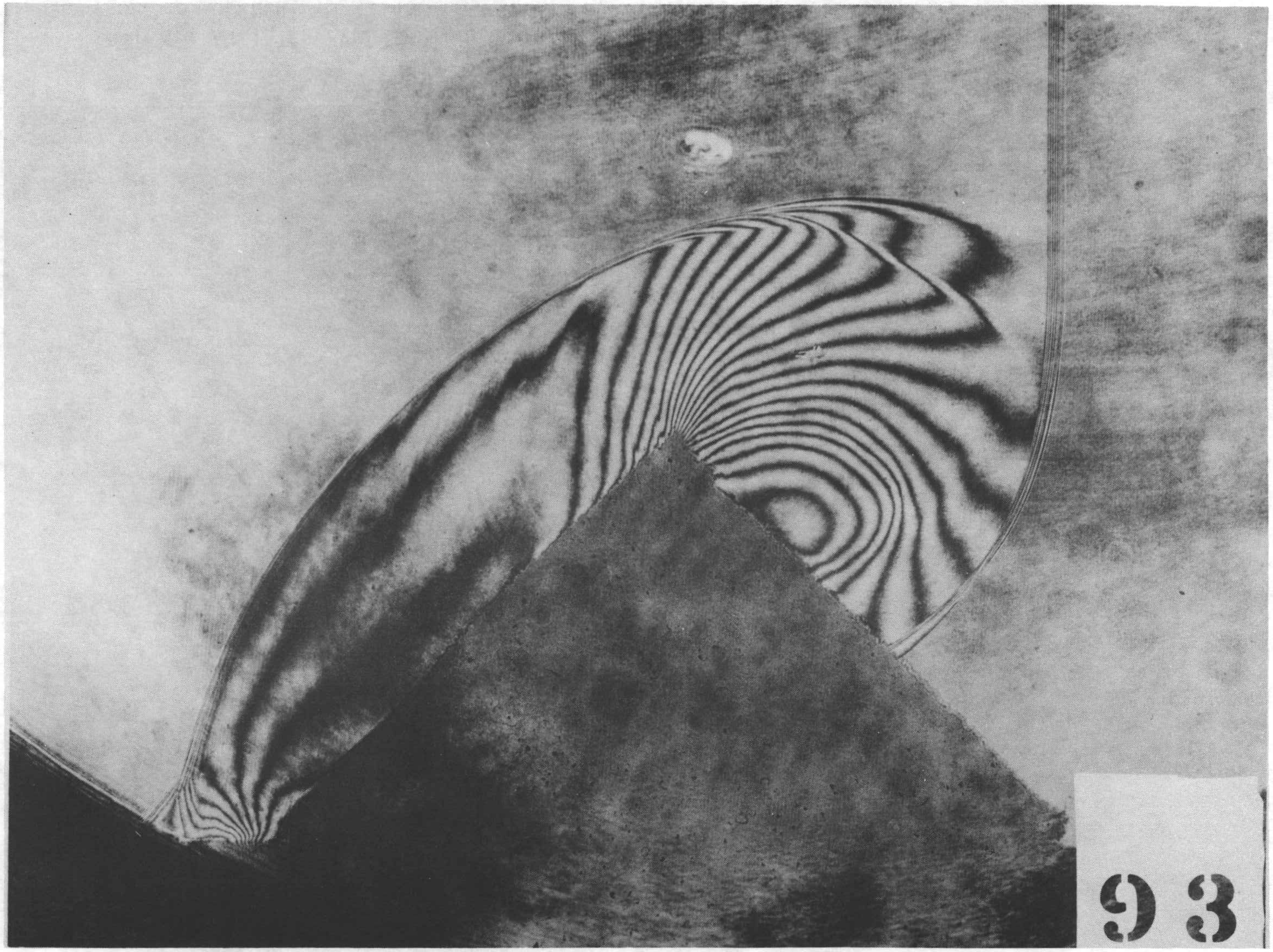

(c) AN INTERFEROGRAM (No. 93) TAKEN AT 77 μs AFTER SHOCK WAVE HITS CORNER; $M_S = 2.45$, $M_1' = 1.17$; $P_0 = 9.20$Kpa, $\rho_0 = 10.81 \times 10^{-2}$kg/m^3, $T_0 = 296.7$°K

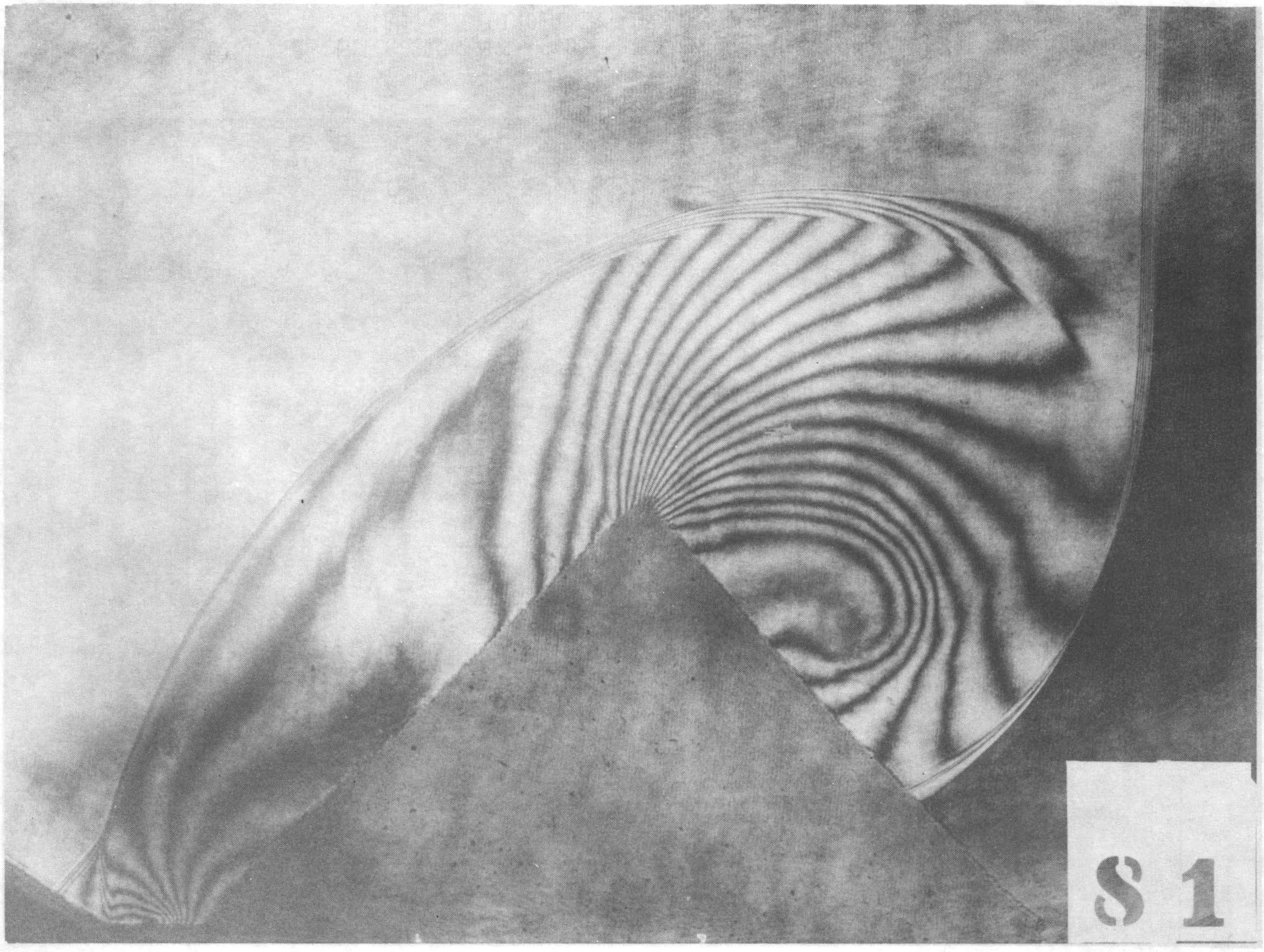

(d) AN INTERFEROGRAM (No. 81) TAKEN AT 88 μs AFTER SHOCK WAVE HITS CORNER; M_s=2.42, M_1'=1.15; P_0=9.20KPa, ρ_0=10.74x10^{-2}kg/m^3, T_0=298.6°K

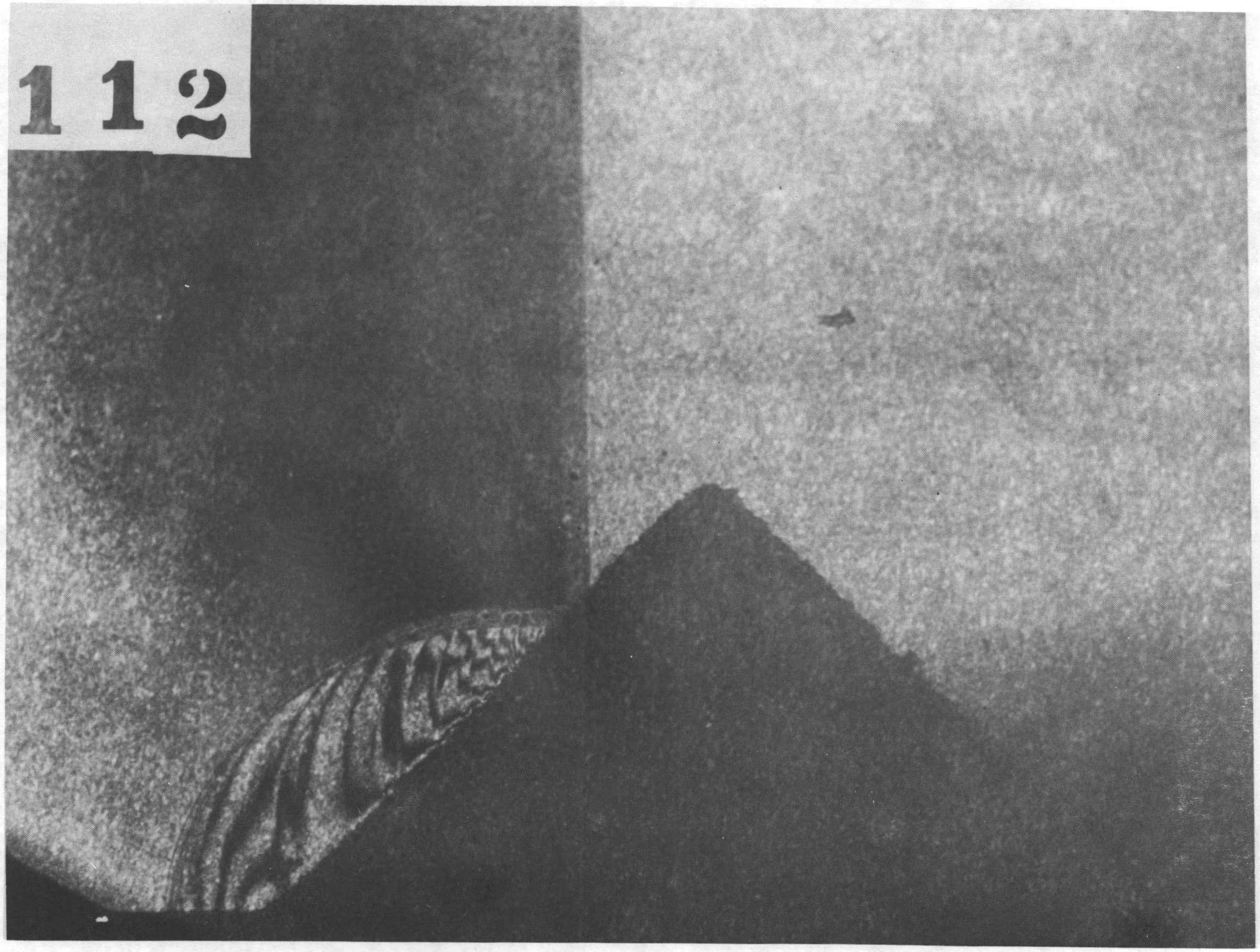

Fig. 14 INTERFEROGRAMS OF DIFFRACTION OF PLANAR SHOCK WAVE OVER A HALF - DIAMOND CYLINDER IN AIR FOR EFFECTS OF SANDPAPER ROUGHNESS, $M_s=1.60$, $M_1'=0.69$, SUBSONIC FLOW.

(a) AN INTERFEROGRAM (No. 112) TAKEN AT 36 μs AFTER SHOCK WAVE HITS CORNER; $M_s=1.60$, $M_1'=0.69$; $P_0=32.53$KPa, $\rho_0=38.19\text{x}10^{-2}$kg/m^3, $T_0=297.1$°K

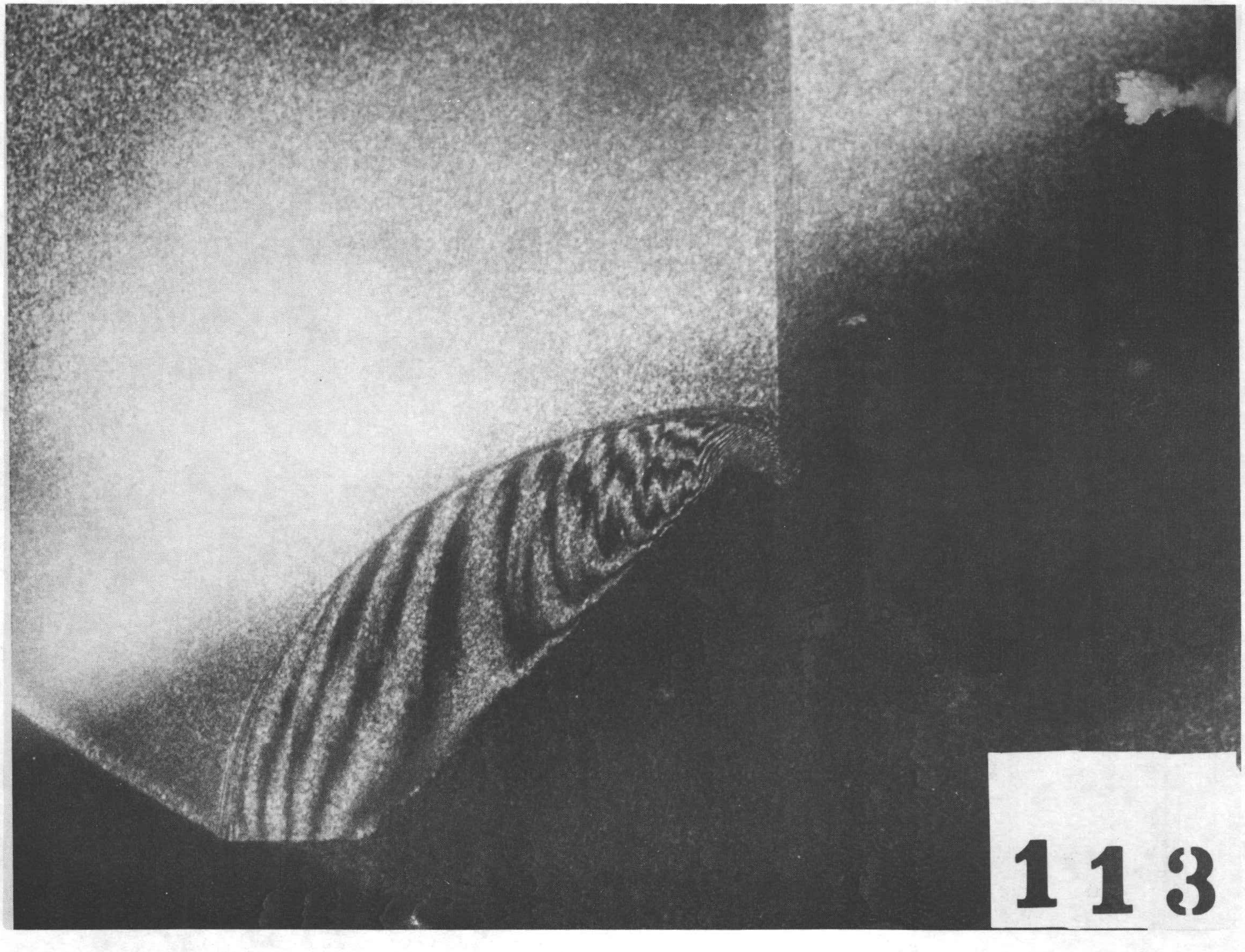

(b) AN INTERFEROGRAM (No. 113) TAKEN AT 58 μs AFTER SHOCK WAVE HITS CORNER; $M_S=1.59$, $M_1'=0.68$; $P_0=32.66$KPa, $\rho_0=38.33 \times 10^{-2}$ kg/m^3, $T_0=297.2$°K

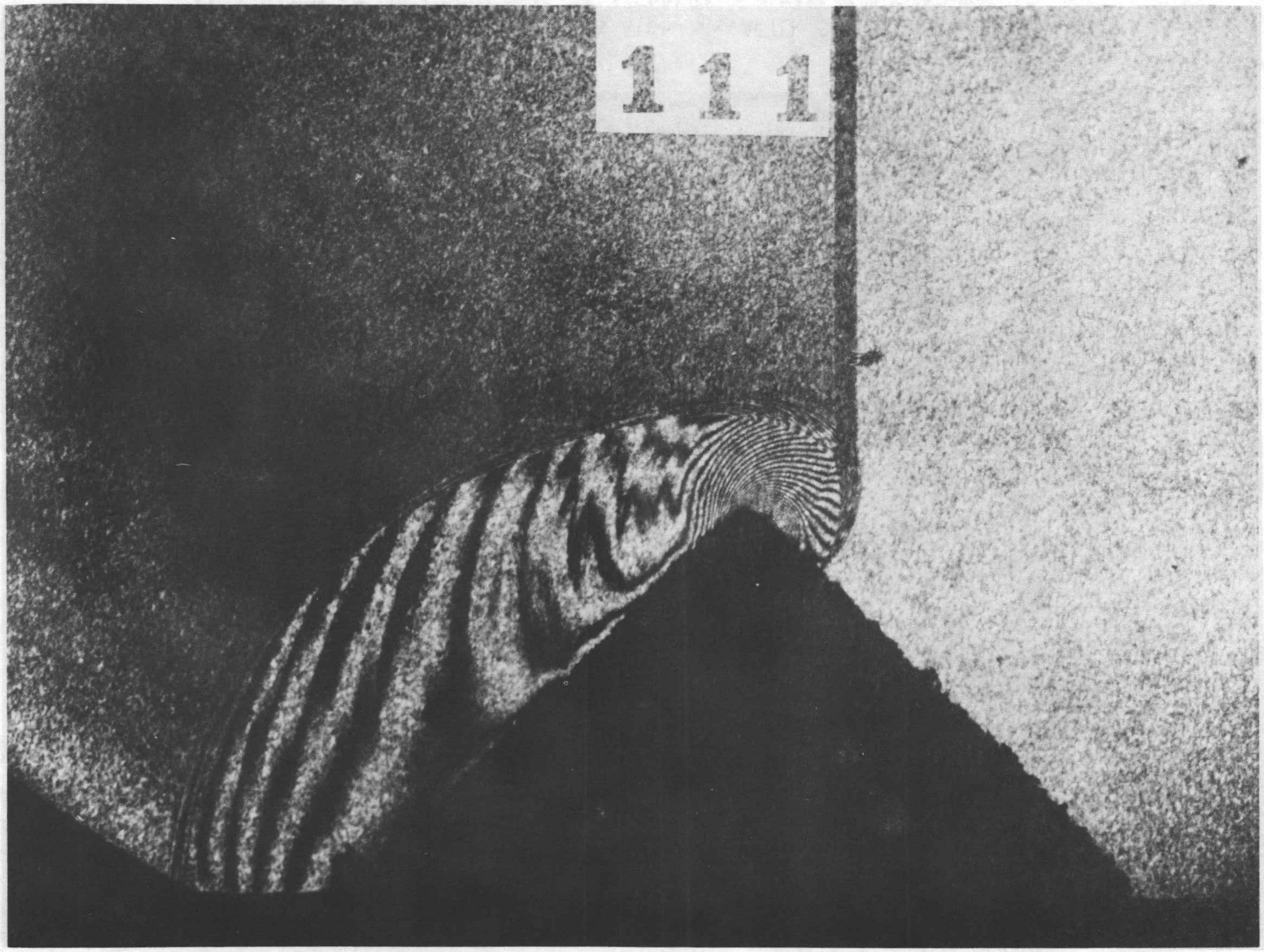

(c) AN INTERFEROGRAM (No. 111) TAKEN AT 67 μs AFTER SHOCK WAVE HITS CORNER; M_S=1.59, M_1'=0.68; P_0=32.53KPa, ρ_0=38.21x10^{-2}kg/m^3, T_0=296.9°K

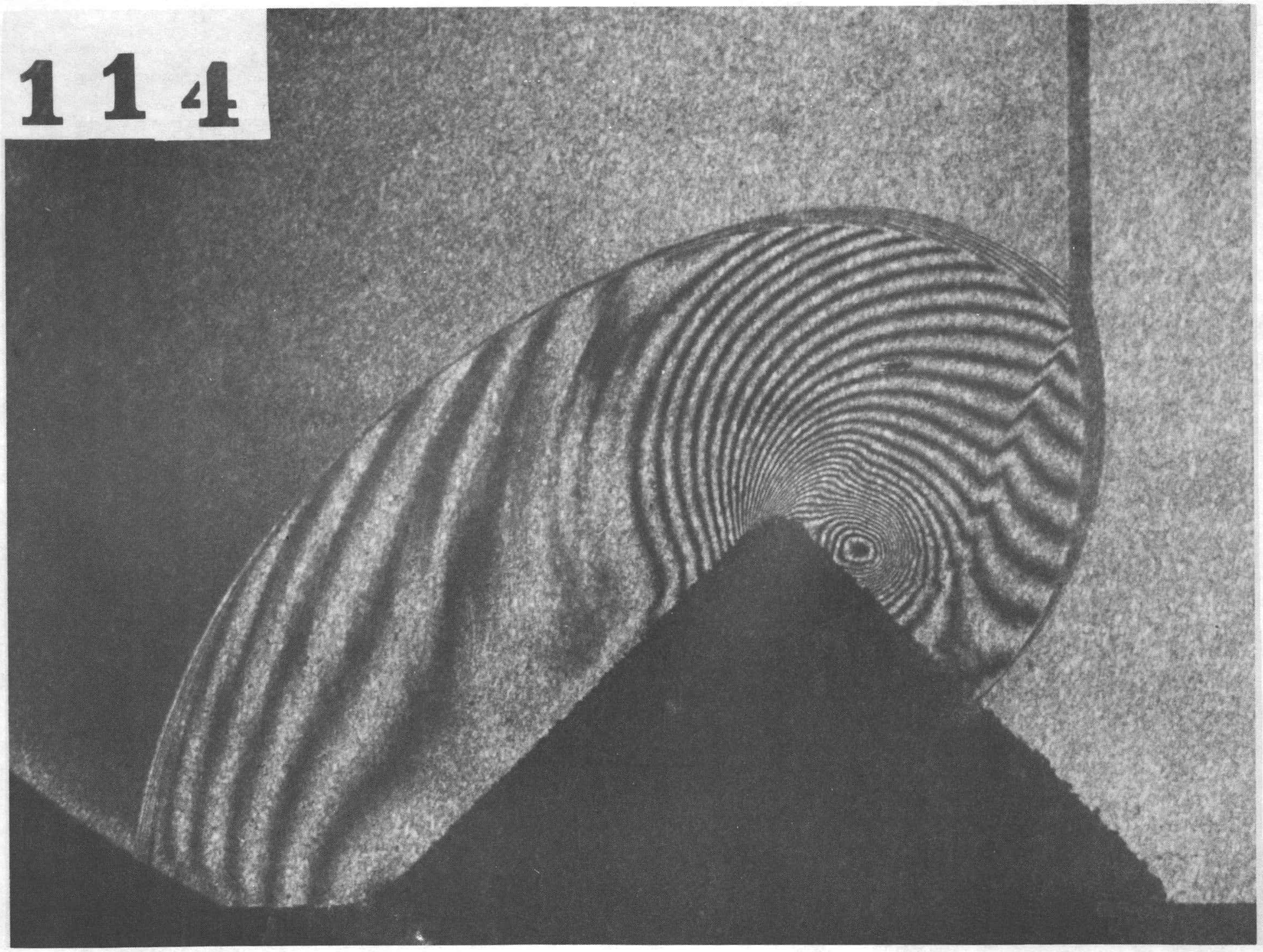

(d) AN INTERFEROGRAM (No. 114) TAKEN AT 94 μs AFTER SHOCK WAVE HITS CORNER; $M_S = 1.60$, $M_1' = 0.69$; $P_0 = 32.53$KPa, $\rho_0 = 38.18 \times 10^{-2}$kg/m^3, $T_0 = 297.2$°K

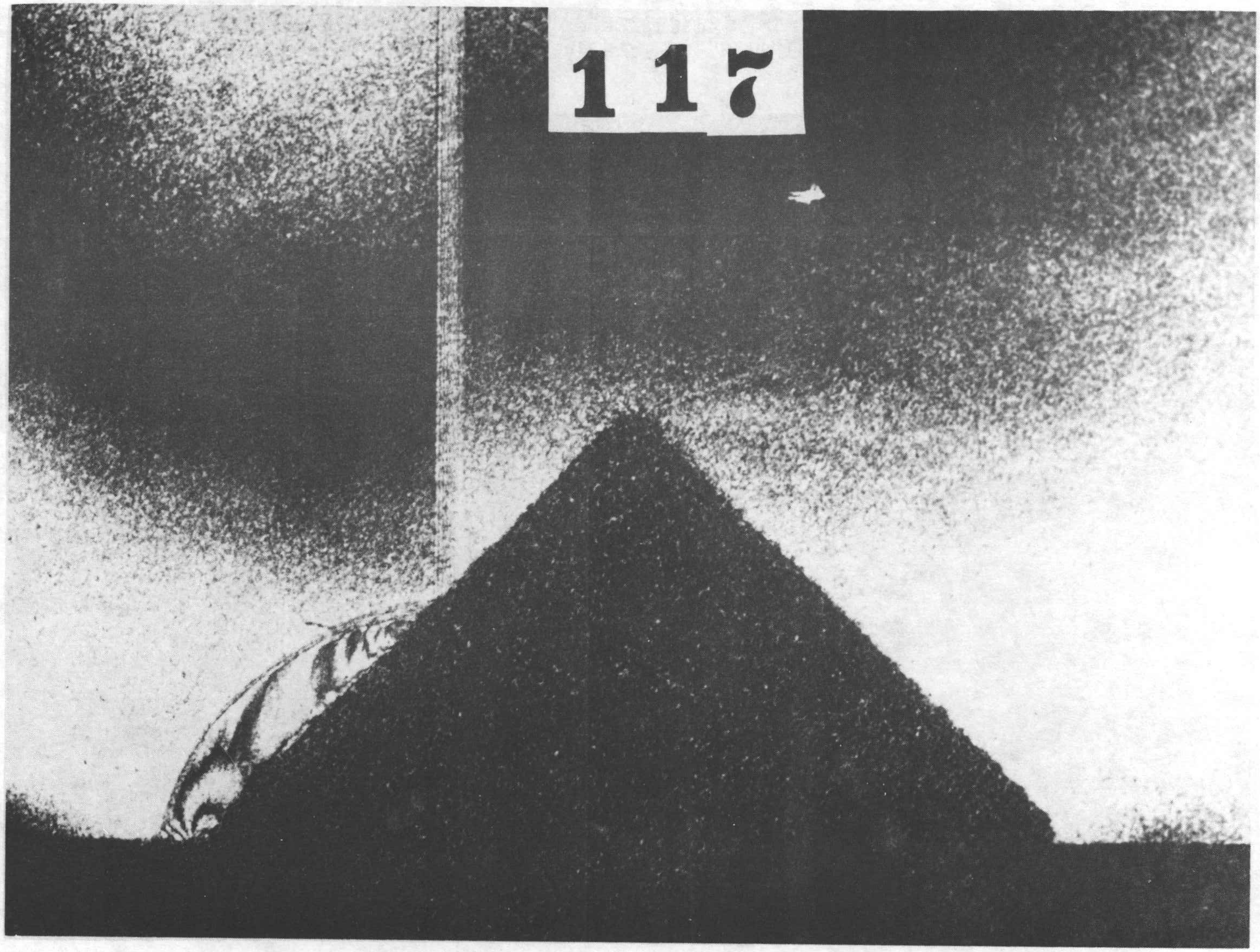

Fig. 15 INTERFEROGRAMS OF DIFFRACTION OF PLANAR SHOCK WAVE OVER A HALF - DIAMOND CYLINDER IN AIR FOR EFFECTS OF SANDPAPER ROUGHNESS, $M_s=2.45$, $M_1'=1.17$, SUPERSONIC FLOW.

(a) AN INTERFEROGRAM (No. 117) TAKEN AT 19 μs AFTER SHOCK WAVE HITS CORNER; $M_s=2.45$, $M_1'=1.17$; $P_0=7.47$KPa, $\rho_0=8.81\times10^{-2}$kg/m^3, $T_0=295.5$°K

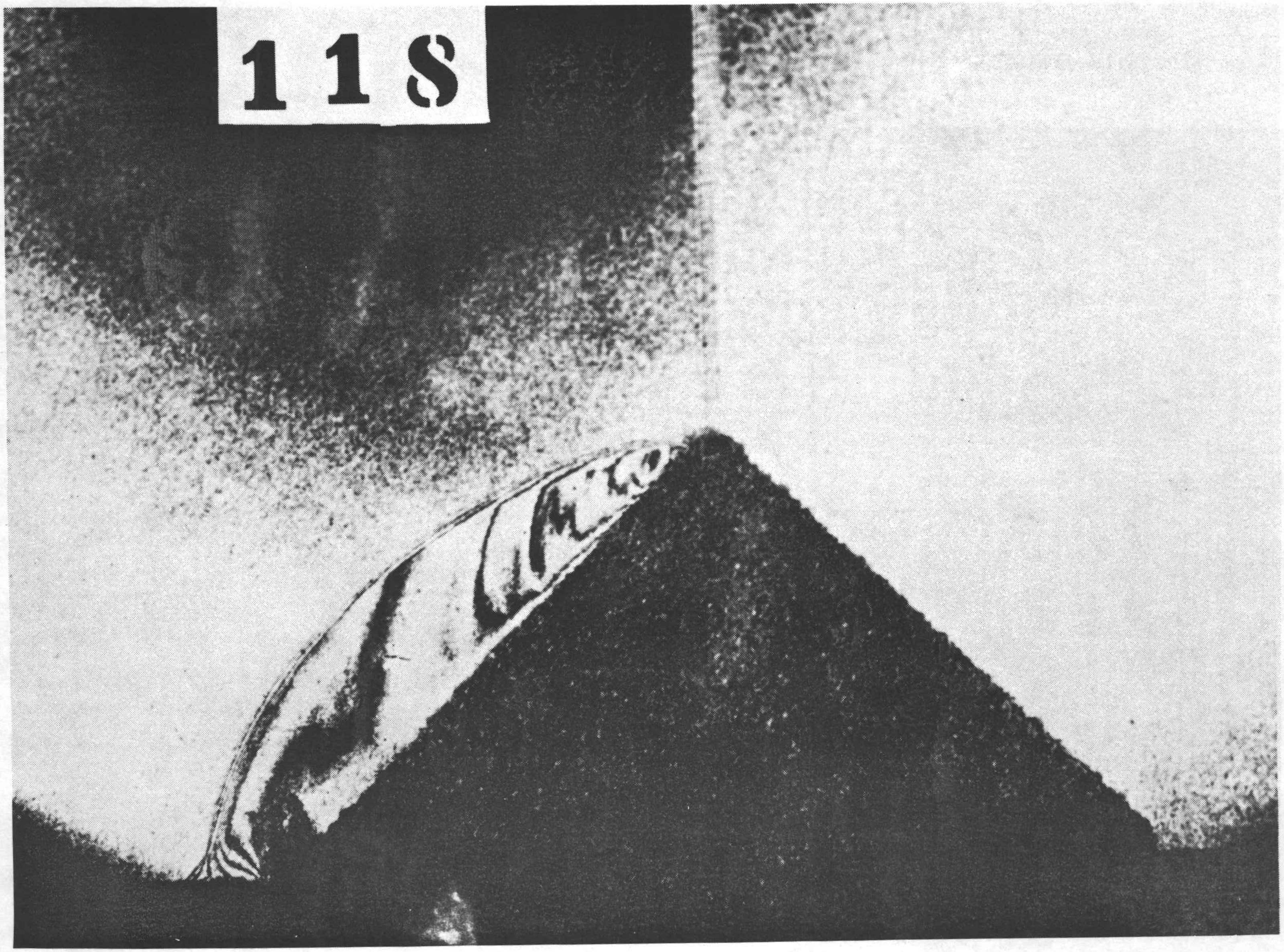

(b) AN INTERFEROGRAM (No. 118) TAKEN AT 33 μs AFTER SHOCK WAVE HITS CORNER; $M_s=2.45$, $M_1'=1.17$; $P_0=7.47$KPa, $\rho_0=8.81\times10^{-2}$kg/m^3, $T_0=295.6$°K

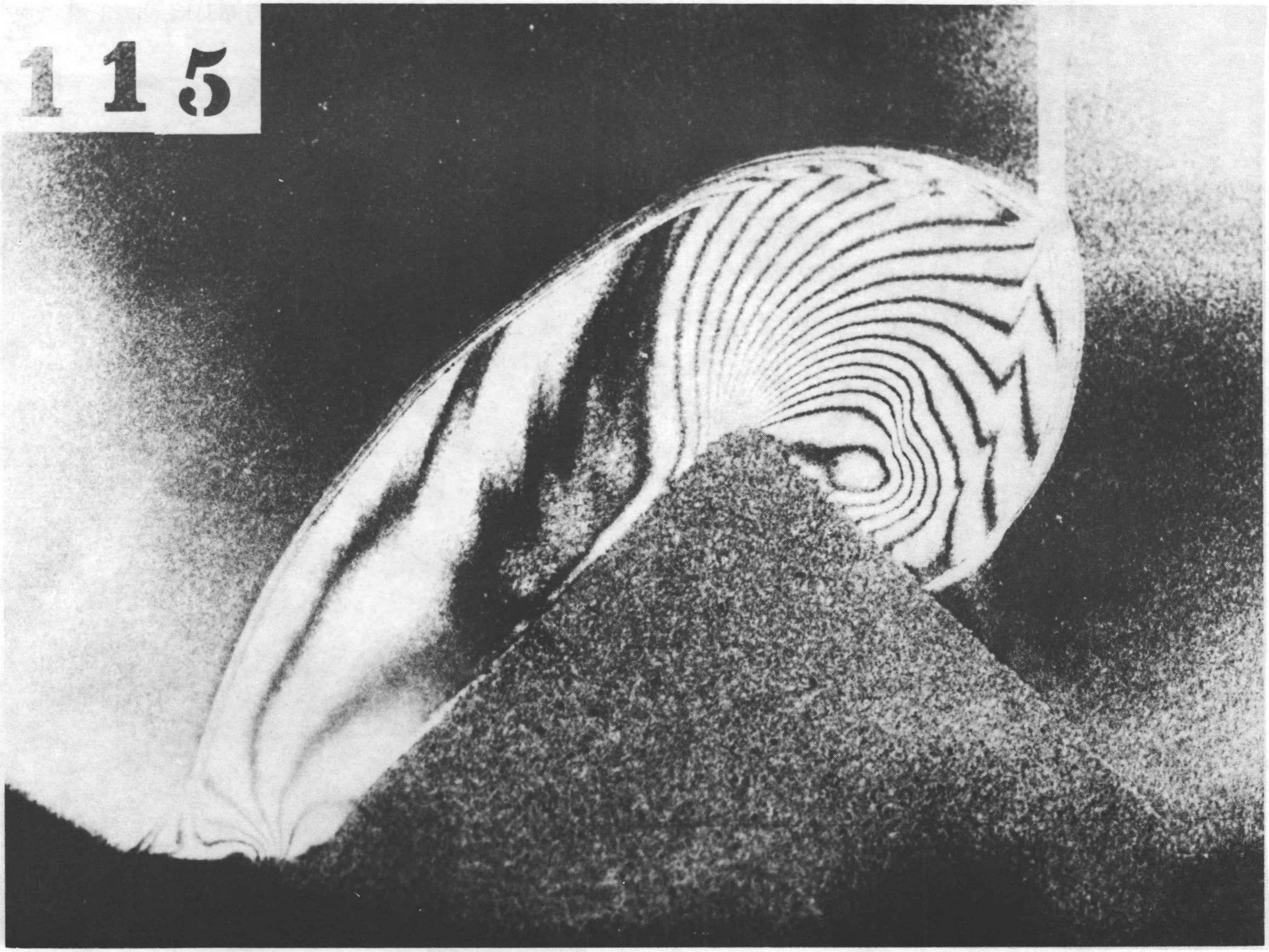

(c) AN INTERFEROGRAM (No. 115) TAKEN AT 58 μs AFTER SHOCK WAVE HITS CORNER; $M_S=2.47$, $M_1'=1.18$; $P_0=7.33$Kpa, $\rho_0=8.63\times10^{-2}$kg/m^3, $T_0=296.2$°K

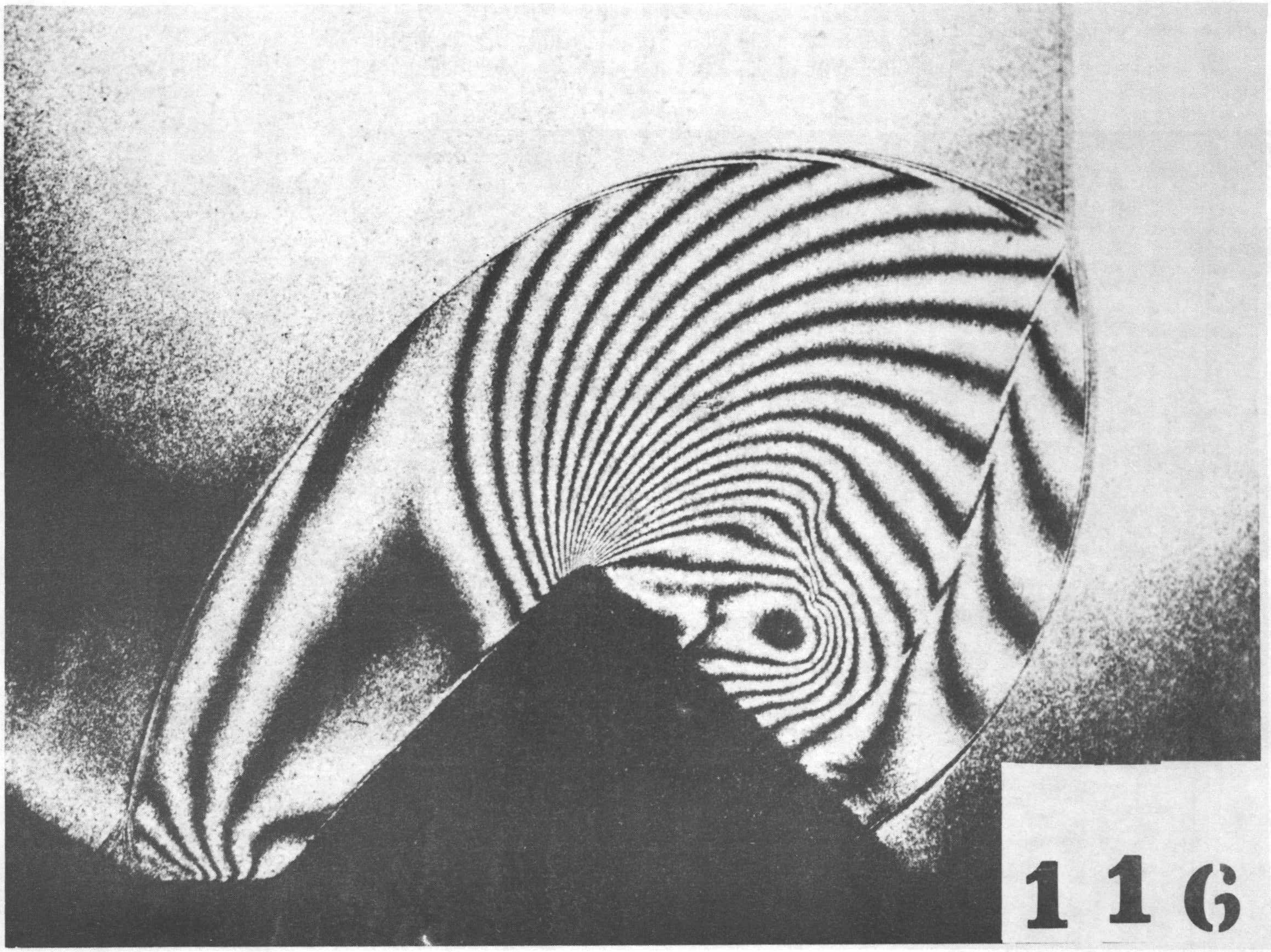

(d) AN INTERFEROGRAM (No. 116) TAKEN AT 86 μs AFTER SHOCK WAVE HITS CORNER; M_s=2.42, M_1'=1.15; P_0=10.66KPa, ρ_0=12.51x10^{-2}kg/m^3, T_0=297.2°K

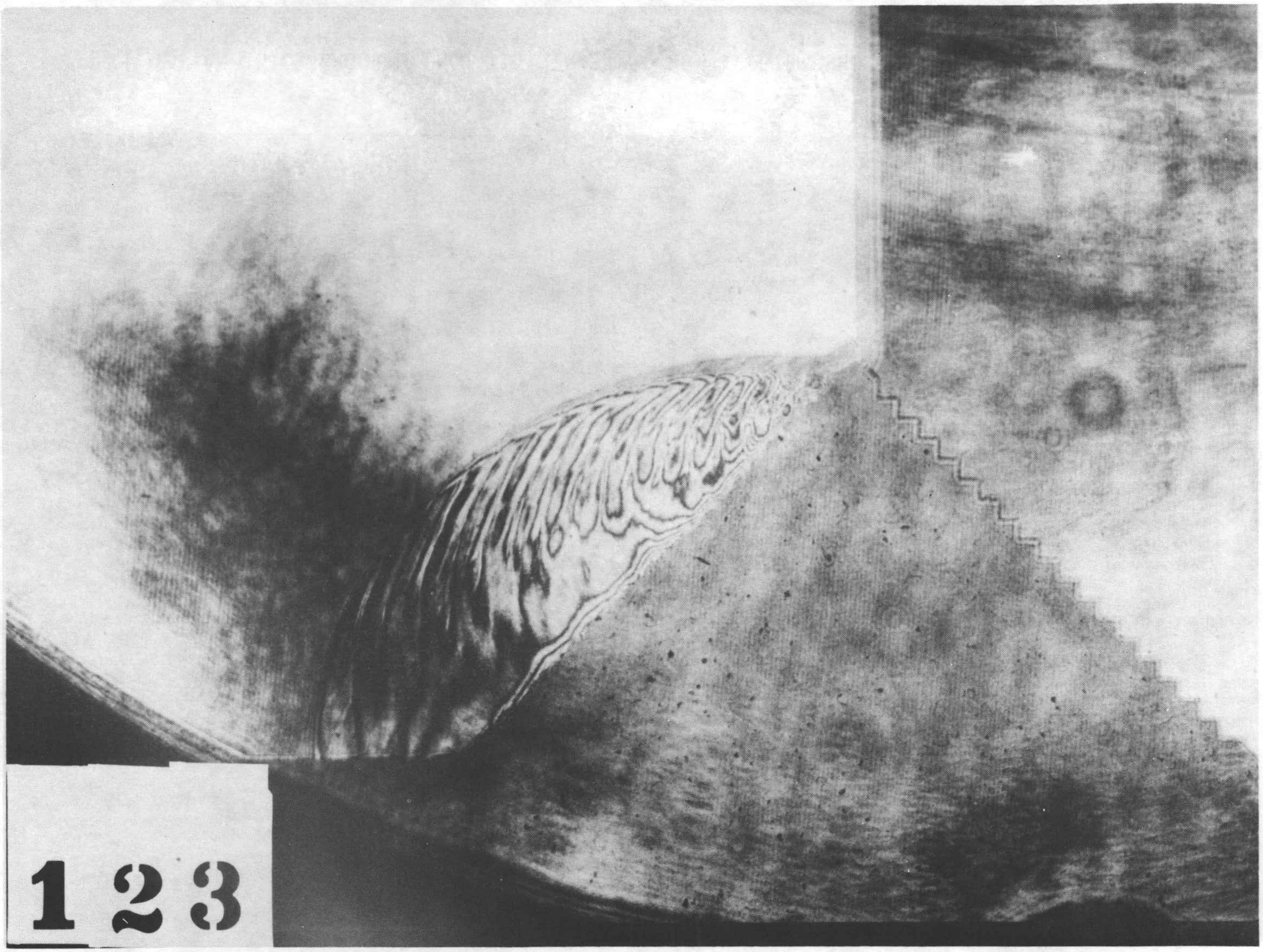

Fig. 16 INTERFEROGRAMS OF DIFFRACTION OF PLANAR SHOCK WAVE OVER A HALF - DIAMOND CYLINDER IN AIR FOR EFFECTS OF SAW - TOOTH MODEL, $M_s=1.60$, $M_1'=0.69$, SUBSONIC FLOW.

(a) AN INTERFEROGRAM (No. 123) TAKEN AT 56 μs AFTER SHOCK WAVE HITS CORNER; $M_s=1.58$, $M_1'=0.67$; $P_0=32.66$KPa, $\rho_0=38.30\times10^{-2}$kg/m^3, $T_0=297.4$°K

(b) AN INTERFEROGRAM (No. 121) TAKEN AT 89 μs AFTER SHOCK WAVE HITS CORNER; $M_s=1.59$, $M_1'=0.68$; $P_0=32.66$KPa, $\rho_0=38.30\times10^{-2}$kg/m^3, $T_0=297.4$°K

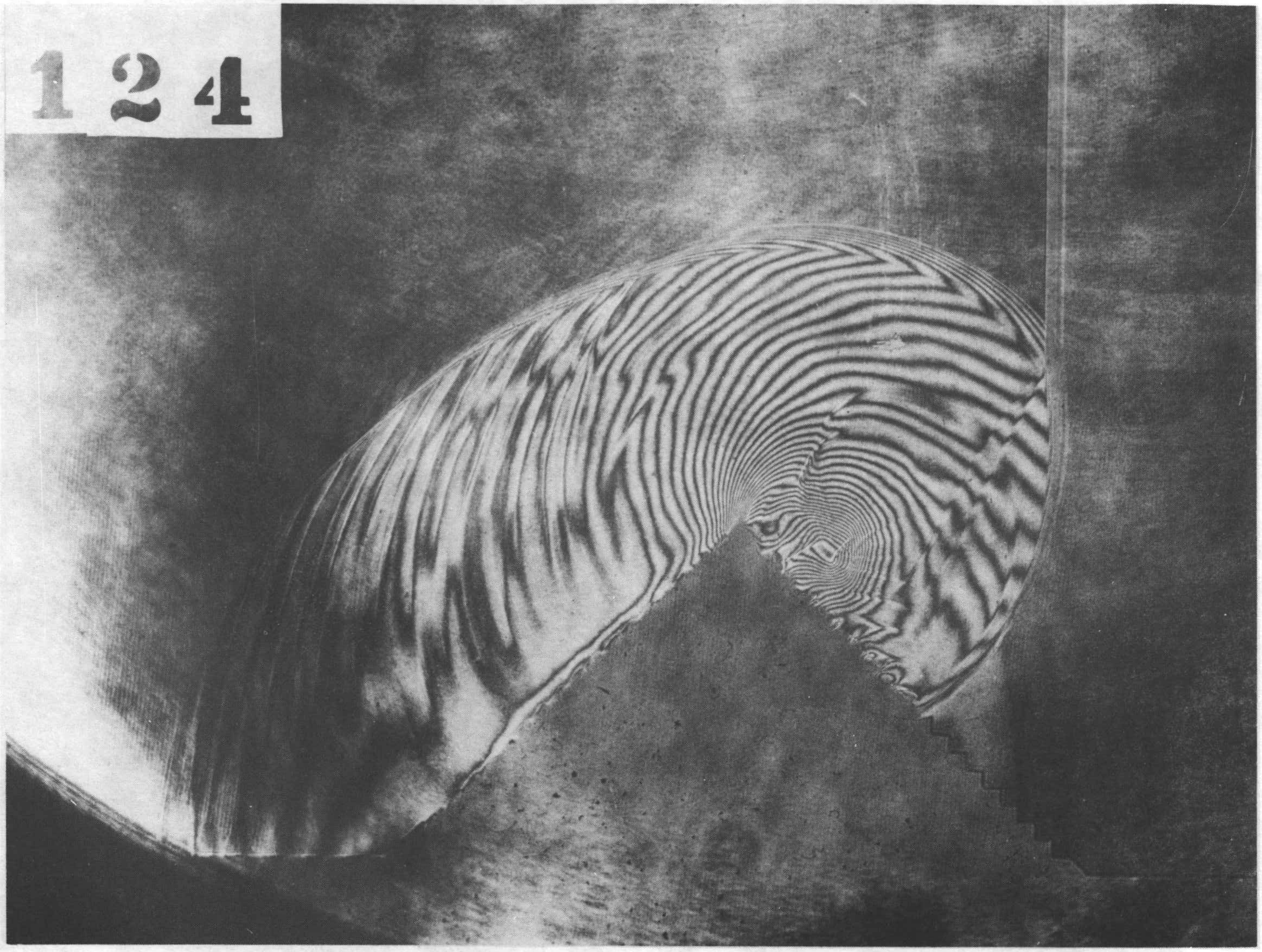

(c) AN INTERFEROGRAM (No. 124) TAKEN AT 100 μs AFTER SHOCK WAVE HITS CORNER; M_s=1.59, M_1'=0.68; P_0=32.66KPa, ρ_0=38.25x10^{-2}kg/m^3, T_0=297.8°K

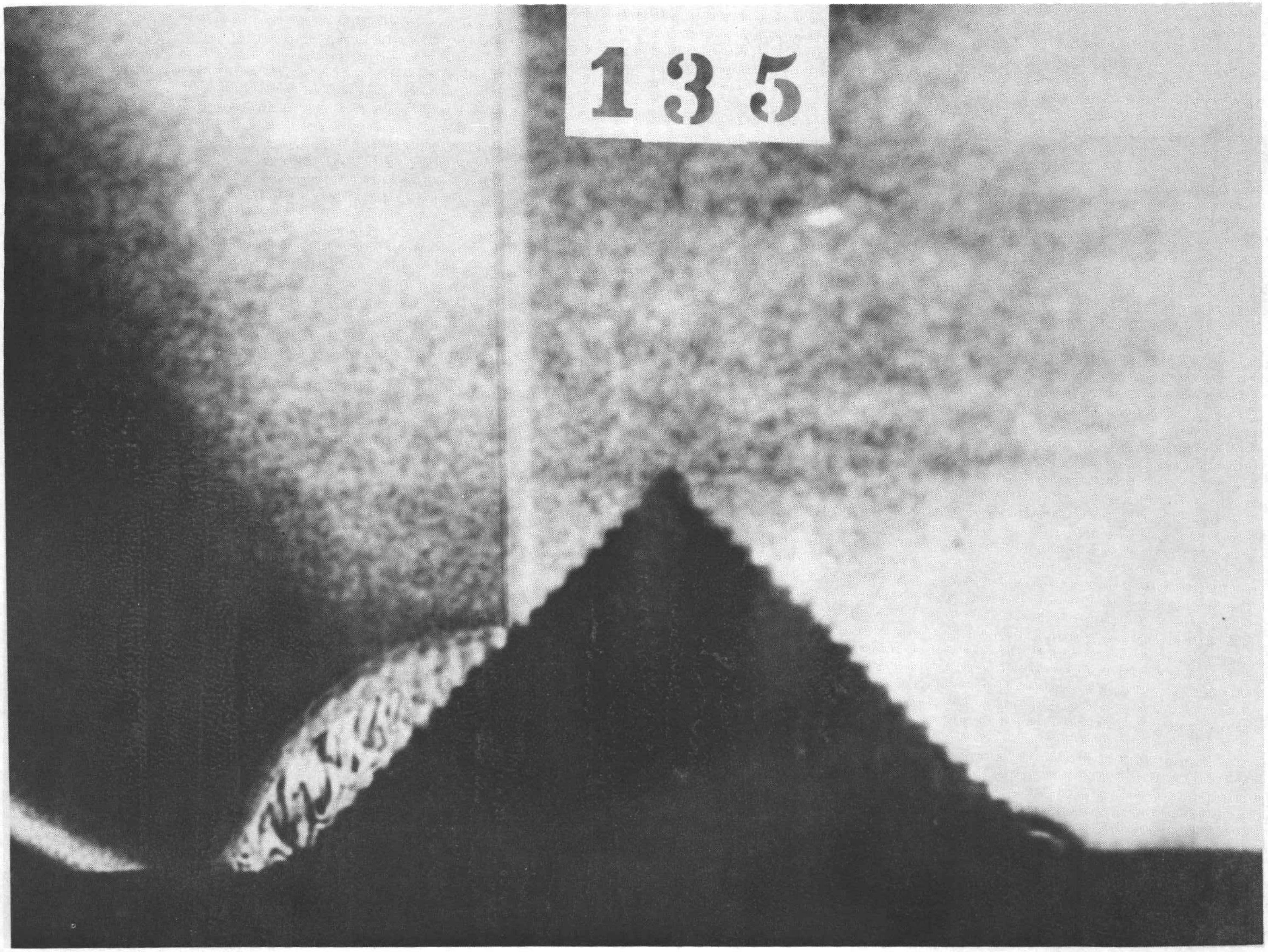

Fig. 17 INTERFEROGRAMS OF DIFFRACTION OF PLANAR SHOCK WAVE OVER A HALF - DIAMOND CYLINDER IN AIR FOR EFFECTS OF SAW - TOOTH MODEL, $M_s=2.45$, $M_1'=1.17$, SUPERSONIC FLOW.

(a) AN INTERFEROGRAM (No. 135) TAKEN AT 19 μs AFTER SHOCK WAVE HITS CORNER; $M_s=2.47$, $M_1'=1.18$; $P_0=7.73$KPa, $\rho_0=9.13\times10^{-2}$kg/m^3, $T_0=295.2$°K

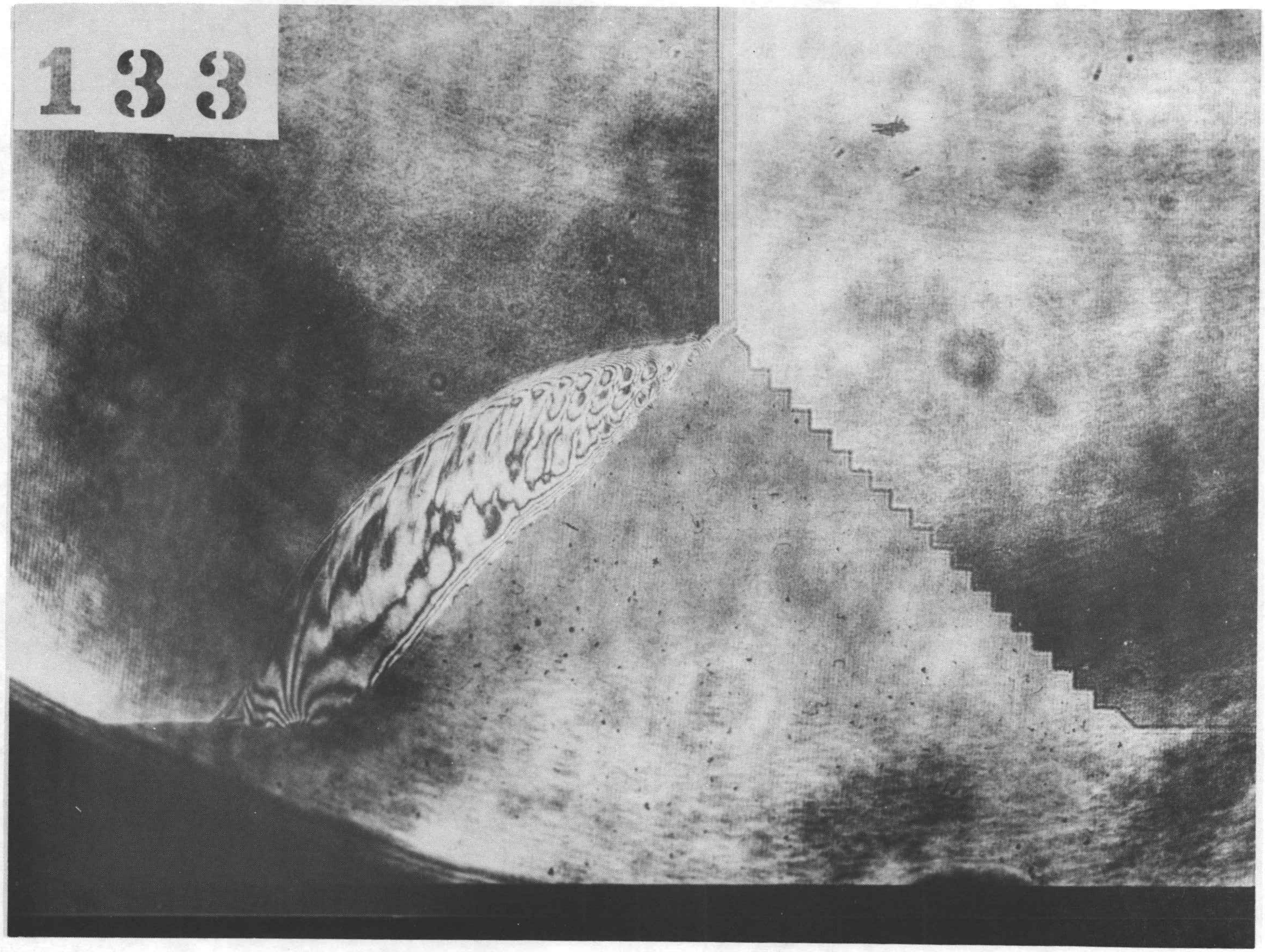

(b) AN INTERFEROGRAM (No. 133) TAKEN AT 33 μs AFTER SHOCK WAVE HITS CORNER; M_S=2.43, M_1'=1.15; P_0=9.33KPa, ρ_0=10.91x10^{-2}kg/m^3, T_0=298.2°K

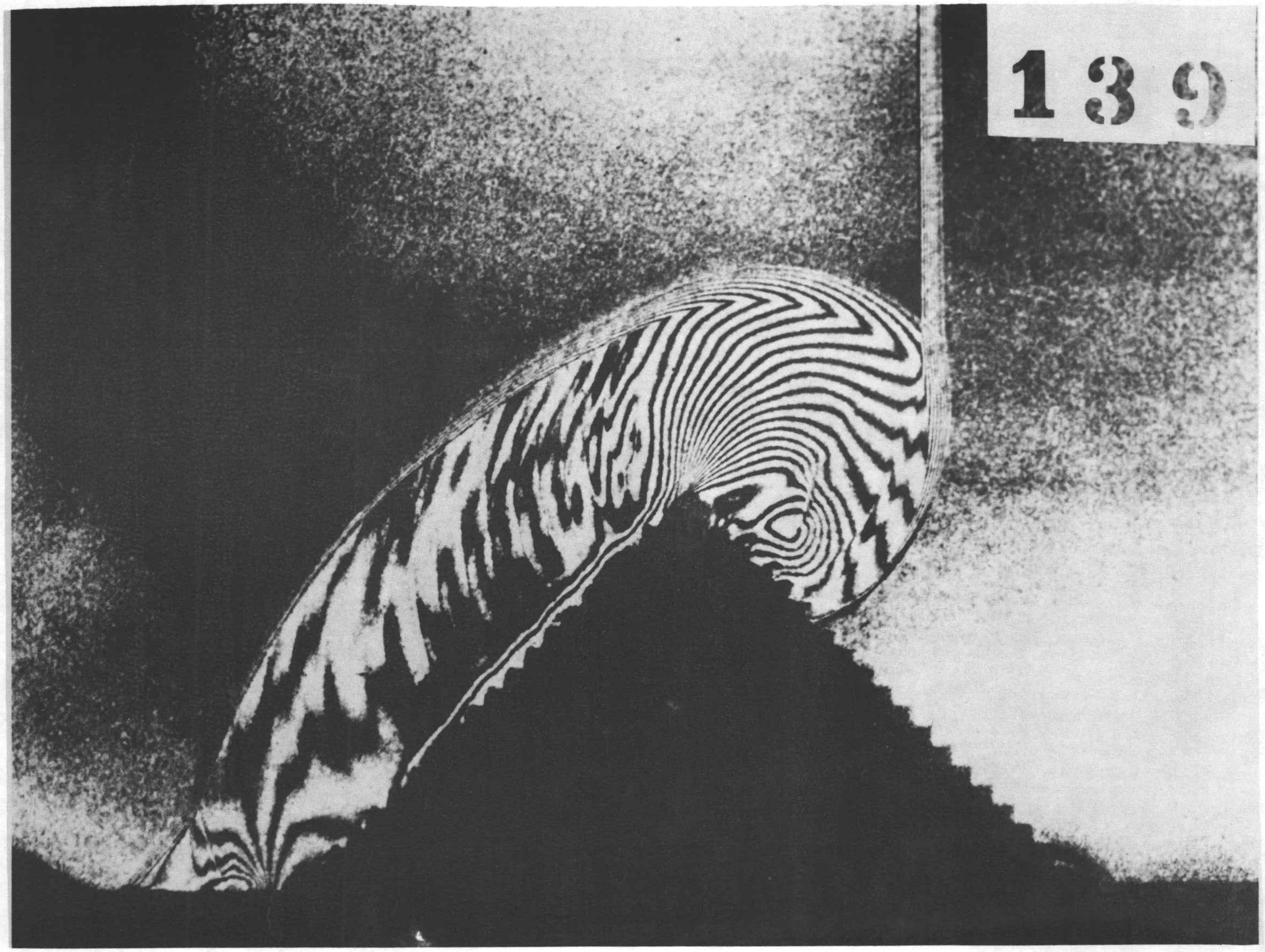

(c) AN INTERFEROGRAM (No. 139) TAKEN AT 55 μs AFTER SHOCK WAVE HITS CORNER; $M_S=2.47$, $M_1'=1.18$; $P_0=7.60$Kpa, $\rho_0=8.98\times10^{-2}$kg/m^3, $T_0=295.2$°K

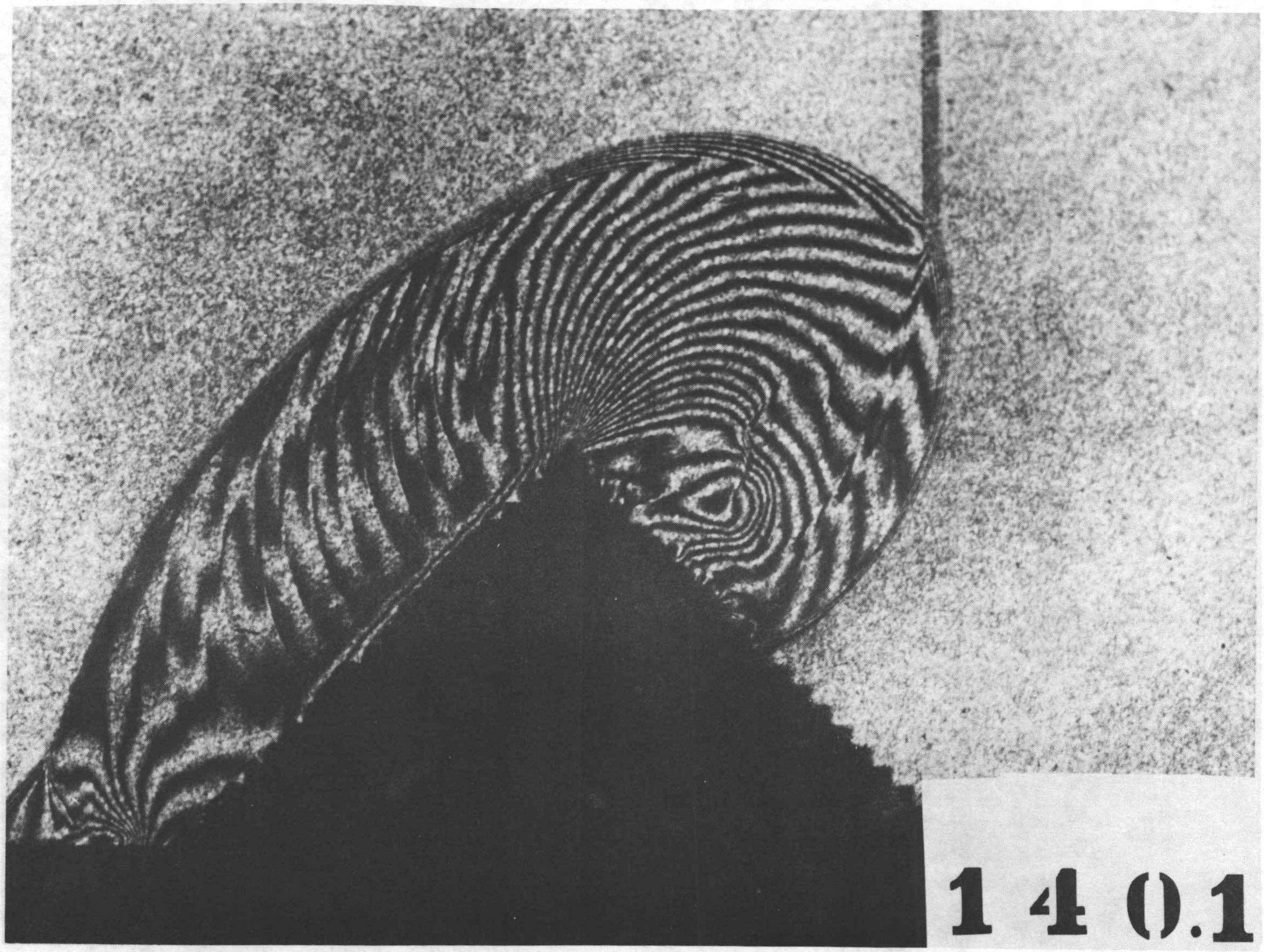

(d) AN INTERFEROGRAM (No. 140.1) TAKEN AT 65 μs AFTER SHOCK WAVE HITS CORNER; $M_s=2.44$, $M_1'=1.16$; $P_0=9.33$KPa, $\rho_0=10.97\times10^{-2}$kg/m^3, $T_0=296.7$°K

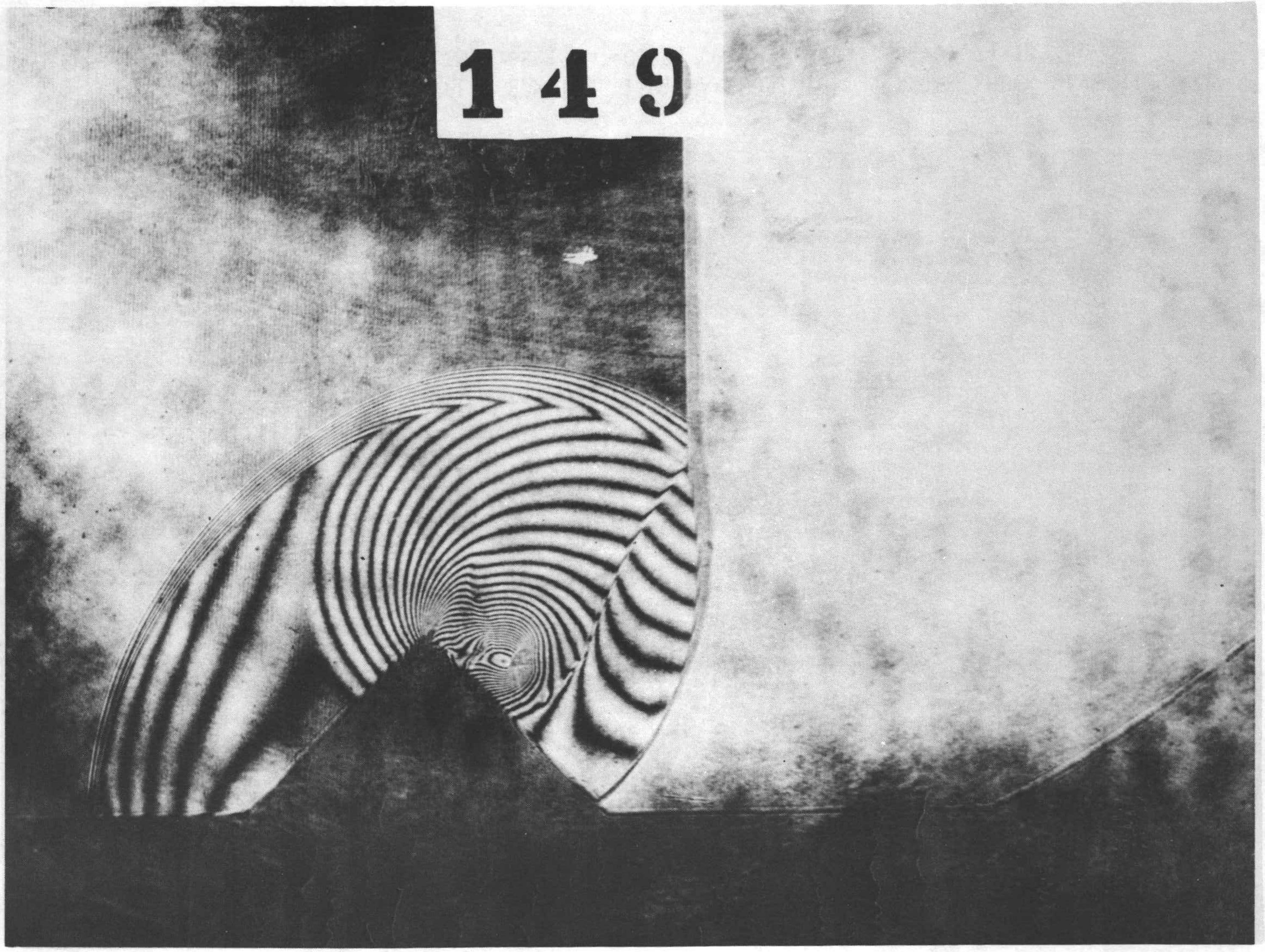

Fig. 18 INTERFEROGRAMS OF DIFFRACTION OF PLANAR SHOCK WAVE OVER A HALF - DIAMOND CYLINDER IN AIR FOR LONG - DURATION FLOWFIELD, $M_s=1.60$, $M_1'=0.69$, SUBSONIC FLOW.

(a) AN INTERFEROGRAM (No. 149) TAKEN AT 67 μs AFTER SHOCK WAVE HITS CORNER; $M_s=1.59$, $M_1'=0.68$; $P_0=32.26$KPa, $\rho_0=37.90\times10^{-2}$kg/m^3, $T_0=296.9$°K

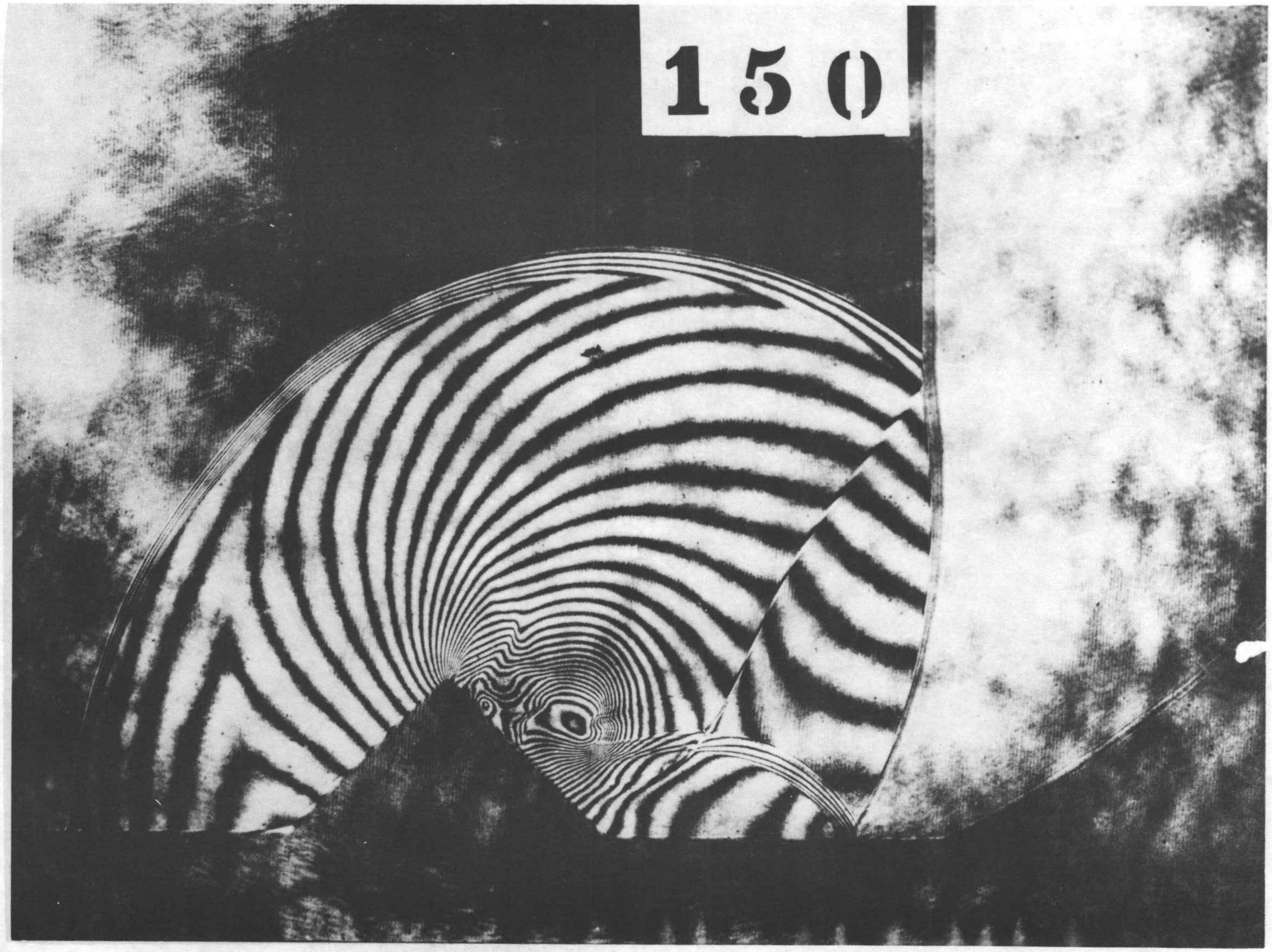

(b) AN INTERFEROGRAM (No. 150) TAKEN AT 105 μs AFTER SHOCK WAVE HITS CORNER; $M_s=1.59$, $M_1'=0.68$; $P_0=32.13$KPa, $\rho_0=37.74\times10^{-2}$kg/m^3, $T_0=296.9$°K

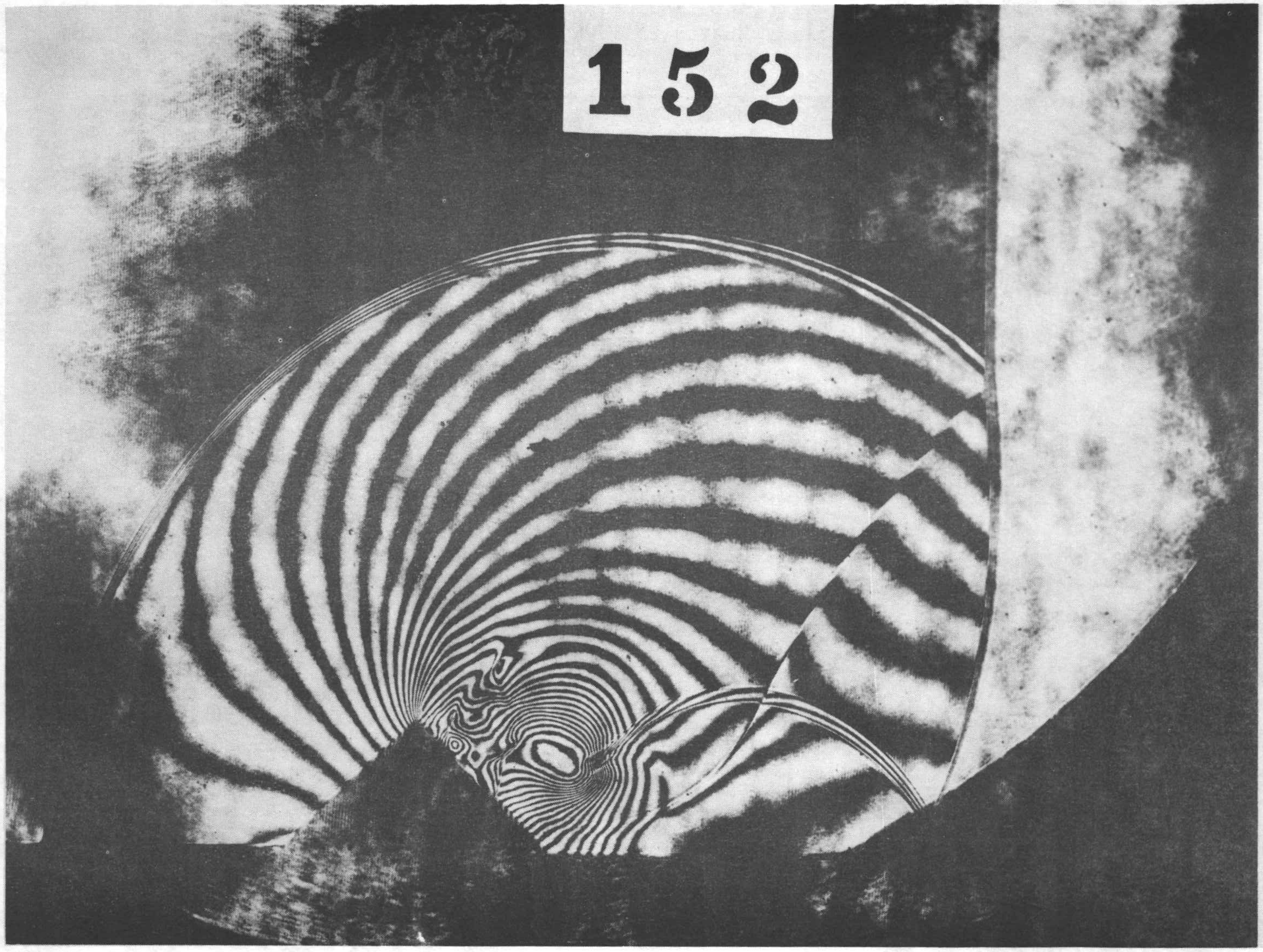

(c) AN INTERFEROGRAM (No. 152) TAKEN AT 142 μs AFTER SHOCK WAVE HITS CORNER; $M_s=1.59$, $M_1'=0.68$; $P_0=32.13$KPa, $\rho_0=37.74\times10^{-2}$kg/m^3, $T_0=296.9$°K

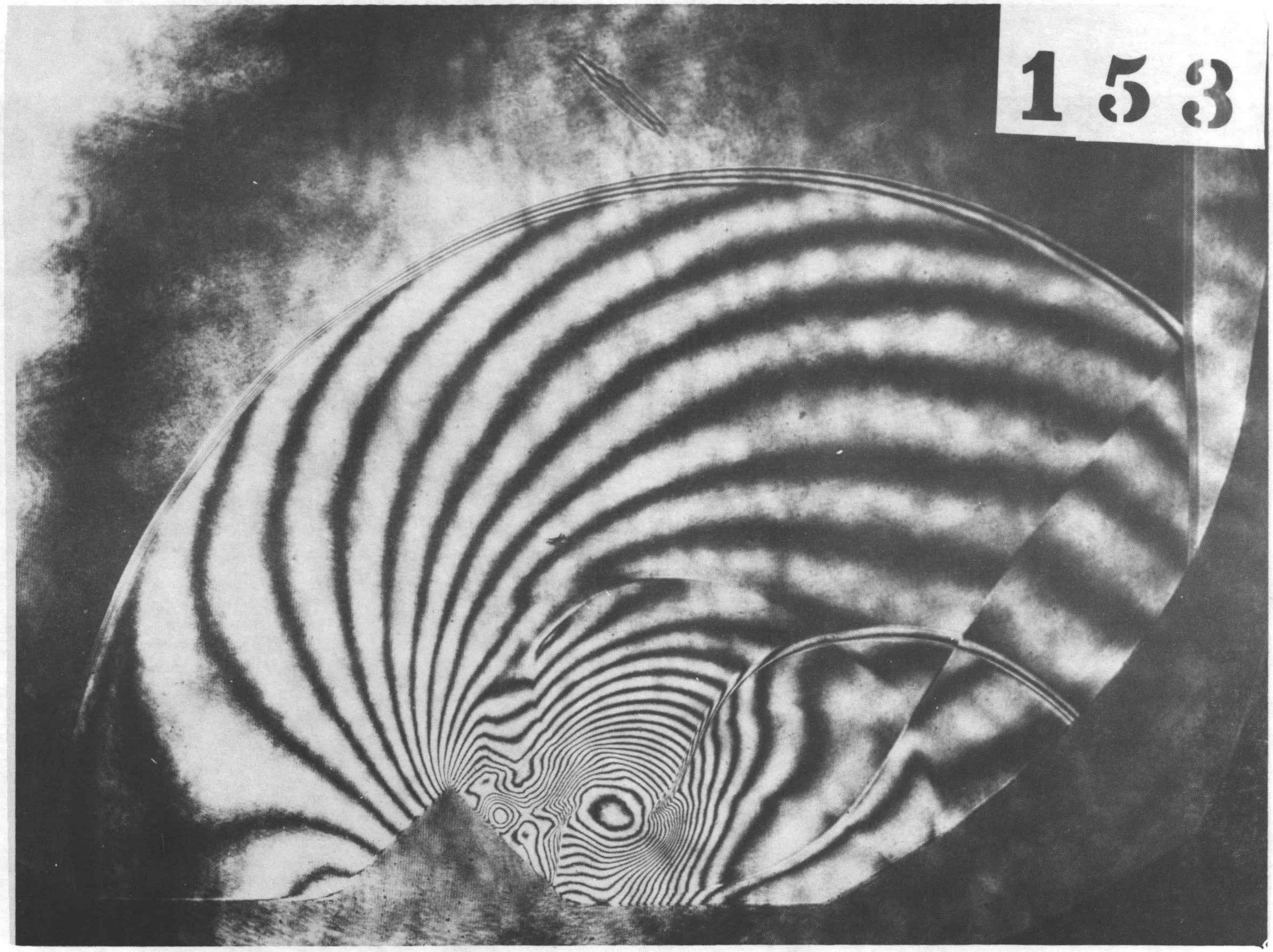

(d) AN INTERFEROGRAM (No. 153) TAKEN AT 192 μs AFTER SHOCK WAVE HITS CORNER; $M_S=1.59$, $M_1'=0.68$; $P_0=32.13$KPa, $\rho_0=37.72\times10^{-2}$kg/m^3, $T_0=297.1$°K

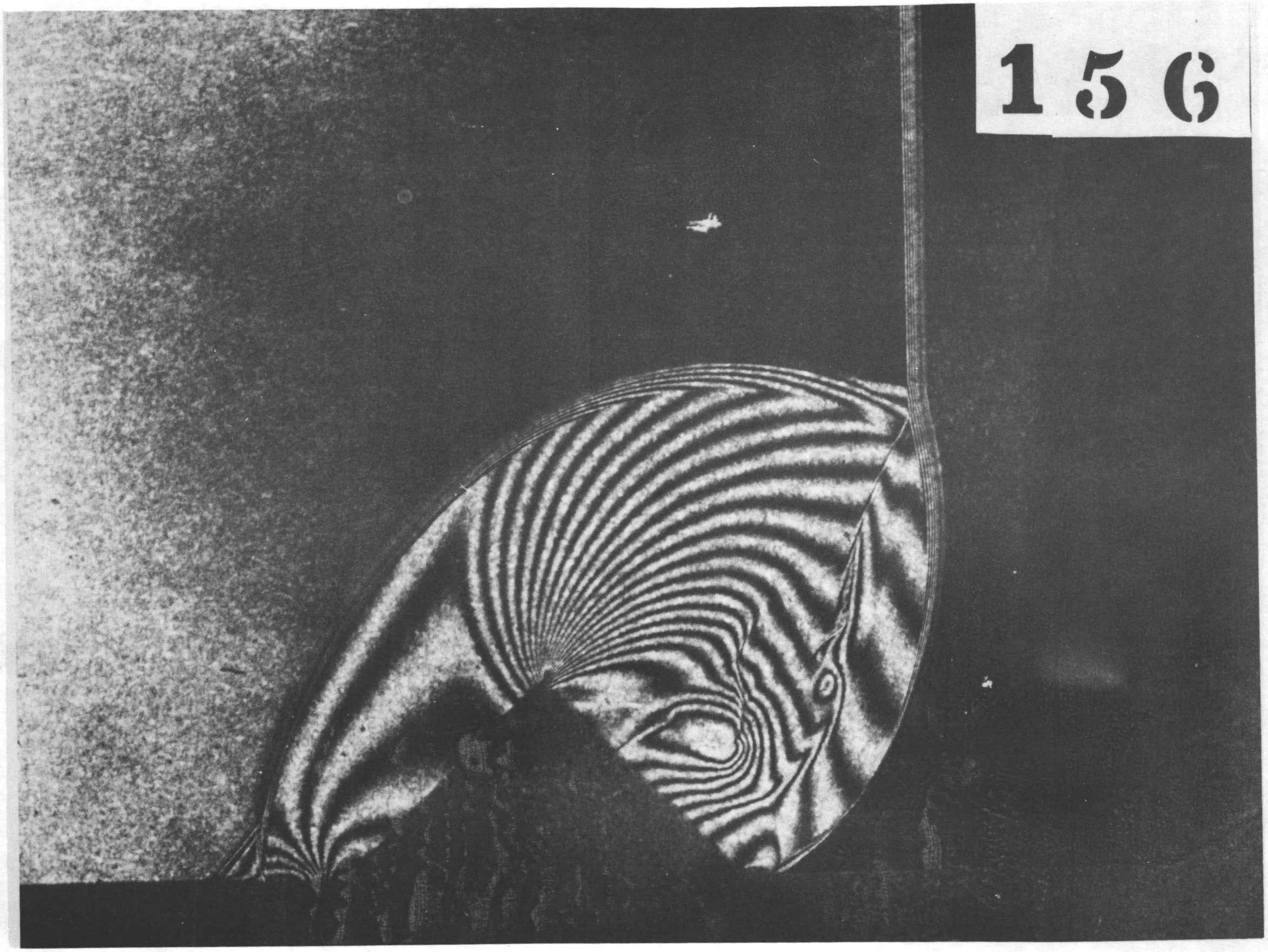

Fig. 19 INTERFEROGRAMS OF DIFFRACTION OF PLANAR SHOCK WAVE OVER A HALF - DIAMOND CYLINDER IN AIR FOR LONG - DURATION FLOWFIELD, $M_s=2.45$, $M_1'=1.17$, SUPERSONIC FLOW.

(a) AN INTERFEROGRAM (No. 156) TAKEN AT 48 μsAFTER SHOCK WAVE HITS CORNER; $M_s=2.48$, $M_1'=1.19$; $P_0=9.33$KPa, $\rho_0=11.0\times10^{-2}$kg/m^3, $T_0=296.0$°K

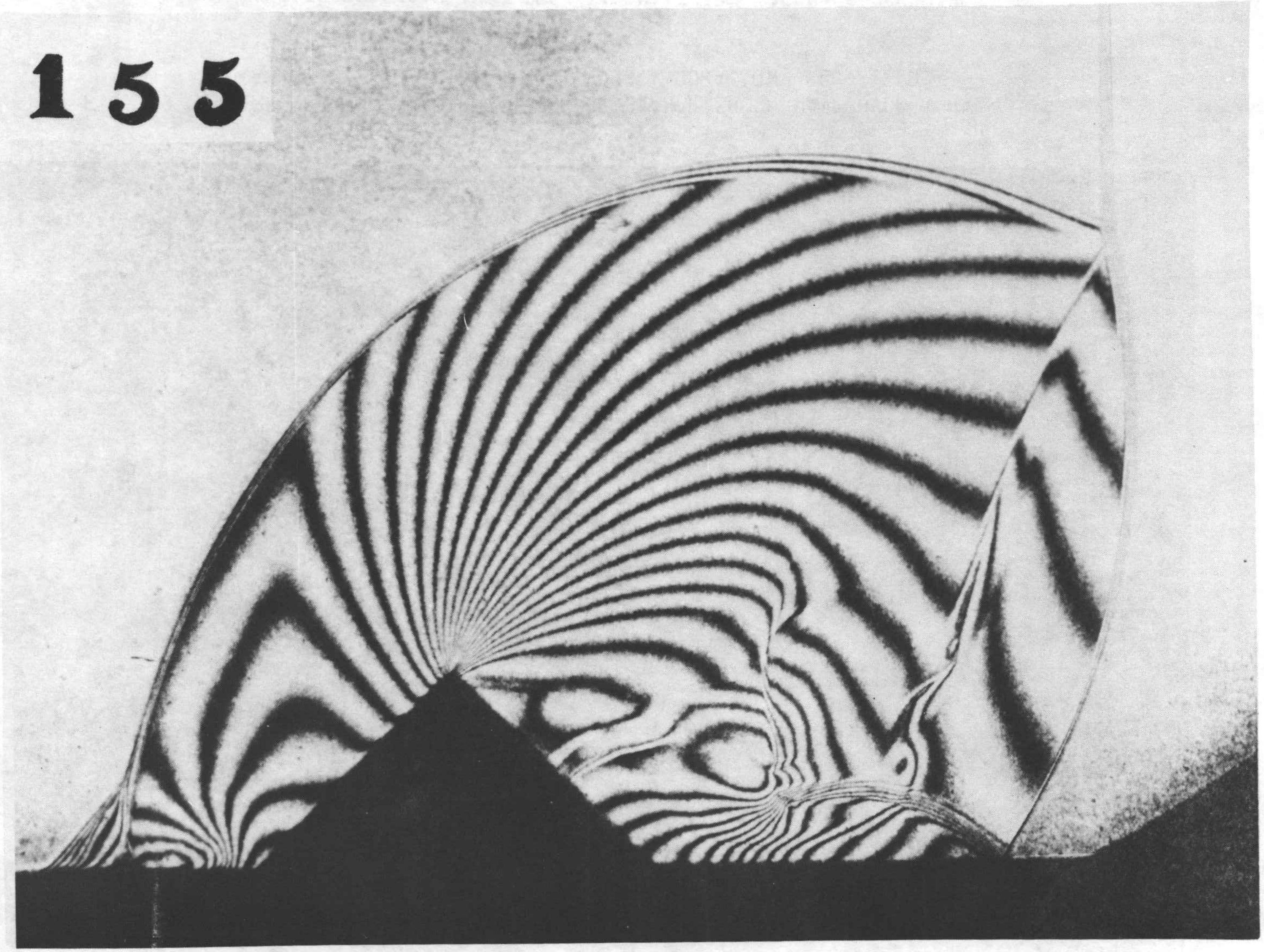

(b) AN INTERFEROGRAM (No. 155) TAKEN AT 70 μs AFTER SHOCK WAVE HITS CORNER; $M_S=2.49$, $M_1'=1.19$; $P_0=9.33$KPa, $\rho_0=11.00\times10^{-2}$kg/m^3, $T_0=295.9$°K

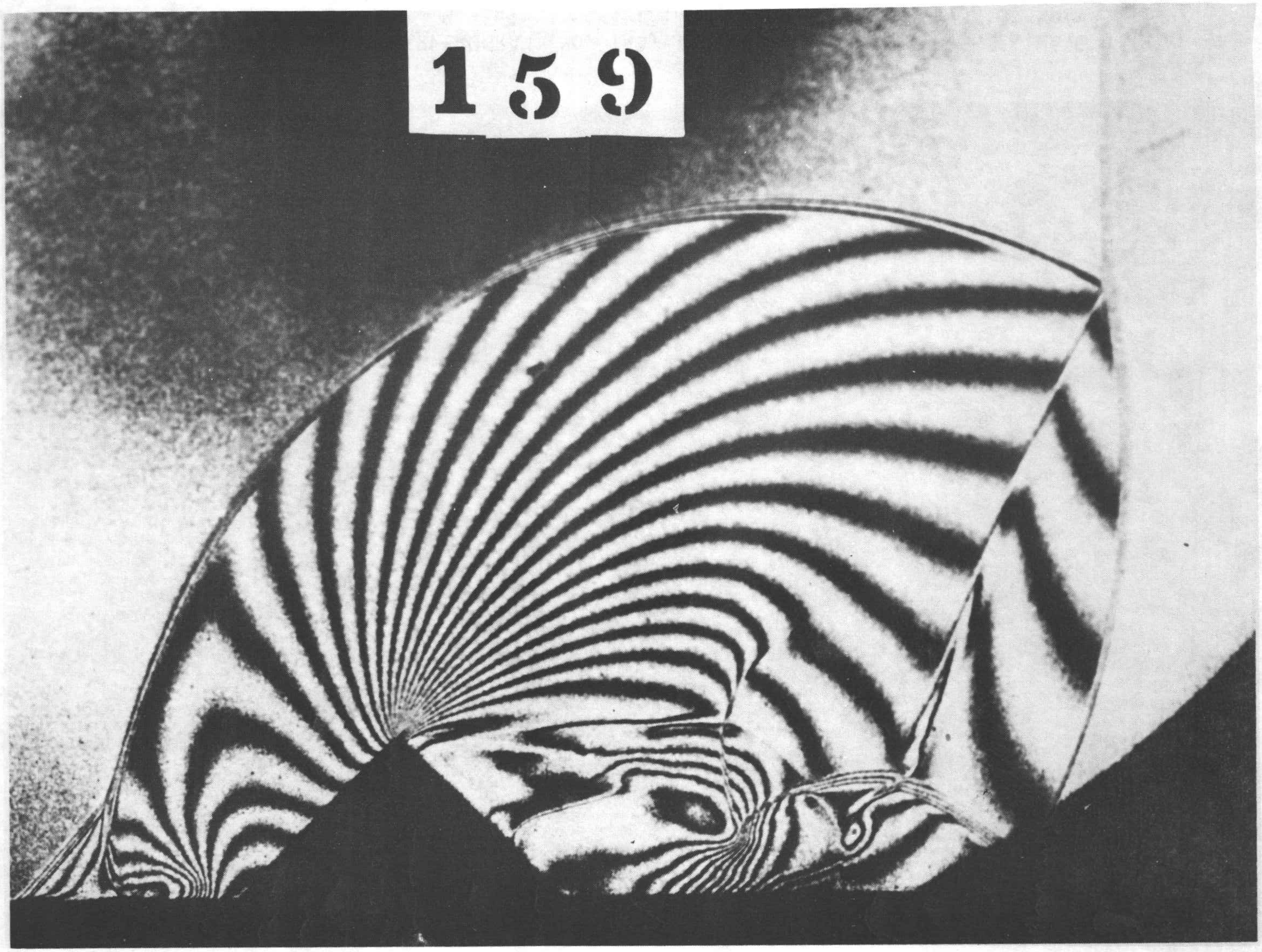

(c) AN INTERFEROGRAM (No. 159) TAKEN AT 89 μs AFTER SHOCK WAVE HITS CORNER; $M_S=2.48$, $M_1'=1.18$; $P_0=9.33$Kpa, $\rho_0=10.98\times10^{-2}$kg/m^3, $T_0=296.4$°K

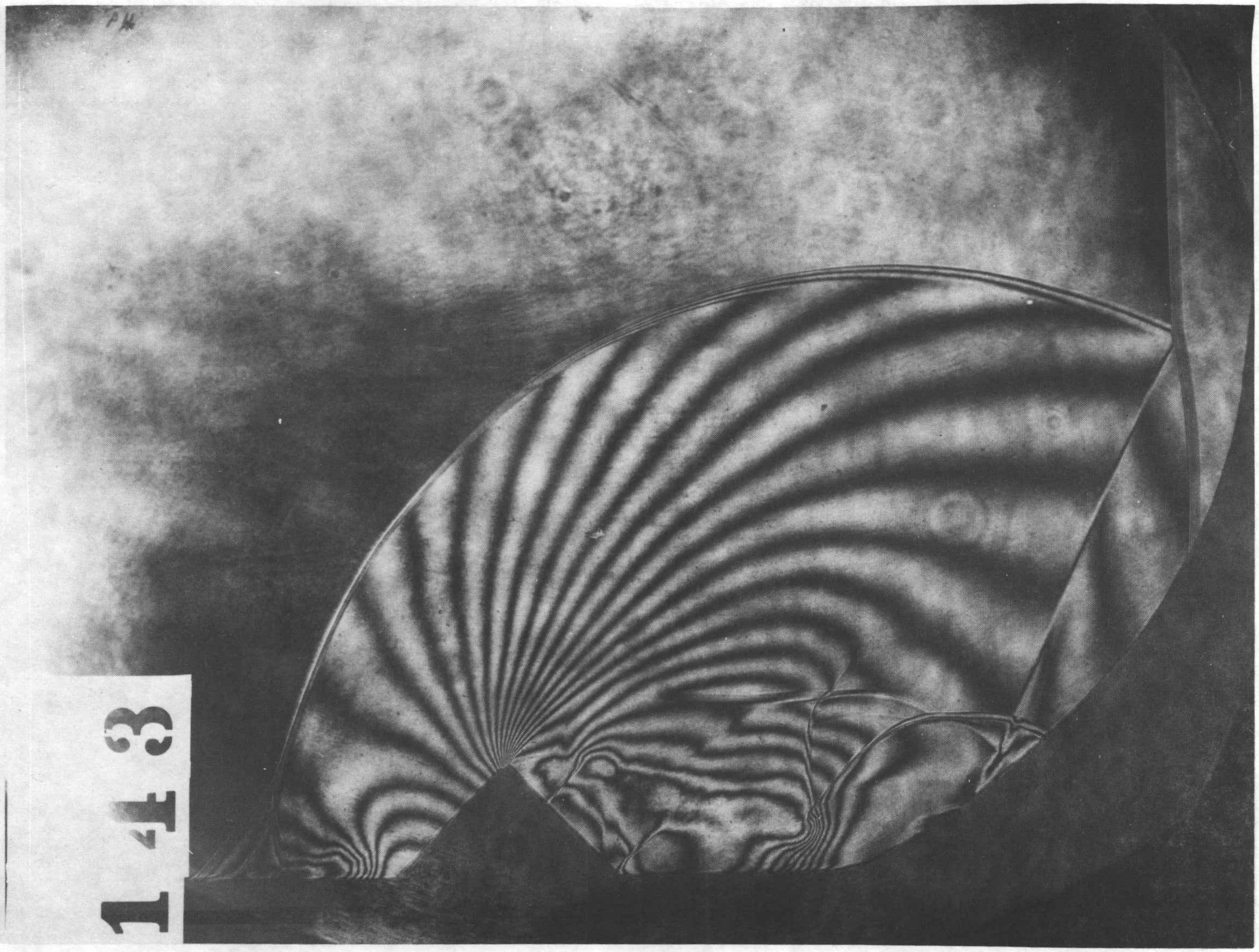

(d) AN INTERFEROGRAM (No. 143) TAKEN AT 116 μs AFTER SHOCK WAVE HITS CORNER; $M_s=2.46$, $M_1'=1.17$; $P_0=9.20$KPa, $\rho_0=10.73\times10^{-2}$kg/m^3, $T_0=298.9$°K

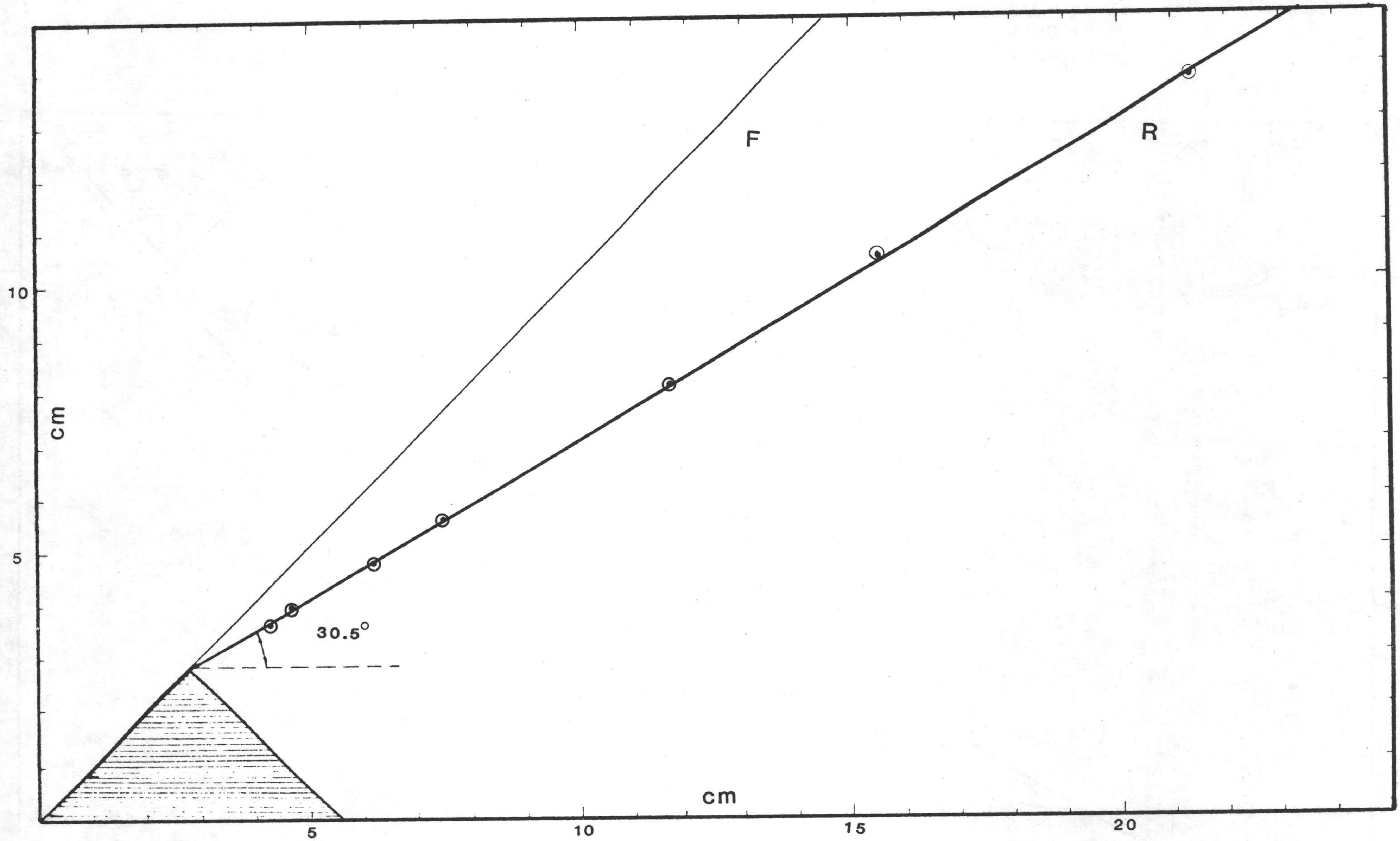

Fig. 20 TRACE OF TRIPLE POINT FOR PLANAR SHOCK WAVE OVER A HALF-DIAMOND CYLINDER IN AIR, F - TRACE AT THE FRONT FACE OF CYLINDER, R - TRACE AT THE REAR FACE OF CYLINDER, α - INCLINED ANGLE.

(a) TRACE OF TRIPLE POINT FOR SMR (M_s=1.60), α=30.5°.

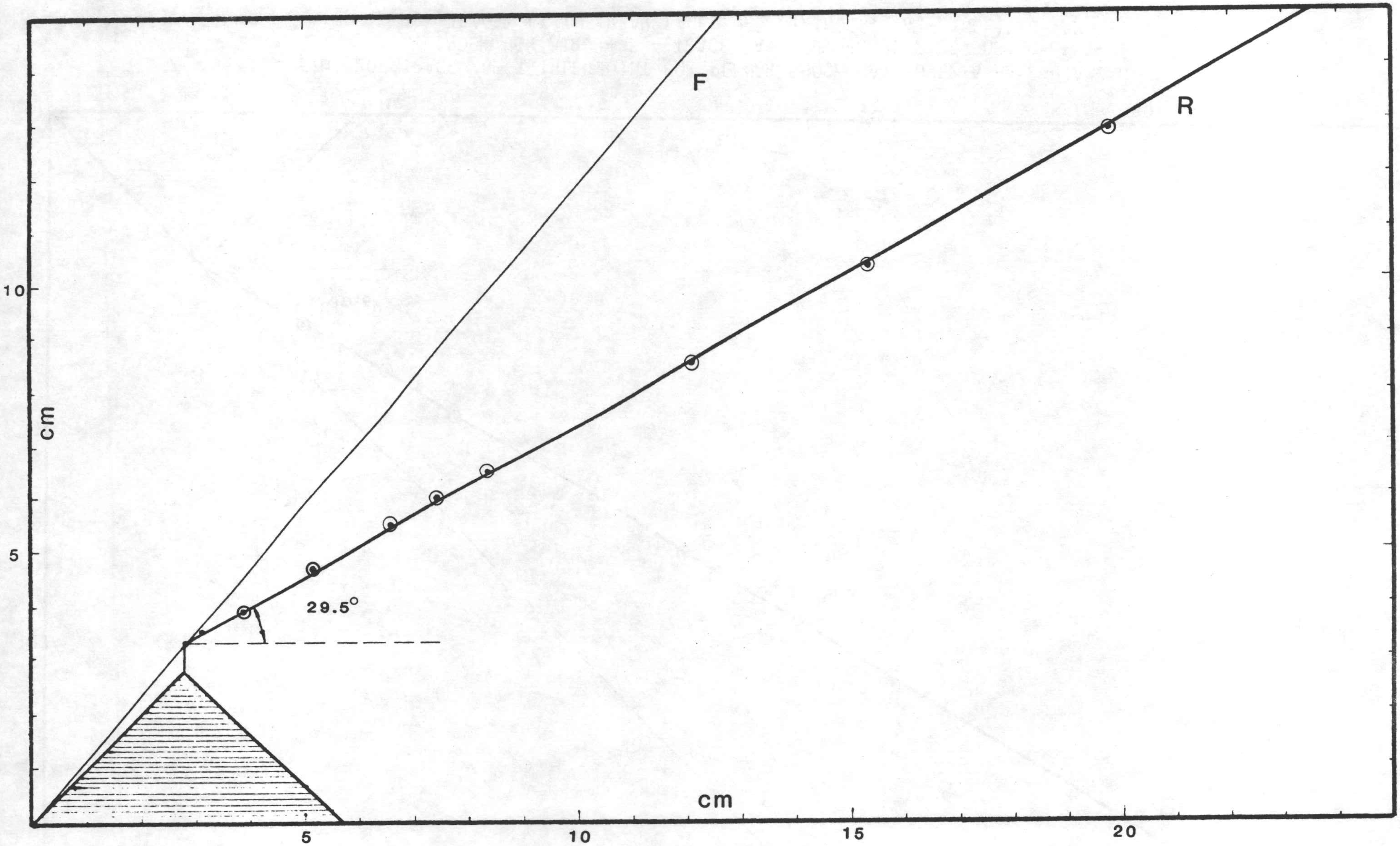

Fig. 20 TRACE OF TRIPLE POINT FOR PLANAR SHOCK WAVE OVER A HALF-DIAMOND CYLINDER IN AIR, F - TRACE AT THE FRONT FACE OF CYLINDER, R - TRACE AT THE REAR FACE OF CYLINDER, α - INCLINED ANGLE.

(b) TRACE OF RTIPLE POINT FOR CMR (M_S=2.45), α=29.5°.

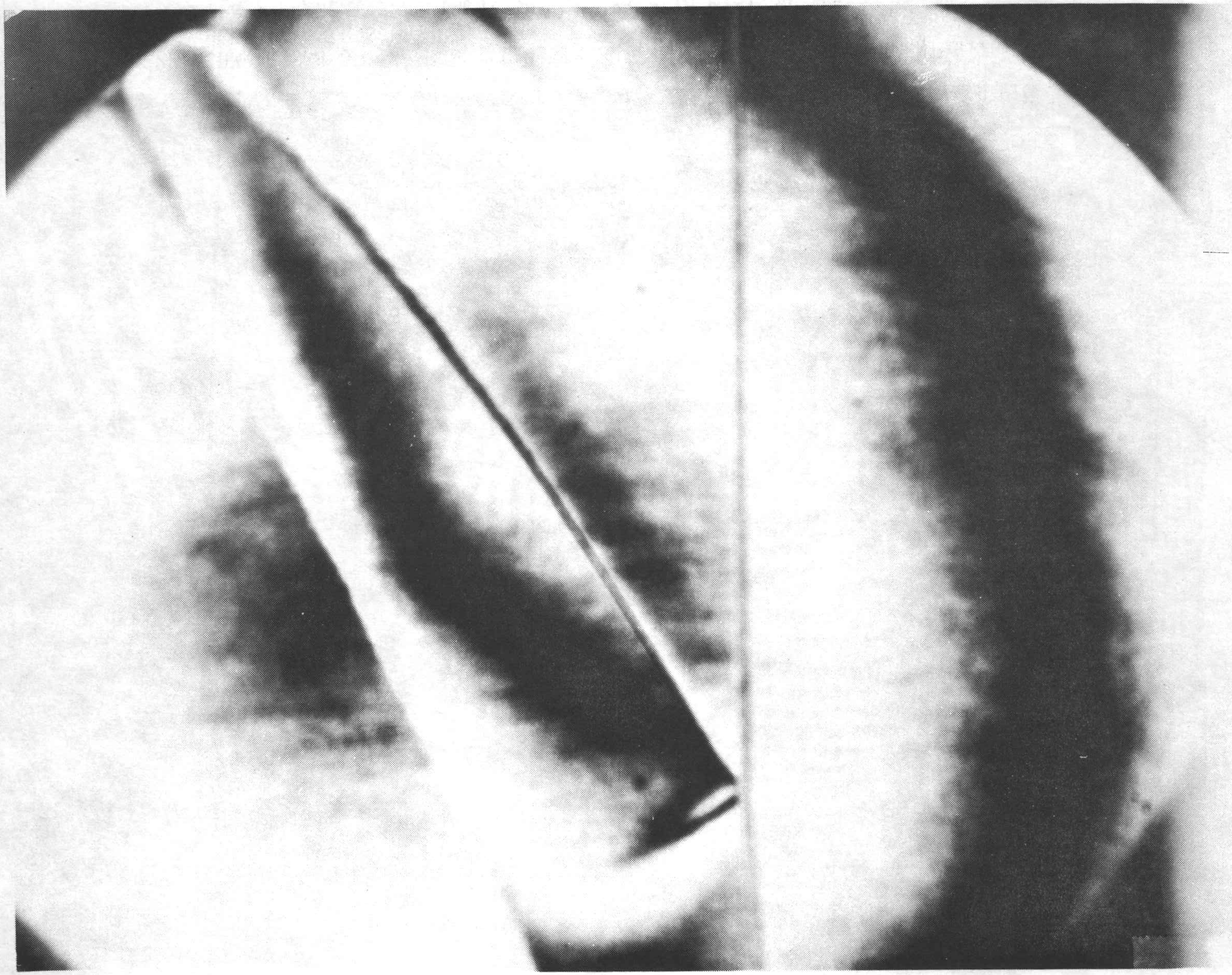

Fig. 21 THE CURVED INCIDENT BOW SHOCK WAVE REFORMS AS A PLANAR SHOCK WAVE

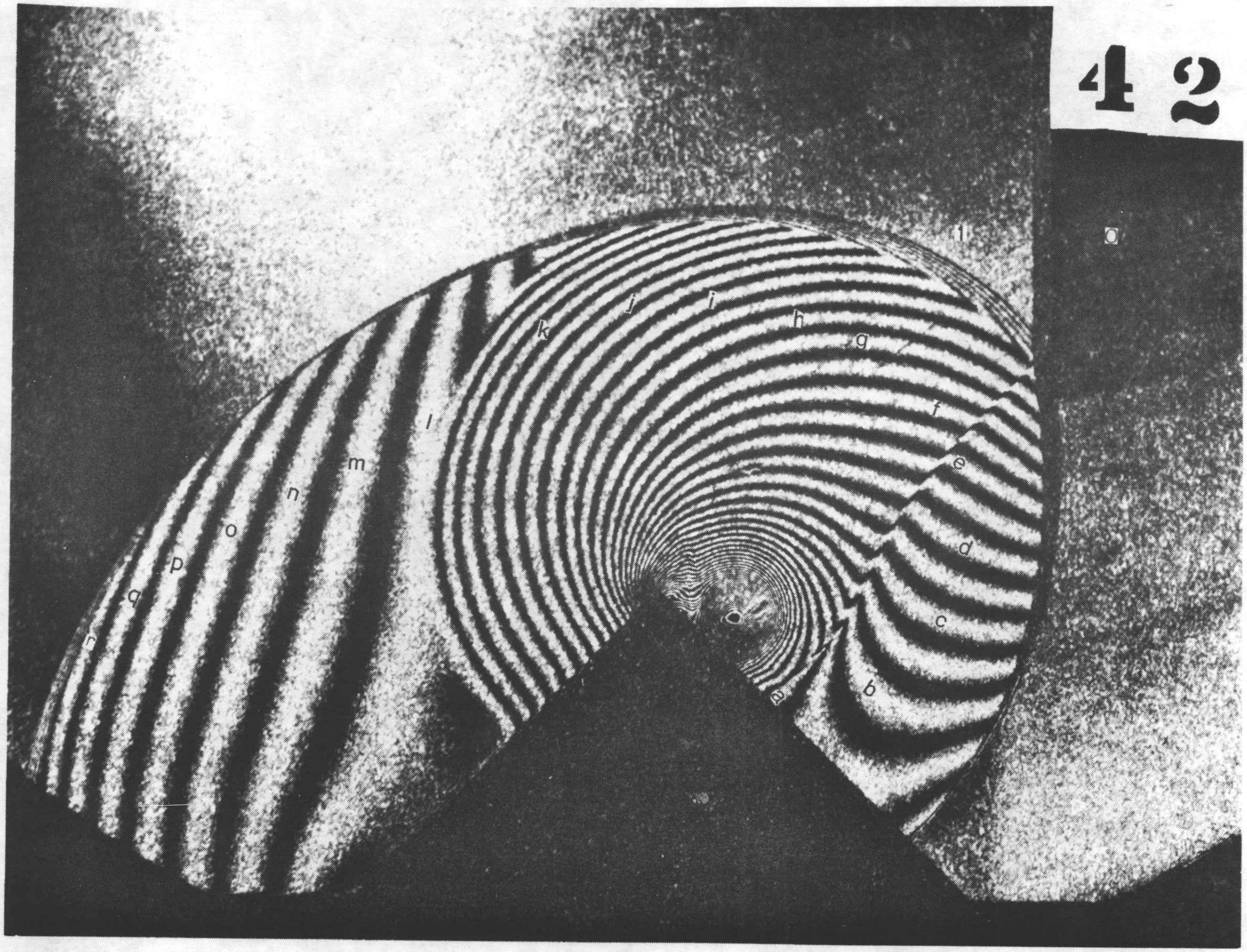

Fig. 22 COMPARISON OF THE DENSITY DISTRIBUTION OF PRESENT EXPERIMENT WITH BLEAKNEY'S RESULT.
(a) PRESENT EXPERIMENT No. 42, RR WITH M_s=1.36, t=138 μs.

Experiments No: 42 , Type of reflection: RR
Test gas: Air , Driver gas: He
shock velocity: 470.73 m/s, Mach number: 1.36
Model: 45° half-diamond, Mach number behind shock 0.47
picture taken time 138 μs after collision with wedge

Initial condition:
P_0 = 80.51 kpa, ρ_0 = 94.08 $\times10^{-2}$ kg/m³, T_0 = 298.5 °k

Parameters behind shock wave:
P_1 = 160.21 kpa, ρ_1 = 152.41 $\times10^{-2}$ kg/m³, T_1 = 370.1 °K
P_2 = ______ kpa, ρ_2 = ______ $\times10^{-2}$ kg/m³, T_2 = ______ °K
P_3 = ______ kpa, ρ_3 = ______ $\times10^{-2}$ kg/m³, T_3 = ______ °K

Wave lenght of light source: 6943 Å, $\nabla\rho/\rho_0$ = 0.032

Region	ρ/ρ_0	Fringe	ρ/ρ_0	Fringe	ρ/ρ_0
(0)	1.00	p	1.81		
(1)	1.62	q	1.78		
(2)		r	1.75		
(3)					
Fringe					
a	1.33				
b	1.40				
c	1.46				
d	1.52				
e	1.59				
f	1.65				
g	1.72				
h	1.75				
i	1.81				
j	1.88				
k	1.94				
l	1.94				
m	1.91				
n	1.88				
o	1.84				

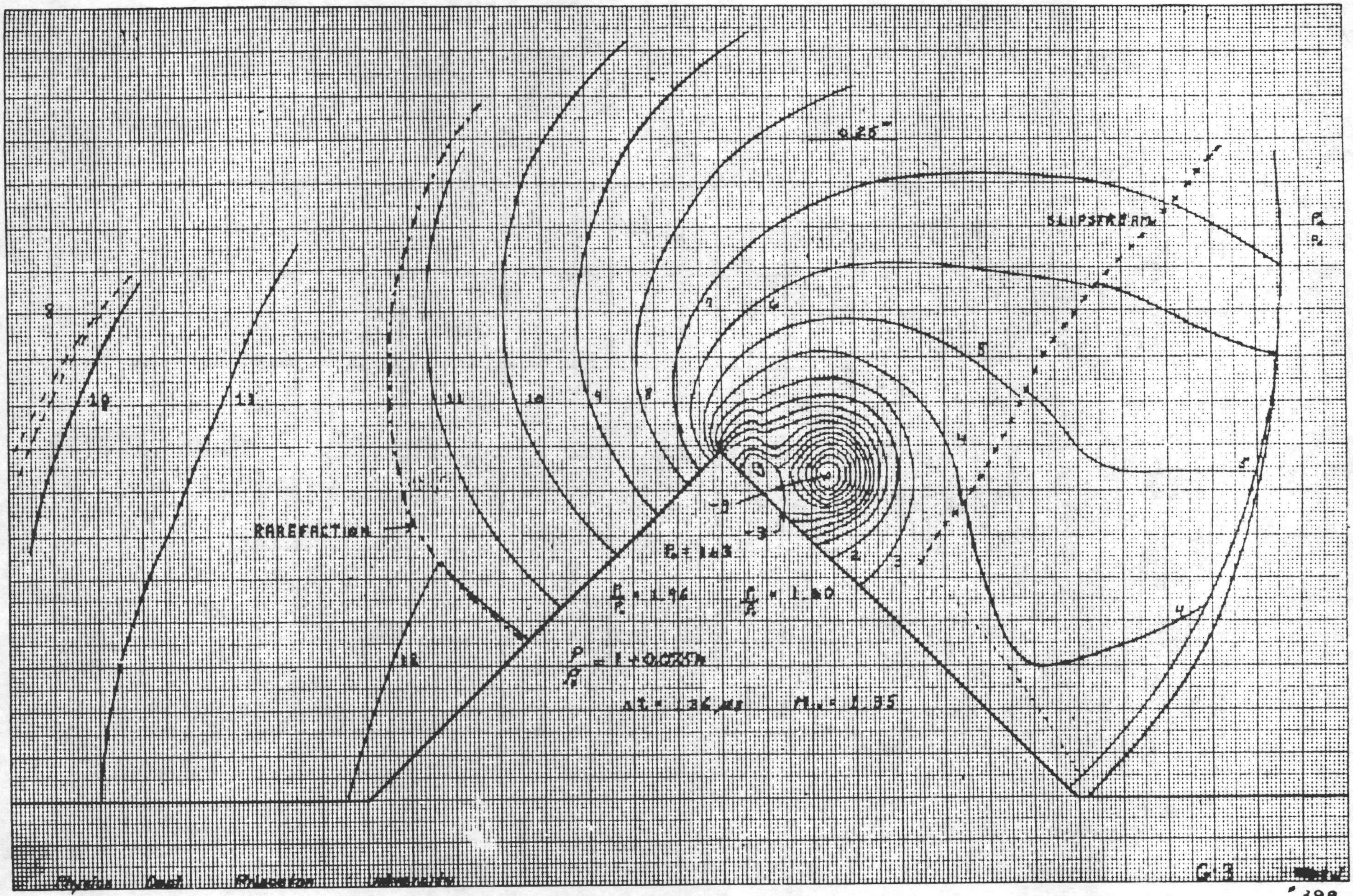

(b) BLEAKNEY'S RESULT OF RR WITH M_s=1.35, t=136 μs.

BLEAKNEY'S RESULT

Experiments No:______, Type of reflection: RR
Test gas: Air , Driver gas: Air
shock velocity: 466.32 m/s, Mach number: 1.35
Model: 45° half-diamond, Mach number behind shock 0.46
picture taken time 136 μs after collision with wedge

Initial condition:
P_0= 21.73 kpa, ρ_0= 25.59 $\times 10^{-2}$ kg/m^3, T_0= 296.2 °k

Parameters behind shock wave:
P_1= 42.59 kpa, ρ_1= 41.02 $\times 10^{-2}$ kg/m^3, T_1= 366.50°K
P_2=______kpa, ρ_2=______$\times 10^{-2}$ kg/m^3, T_2=______°K
P_3=______kpa, ρ_3=______$\times 10^{-2}$ kg/m^3, T_3=______°K

Wave lenght of light source:______Å, $\nabla\rho/\rho_0$=______

Region	ρ/ρ_0	Fringe	ρ/ρ_0	Fringe	ρ/ρ_0
(0)	1.00				
(1)	1.60				
(2)					
(3)					
Fringe					
1	1.08				
2	1.15				
3	1.23				
4	1.30				
5	1.38				
6	1.45				
7	1.53				
8	1.60				
9	1.68				
10	1.75				
11	1.83				
12	1.90				
13	1.98				
14	2.05				
15	2.13				

APPENDIX A

CALCULATION OF PRESSURE DISTRIBUTION AND TOTAL LOAD

In order to give the readers a feeling for the pressure distribution and total load and to illustrate the method of computation, using the equations described in Section 7.3

$$P/P_0=(P_2/P_0)(\rho_0/\rho_2)^\gamma(\rho/\rho_0)^\gamma,$$

the pressure distribution and total load on the front and rear faces are plotted in Figs. A-1 and A-2. These figures, obtained from Fig. 7 (a, b, c, d, e), correspond to the case of $M_S = 1.35$. As shown in Fig. A-1, the number attached to each curve is the dimensionless time. The ordinate is the pressure in atmospheres (given by $(P - P_0)/P_0$). The time is made nondimensional by dividing the actual time by t_0 (59 μs), which is the time taken by the shock wave to go from the corner to the apex. The area between each curve and the corresponding face is a measure of the total force on that face at the designated time, which is plotted in Fig. A-2. In Fig. A-2, the relation between the total load (kg) and time (μs) are shown.

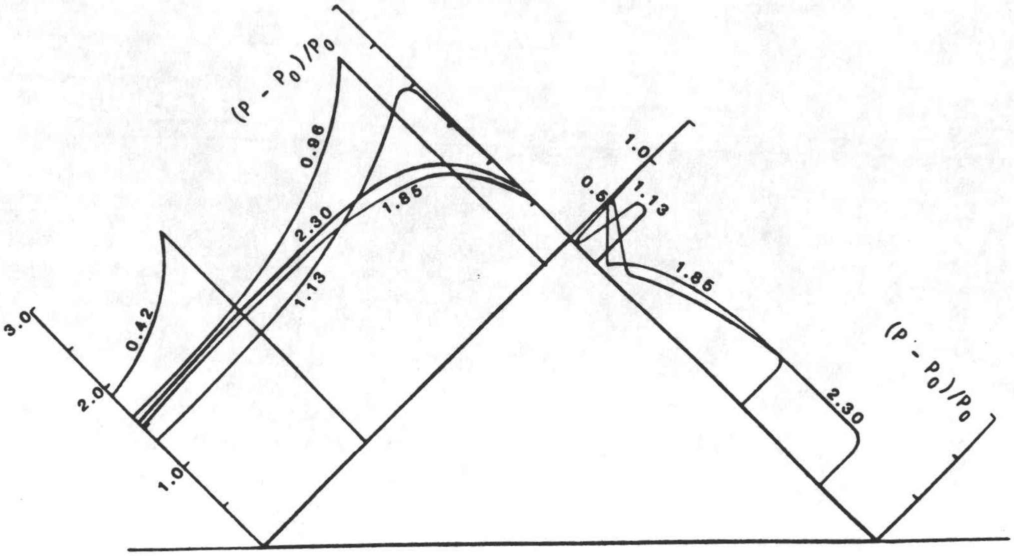

Fig. A-1 PRESSURES ON FACES OF HALF-DIAMOND CYLINDER AT VARIOUS DIMENSIONLESS TIMES, PLOTTED VERTICALLY TO CORRESPONDING FACE.

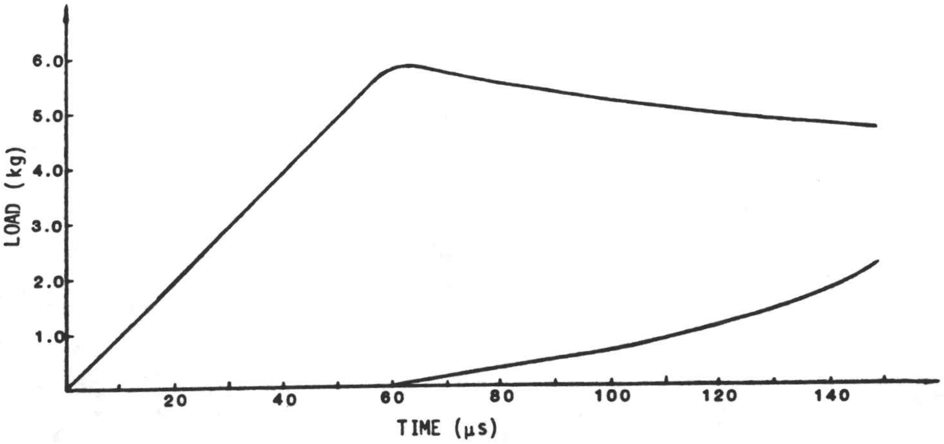

Fig. A-2 TOTAL LOAD ON EACH FACE AS FUNCTION OF TIME. (EACH POINT REPRESENTS AREA UNDER A CURVE SUCH AS THOSE APPEARING IN FIG. A-1, THE LENGTH OF CORRESPONDING FACE BEING TAKEN AS UNITY.)

UTIAS Report No. 322

University of Toronto, Institute for Aerospace Studies (UTIAS)
4925 Dufferin Street, Downsview, Ontario, Canada, M3H 5T6

AN INTERFEROMETRIC INVESTIGATION OF THE DIFFRACTION OF PLANAR SHOCK WAVES OVER A HALF-DIAMOND CYLINDER IN AIR

Zhang, D. L., Glass, I. I.

1. Oblique shock waves 2. Shock wave diffraction over half-diamond cylinder
3. Interferometric analysis

I. UTIAS Report No. 322 II. Zhang, D. L., Glass, I. I.

In this study an experimental investigation was conducted on the diffraction of planar shock waves over a half-diamond (45° wedge angles) cylinder (28 mm x 28 mm x 56 mm cross-section) in air at initial pressures ranging from 6.67 Kpa to 80.3 Kpa (50 torr to 605 torr), at an initial temperature near 300 K in all cases and at initial Mach numbers ranging from $1.35 < M_S < 2.82$. Over 150 experiments were conducted including models with smooth, spongy (plastic), rough (sandpaper) and saw-tooth surfaces. Infinite fringe interferograms were used throughout. The UTIAS 10 cm x 18 cm hypervelocity shock tube and the 23 cm diam field-of-view Mach-Zehnder interferometer were utilized for this purpose. The induced flows behind the incident shock waves were subsonic, transonic and supersonic. The subsequent intersections with the initial wedge produced regular, single Mach, complex Mach and double Mach reflections. The isopycnics over the entire flowfields were evaluated and the pressure fields determined using the isentropic equation of state. A half-size model was also used to study the effects of longer flow durations. The present experimental data should prove very useful for comparison with numerical simulations and for evaluating the blast loading of structures.

Available copies of this report are limited. Return this card to UTIAS, if you require a copy.

UTIAS Report No. 322

University of Toronto, Institute for Aerospace Studies (UTIAS)
4925 Dufferin Street, Downsview, Ontario, Canada, M3H 5T6

AN INTERFEROMETRIC INVESTIGATION OF THE DIFFRACTION OF PLANAR SHOCK WAVES OVER A HALF-DIAMOND CYLINDER IN AIR

Zhang, D. L., Glass, I. I.

1. Oblique shock waves 2. Shock wave diffraction over half-diamond cylinder
3. Interferometric analysis

I. UTIAS Report No. 322 II. Zhang, D. L., Glass, I. I.

In this study an experimental investigation was conducted on the diffraction of planar shock waves over a half-diamond (45° wedge angles) cylinder (28 mm x 28 mm x 56 mm cross-section) in air at initial pressures ranging from 6.67 Kpa to 80.3 Kpa (50 torr to 605 torr), at an initial temperature near 300 K in all cases and at initial Mach numbers ranging from $1.35 < M_S < 2.82$. Over 150 experiments were conducted including models with smooth, spongy (plastic), rough (sandpaper) and saw-tooth surfaces. Infinite fringe interferograms were used throughout. The UTIAS 10 cm x 18 cm hypervelocity shock tube and the 23 cm diam field-of-view Mach-Zehnder interferometer were utilized for this purpose. The induced flows behind the incident shock waves were subsonic, transonic and supersonic. The subsequent intersections with the initial wedge produced regular, single Mach, complex Mach and double Mach reflections. The isopycnics over the entire flowfields were evaluated and the pressure fields determined using the isentropic equation of state. A half-size model was also used to study the effects of longer flow durations. The present experimental data should prove very useful for comparison with numerical simulations and for evaluating the blast loading of structures.

Available copies of this report are limited. Return this card to UTIAS, if you require a copy.

UTIAS Report No. 322

University of Toronto, Institute for Aerospace Studies (UTIAS)
4925 Dufferin Street, Downsview, Ontario, Canada, M3H 5T6

AN INTERFEROMETRIC INVESTIGATION OF THE DIFFRACTION OF PLANAR SHOCK WAVES OVER A HALF-DIAMOND CYLINDER IN AIR

Zhang, D. L., Glass, I. I.

1. Oblique shock waves 2. Shock wave diffraction over half-diamond cylinder
3. Interferometric analysis

I. UTIAS Report No. 322 II. Zhang, D. L., Glass, I. I.

In this study an experimental investigation was conducted on the diffraction of planar shock waves over a half-diamond (45° wedge angles) cylinder (28 mm x 28 mm x 56 mm cross-section) in air at initial pressures ranging from 6.67 Kpa to 80.3 Kpa (50 torr to 605 torr), at an initial temperature near 300 K in all cases and at initial Mach numbers ranging from $1.35 < M_S < 2.82$. Over 150 experiments were conducted including models with smooth, spongy (plastic), rough (sandpaper) and saw-tooth surfaces. Infinite fringe interferograms were used throughout. The UTIAS 10 cm x 18 cm hypervelocity shock tube and the 23 cm diam field-of-view Mach-Zehnder interferometer were utilized for this purpose. The induced flows behind the incident shock waves were subsonic, transonic and supersonic. The subsequent intersections with the initial wedge produced regular, single Mach, complex Mach and double Mach reflections. The isopycnics over the entire flowfields were evaluated and the pressure fields determined using the isentropic equation of state. A half-size model was also used to study the effects of longer flow durations. The present experimental data should prove very useful for comparison with numerical simulations and for evaluating the blast loading of structures.

Available copies of this report are limited. Return this card to UTIAS, if you require a copy.

UTIAS Report No. 322

University of Toronto, Institute for Aerospace Studies (UTIAS)
4925 Dufferin Street, Downsview, Ontario, Canada, M3H 5T6

AN INTERFEROMETRIC INVESTIGATION OF THE DIFFRACTION OF PLANAR SHOCK WAVES OVER A HALF-DIAMOND CYLINDER IN AIR

Zhang, D. L., Glass, I. I.

1. Oblique shock waves 2. Shock wave diffraction over half-diamond cylinder
3. Interferometric analysis

I. UTIAS Report No. 322 II. Zhang, D. L., Glass, I. I.

In this study an experimental investigation was conducted on the diffraction of planar shock waves over a half-diamond (45° wedge angles) cylinder (28 mm x 28 mm x 56 mm cross-section) in air at initial pressures ranging from 6.67 Kpa to 80.3 Kpa (50 torr to 605 torr), at an initial temperature near 300 K in all cases and at initial Mach numbers ranging from $1.35 < M_S < 2.82$. Over 150 experiments were conducted including models with smooth, spongy (plastic), rough (sandpaper) and saw-tooth surfaces. Infinite fringe interferograms were used throughout. The UTIAS 10 cm x 18 cm hypervelocity shock tube and the 23 cm diam field-of-view Mach-Zehnder interferometer were utilized for this purpose. The induced flows behind the incident shock waves were subsonic, transonic and supersonic. The subsequent intersections with the initial wedge produced regular, single Mach, complex Mach and double Mach reflections. The isopycnics over the entire flowfields were evaluated and the pressure fields determined using the isentropic equation of state. A half-size model was also used to study the effects of longer flow durations. The present experimental data should prove very useful for comparison with numerical simulations and for evaluating the blast loading of structures.

Available copies of this report are limited. Return this card to UTIAS, if you require a copy.

UTIAS Report No. 322

University of Toronto, Institute for Aerospace Studies (UTIAS)
4925 Dufferin Street, Downsview, Ontario, Canada, M3H 5T6

AN INTERFEROMETRIC INVESTIGATION OF THE DIFFRACTION OF PLANAR SHOCK WAVES OVER A HALF-DIAMOND CYLINDER IN AIR

Zhang, D. L., Glass, I. I.

1. Oblique shock waves 2. Shock wave diffraction over half-diamond cylinder
3. Interferometric analysis

I. UTIAS Report No. 322 II. Zhang, D. L., Glass, I. I.

In this study an experimental investigation was conducted on the diffraction of planar shock waves over a half-diamond (45° wedge angles) cylinder (28 mm x 28 mm x 56 mm cross-section) in air at initial pressures ranging from 6.67 Kpa to 80.3 Kpa (50 torr to 605 torr), at an initial temperature near 300 K in all cases and at initial Mach numbers ranging from $1.35 < M_s < 2.82$. Over 150 experiments were conducted including models with smooth, spongy (plastic), rough (sandpaper) and saw-tooth surfaces. Infinite fringe interferograms were used throughout. The UTIAS 10 cm x 18 cm hypervelocity shock tube and the 23 cm diam field-of-view Mach-Zehnder interferometer were utilized for this purpose. The induced flows behind the incident shock waves were subsonic, transonic and supersonic. The subsequent intersections with the initial wedge produced regular, single Mach, complex Mach and double Mach reflections. The isopycnics over the entire flowfields were evaluated and the pressure fields determined using the isentropic equation of state. A half-size model was also used to study the effects of longer flow durations. The present experimental data should prove very useful for comparison with numerical simulations and for evaluating the blast loading of structures.

Available copies of this report are limited. Return this card to UTIAS, if you require a copy.

UTIAS Report No. 322

University of Toronto, Institute for Aerospace Studies (UTIAS)
4925 Dufferin Street, Downsview, Ontario, Canada, M3H 5T6

AN INTERFEROMETRIC INVESTIGATION OF THE DIFFRACTION OF PLANAR SHOCK WAVES OVER A HALF-DIAMOND CYLINDER IN AIR

Zhang, D. L., Glass, I. I.

1. Oblique shock waves 2. Shock wave diffraction over half-diamond cylinder
3. Interferometric analysis

I. UTIAS Report No. 322 II. Zhang, D. L., Glass, I. I.

In this study an experimental investigation was conducted on the diffraction of planar shock waves over a half-diamond (45° wedge angles) cylinder (28 mm x 28 mm x 56 mm cross-section) in air at initial pressures ranging from 6.67 Kpa to 80.3 Kpa (50 torr to 605 torr), at an initial temperature near 300 K in all cases and at initial Mach numbers ranging from $1.35 < M_s < 2.82$. Over 150 experiments were conducted including models with smooth, spongy (plastic), rough (sandpaper) and saw-tooth surfaces. Infinite fringe interferograms were used throughout. The UTIAS 10 cm x 18 cm hypervelocity shock tube and the 23 cm diam field-of-view Mach-Zehnder interferometer were utilized for this purpose. The induced flows behind the incident shock waves were subsonic, transonic and supersonic. The subsequent intersections with the initial wedge produced regular, single Mach, complex Mach and double Mach reflections. The isopycnics over the entire flowfields were evaluated and the pressure fields determined using the isentropic equation of state. A half-size model was also used to study the effects of longer flow durations. The present experimental data should prove very useful for comparison with numerical simulations and for evaluating the blast loading of structures.

Available copies of this report are limited. Return this card to UTIAS, if you require a copy.

UTIAS Report No. 322

University of Toronto, Institute for Aerospace Studies (UTIAS)
4925 Dufferin Street, Downsview, Ontario, Canada, M3H 5T6

AN INTERFEROMETRIC INVESTIGATION OF THE DIFFRACTION OF PLANAR SHOCK WAVES OVER A HALF-DIAMOND CYLINDER IN AIR

Zhang, D. L., Glass, I. I.

1. Oblique shock waves 2. Shock wave diffraction over half-diamond cylinder
3. Interferometric analysis

I. UTIAS Report No. 322 II. Zhang, D. L., Glass, I. I.

In this study an experimental investigation was conducted on the diffraction of planar shock waves over a half-diamond (45° wedge angles) cylinder (28 mm x 28 mm x 56 mm cross-section) in air at initial pressures ranging from 6.67 Kpa to 80.3 Kpa (50 torr to 605 torr), at an initial temperature near 300 K in all cases and at initial Mach numbers ranging from $1.35 < M_s < 2.82$. Over 150 experiments were conducted including models with smooth, spongy (plastic), rough (sandpaper) and saw-tooth surfaces. Infinite fringe interferograms were used throughout. The UTIAS 10 cm x 18 cm hypervelocity shock tube and the 23 cm diam field-of-view Mach-Zehnder interferometer were utilized for this purpose. The induced flows behind the incident shock waves were subsonic, transonic and supersonic. The subsequent intersections with the initial wedge produced regular, single Mach, complex Mach and double Mach reflections. The isopycnics over the entire flowfields were evaluated and the pressure fields determined using the isentropic equation of state. A half-size model was also used to study the effects of longer flow durations. The present experimental data should prove very useful for comparison with numerical simulations and for evaluating the blast loading of structures.

Available copies of this report are limited. Return this card to UTIAS, if you require a copy.

UTIAS Report No. 322

University of Toronto, Institute for Aerospace Studies (UTIAS)
4925 Dufferin Street, Downsview, Ontario, Canada, M3H 5T6

AN INTERFEROMETRIC INVESTIGATION OF THE DIFFRACTION OF PLANAR SHOCK WAVES OVER A HALF-DIAMOND CYLINDER IN AIR

Zhang, D. L., Glass, I. I.

1. Oblique shock waves 2. Shock wave diffraction over half-diamond cylinder
3. Interferometric analysis

I. UTIAS Report No. 322 II. Zhang, D. L., Glass, I. I.

In this study an experimental investigation was conducted on the diffraction of planar shock waves over a half-diamond (45° wedge angles) cylinder (28 mm x 28 mm x 56 mm cross-section) in air at initial pressures ranging from 6.67 Kpa to 80.3 Kpa (50 torr to 605 torr), at an initial temperature near 300 K in all cases and at initial Mach numbers ranging from $1.35 < M_s < 2.82$. Over 150 experiments were conducted including models with smooth, spongy (plastic), rough (sandpaper) and saw-tooth surfaces. Infinite fringe interferograms were used throughout. The UTIAS 10 cm x 18 cm hypervelocity shock tube and the 23 cm diam field-of-view Mach-Zehnder interferometer were utilized for this purpose. The induced flows behind the incident shock waves were subsonic, transonic and supersonic. The subsequent intersections with the initial wedge produced regular, single Mach, complex Mach and double Mach reflections. The isopycnics over the entire flowfields were evaluated and the pressure fields determined using the isentropic equation of state. A half-size model was also used to study the effects of longer flow durations. The present experimental data should prove very useful for comparison with numerical simulations and for evaluating the blast loading of structures.

Available copies of this report are limited. Return this card to UTIAS, if you require a copy.